Water Availability and Use Science Program

Construction and Calibration of a Groundwater-Flow Model to Assess Groundwater Availability in the Uppermost Principal Aquifer Systems of the Williston Basin, United States and Canada

Scientific Investigations Report 2017–5158

U.S. Department of the Interior
U.S. Geological Survey

Cover. Photograph of lower Tertiary aquifer system, 8 miles south of Medora, North Dakota. Photograph by Whitten Photography, July 2012, used with permission.

Construction and Calibration of a Groundwater-Flow Model to Assess Groundwater Availability in the Uppermost Principal Aquifer Systems of the Williston Basin, United States and Canada

By Kyle W. Davis and Andrew J. Long

Water Availability and Use Science Program

Scientific Investigations Report 2017–5158

U.S. Department of the Interior
U.S. Geological Survey

U.S. Department of the Interior
RYAN K. ZINKE, Secretary

U.S. Geological Survey
James F. Reilly II, Director

U.S. Geological Survey, Reston, Virginia: 2018

For more information on the USGS—the Federal source for science about the Earth, its natural and living resources, natural hazards, and the environment—visit https://www.usgs.gov or call 1–888–ASK–USGS.

For an overview of USGS information products, including maps, imagery, and publications, visit https://store.usgs.gov.

Any use of trade, firm, or product names is for descriptive purposes only and does not imply endorsement by the U.S. Government.

Although this information product, for the most part, is in the public domain, it also may contain copyrighted materials as noted in the text. Permission to reproduce copyrighted items must be secured from the copyright owner.

Suggested citation:
Davis, K.W., and Long, A.J., 2018, Construction and calibration of a groundwater-flow model to assess groundwater availability in the uppermost principal aquifer systems of the Williston Basin, United States and Canada: U.S. Geological Survey Scientific Investigations Report 2017–5158, 70 p., https://doi.org/10.3133/sir20175158.

ISSN 2328-0328 (online)

Acknowledgments

The authors thank Jon Reiten and Kevin Chandler (Montana Bureau of Mines and Geology), Kimberly Fischer (North Dakota State Water Commission), Attila Folnagy (Montana Department of Natural Resources and Conservation), Kei Lo (Saskatchewan Water Security Agency), Graham Phipps (Manitoba Sustainable Development), and Yves Michaud and Alfonso Rivera (Geological Survey of Canada), for their participation in monthly technical conference calls as part of the Williston Area Aquifers Modeling Consortium to discuss the groundwater resources of the Williston Basin. The authors would also like to thank Kimberly Fischer for providing insightful comments for this report as a technical reviewer.

The authors thank the U.S. Geological Survey (USGS) Water Availability and Use Science Program, which includes the former Groundwater Resources Program, for their support of this study. Several USGS personnel have contributed through technical assistance and guidance throughout the project. Kevin Dennehy (retired), Geoff Delin (retired), Howard Reeves, Mike Fienen, Randy Hansen, Tom Reilly (emeritus), Arlen Harbaugh, Chris Langevin, and Seth Haines (USGS) have provided technical guidance and comments throughout the study. The authors would also like to thank Brian Clark (USGS) for providing technical review of the report and Daniel Feinstein (USGS) for technical review of the model files available in the accompanying data release.

Contents

Abstract 1
Introduction 2
Purpose and Scope 2
Description of Model Area 4
Previous Investigations 4
Hydrogeologic Framework 4
Overview of Groundwater Flow 5
Methods Overview 6
Model Design and Construction 7
Spatial Discretization and Vertical Layering 7
Temporal Discretization 10
Hydraulic Properties 10
Boundary Conditions 14
Lateral and Lower Boundaries 14
Precipitation Recharge 14
Surface-Water Features 16
Groundwater Withdrawal 18
Model Calibration 19
Calibration Targets 20
Groundwater Levels 21
Exchanges Between Groundwater and Surface Water 21
Discharge From Flowing Artesian Wells 22
Calibration Results 22
Optimal Parameter Estimates 22
Assessment of Model Fit 28
Potentiometric Surfaces 28
Calibration Targets 32
Groundwater Flow 39
Flowing Artesian Wells 53
Parameter Sensitivity and Identifiability 54
Model Limitations and Assumptions 57
Summary 58
References Cited 59
Glossary 65
Appendix 1. Model Calibration Targets and Optimized Parameter Estimates 68
Appendix 2. Model Calibration Weights 69

Figures

1. Map showing structural basins, outcrops or subcrops of hydrogeologic units of the principal aquifers in the Northern Great Plains, numerical model grid, and spatial extent of the active model area....3
2. Conceptual block diagram of groundwater flow in the Williston Basin, as viewed from the southeast....6
3. Diagram showing example of the relation of aquifer systems and property zones to model layers, shown in vertical profile along a generalized south to north profile....9
4. Maps showing property zones and pilot point locations for each model layer....11
5. Map showing active-extent boundaries for the steady-state and transient models, and recharge and pumping wells for the steady-state model....15
6. Map showing simulated stream cells used in the River, Drain, and Streamflow-Routing Packages, and simulated flowing wells represented by the Multi-Node Well Package....17
7. Maps showing horizontal hydraulic conductivity and pilot points for *A*, layer 1; *B*, layer 2; *C*, layer 3; *D*, layer 4; *E*, layer 5; *F*, layer 6; *G*, layer 7; and *H*, layer 8, estimated by model calibration....23
8. Maps showing vertical hydraulic conductivity and pilot points for *A*, layer 1; *B*, layer 2; *C*, layer 3; *D*, layer 4; *E*, layer 5; *F*, layer 6; *G*, layer 7; and *H*, layer 8, estimated by model calibration....25
9. Map showing comparison of observed and simulated steady-state potentiometric surfaces for the upper Fort Union aquifer....29
10. Map showing comparison of observed and simulated steady-state potentiometric surfaces for the lower Fort Union aquifer....30
11. Map showing comparison of observed and simulated steady-state potentiometric surfaces for the Fox Hills aquifer....31
12. Graph showing relation between observed and simulated hydraulic heads for the steady-state model....32
13. Maps showing hydraulic head residuals for the steady-state model for the *A*, upper part of the glacial aquifer system; *B*, lower part of the glacial aquifer system; *C*, upper Fort Union aquifer; *D*, lower Fort Union aquifer; *E*, lower Hell Creek aquifer; and *F*, Fox Hills aquifer....33
14. Histogram of hydraulic head residuals for the transient model....39
15. Maps and selected hydrographs showing observed and simulated hydraulic head for the transient model for the *A*, upper part of the glacial aquifer system; *B*, lower part of the glacial aquifer system; *C*, upper Fort Union aquifer; *D*, lower Fort Union aquifer; *E*, lower Hell Creek aquifer; and *F*, Fox Hills aquifer....40
16. Graphs showing comparison of observed and simulated base flow for the *A*, steady-state model and *B*, transient model....46
17. Map showing base-flow or stream-flux residuals for the Gage Package and base flow from the Streamflow-Routing Package for the steady-state model....47
18. Graphs showing observed hydrographs and simulated hydrographs using the transient model for streamgages with 10 or more years of streamflow record and contributing drainage area entirely within the model area....48
19. Graph showing simulated groundwater budgets for the steady-state and transient models....51

20. Graph showing total discharge to flowing artesian wells and mean flowing artesian well discharge as simulated by the Multi-Node Well Package for the transient model 53
21. Graph showing identifiability of all parameters with values greater than 0.5 for the steady-state model, when the 50 highest ranking singular-value parameters are considered 55

Tables

1. Estimated mean groundwater recharge and discharge components for 1981–2005 for a control volume within the model area 5
2. Relation of hydrogeologic units to numerical-model layers and hydraulic-property zones, description of zone properties, and mean simulated thickness....8
3. Summary statistics of hydraulic properties from Thamke and others (2014)....13
4. Previously published aquifer storage properties 13
5. Summary of parameters estimated during model calibration 20
6. Summary statistics of model-estimated aquifer properties by hydraulic property zone 27
7. Summary statistics of simulated hydraulic head for the steady-state model....39
8. Simulated steady-state groundwater recharge and discharge components for 1981–2005 for the upper Fort Union aquifer....52
9. Simulated steady-state groundwater recharge and discharge components for 1981–2005 for the lower Fort Union aquifer....52
10. Simulated steady-state groundwater recharge and discharge components for 1981–2005 for the Fox Hills aquifer....53
11. Parameters with identifiability values greater than 0.5 for the steady-state model 56

Conversion Factors

U.S. customary units to International System of Units

Multiply	By	To obtain
	Length	
inch (in.)	2.54	centimeter (cm)
foot (ft)	0.3048	meter (m)
mile (mi)	1.609	kilometer (km)
	Area	
square mile (mi^2)	2.590	square kilometer (km^2)
	Flow rate	
foot per day (ft/d)	0.3048	meter per day (m/d)
foot per year (ft/yr)	0.3048	meter per year (m/yr)
cubic foot per second (ft^3/s)	0.02832	cubic meter per second (m^3/s)
gallon per minute (gal/min)	0.06309	liter per second (L/s)
inch per year (in/yr)	25.4	millimeter per year (mm/yr)

Vertical coordinate information is referenced to the North American Vertical Datum of 1988 (NAVD 88).

Horizontal coordinate information is referenced to the North American Datum of 1983 (NAD 83).

Altitude, as used in this report, refers to distance above the vertical datum.

*Transmissivity: The standard unit for transmissivity is cubic foot per day per square foot times foot of aquifer thickness ($[ft^3/d]/ft^2$)ft. In this report, the mathematically reduced form, foot squared per day (ft^2/d), is used for convenience.

Abbreviations

CHD	Time-Variant Specified-Head Option
DEM	digital elevation model
DRN	Drain (Package)
FH	Fox Hills aquifer
GIS	geographic information system
K	hydraulic conductivity
LFU	lower Fort Union aquifer
LGh	sand and gravel outwash in bedrock valleys in the lower part of glacial aquifer system
LGl	till in the lower part of the glacial aquifer system
LHC	lower Hell Creek aquifer
MFU	middle Fort Union hydrogeologic unit

MNW	Multi-Node Well (Package)
NED	National Elevation Dataset
NHDPlus v2	National Hydrography Dataset
NHN	National Hydro Network
NOAA	National Oceanic and Atmospheric Administration
PEST	Parameter ESTimation [software]
RCH	Recharge (Package)
RIV	River (Package)
SFR2	Streamflow-Routing (Package)
SVD	singular-value decomposition
SWB	Soil-Water-Balance
UFU	upper Fort Union aquifer
UGh	glaciofluvial, loess, and eolian deposits in upper part of glacial aquifer system
UGl	till in upper part of glacial aquifer system
UGm	glaciolacustrine and glaciotectonic deposits in the upper part of the glacial aquifer system
UGu	deposits of unknown origin in the upper part of the glacial aquifer system
UHC	upper Hell Creek hydrogeologic unit
UPW	Upstream Weighting (Package)
USGS	U.S. Geological Survey
WEL	Well (Package)

Construction and Calibration of a Groundwater-Flow Model to Assess Groundwater Availability in the Uppermost Principal Aquifer Systems of the Williston Basin, United States and Canada

By Kyle W. Davis and Andrew J. Long

Abstract

The U.S. Geological Survey developed a groundwater-flow model for the uppermost principal aquifer systems in the Williston Basin in parts of Montana, North Dakota, and South Dakota in the United States and parts of Manitoba and Saskatchewan in Canada as part of a detailed assessment of the groundwater availability in the area. The assessment was done because of the potential for increased demands and stresses on groundwater associated with large-scale energy development in the area. As part of this assessment, a three-dimensional groundwater-flow model was developed as a tool that can be used to simulate how the groundwater-flow system responds to changes in hydrologic stresses at a regional scale.

The three-dimensional groundwater-flow model was developed using the U.S. Geological Survey's numerical finite-difference groundwater model with the Newton-Rhapson solver, MODFLOW–NWT, to represent the glacial, lower Tertiary, and Upper Cretaceous aquifer systems for steady-state (mean) hydrological conditions for 1981–2005 and for transient (temporally varying) conditions using a combination of a steady-state period for pre-1960 and transient periods for 1961–2005. The numerical model framework was constructed based on existing and interpreted hydrogeologic and geospatial data and consisted of eight layers. Two layers were used to represent the glacial aquifer system in the model; layer 1 represented the upper one-half and layer 2 represented the lower one-half of the glacial aquifer system. Three layers were used to represent the lower Tertiary aquifer system in the model; layer 3 represented the upper Fort Union aquifer, layer 4 represented the middle Fort Union hydrogeologic unit, and layer 5 represented the lower Fort Union aquifer. Three layers were used to represent the Upper Cretaceous aquifer system in the model; layer 6 represented the upper Hell Creek hydrogeologic unit, layer 7 represented the lower Hell Creek aquifer, and layer 8 represented the Fox Hills aquifer. The numerical model was constructed using a uniform grid with square cells that are about 1 mile (1,600 meters) on each side with a total of about 657,000 active cells.

Model calibration was completed by linking Parameter ESTimation (PEST) software with MODFLOW–NWT. The PEST software uses statistical parameter estimation techniques to identify an optimum set of input parameters by adjusting individual model input parameters and assessing the differences, or residuals, between observed (measured or estimated) data and simulated values. Steady-state model calibration consisted of attempting to match mean simulated values to measured or estimated values of (1) hydraulic head, (2) hydraulic head differences between model layers, (3) stream infiltration, and (4) discharge to streams. Calibration of the transient model consisted of attempting to match simulated and measured temporally distributed values of hydraulic head changes, stream base flow, and groundwater discharge to artesian flowing wells. Hydraulic properties estimated through model calibration included hydraulic conductivity, vertical hydraulic conductivity, aquifer storage, and riverbed hydraulic conductivity in addition to groundwater recharge and well skin.

The ability of the numerical model to accurately simulate groundwater flow in the Williston Basin was assessed primarily by its ability to match calibration targets for hydraulic head, stream base flow, and flowing well discharge. The steady-state model also was used to assess the simulated potentiometric surfaces in the upper Fort Union aquifer, the lower Fort Union aquifer, and the Fox Hills aquifer. Additionally, a previously estimated regional groundwater-flow budget was compared with the simulated steady-state groundwater-flow budget for the Williston Basin. The simulated potentiometric surfaces typically compared well with the estimated potentiometric surfaces based on measured hydraulic head data and indicated localized groundwater-flow gradients that were topographically controlled in outcrop areas and more generalized regional gradients where the aquifers were confined. The differences between the measured and simulated (residuals) hydraulic head values for 11,109 wells were assessed, which indicated that the steady-state model generally underestimated hydraulic head in the model area. This underestimation is indicated by a positive mean residual of 11.2 feet for all model layers. Layer 7, which represents

the lower Hell Creek aquifer, is the only layer for which the steady-state model overestimated hydraulic head. Simulated groundwater-level changes for the transient model matched within plus or minus 2.5 feet of the measured values for more than 60 percent of all measurements and to within plus or minus 17.5 feet for 95 percent of all measurements; however, the transient model underestimated groundwater-level changes for all model layers. A comparison between simulated and estimated base flows for the steady-state and transient models indicated that both models overestimated base flow in streams and underestimated annual fluctuations in base flow.

The estimated and simulated groundwater budgets indicate the model area received a substantial amount of recharge from precipitation and stream infiltration. The steady-state model indicated that reservoir seepage was a larger component of recharge in the Williston Basin than was previously estimated. Irrigation recharge and groundwater inflow from outside the Williston Basin accounted for a relatively small part of total groundwater recharge when compared with recharge from precipitation, stream infiltration, and reservoir seepage. Most of the estimated and simulated groundwater discharge in the Williston Basin was to streams and reservoirs. Simulated groundwater withdrawal, discharge to reservoirs, and groundwater outflow in the Williston Basin accounted for a smaller part of total groundwater discharge.

The transient model was used to simulate discharge to 571 flowing artesian wells within the model area. Of the 571 established flowing artesian wells simulated by the model, 271 wells did not flow at any time during the simulation because hydraulic head was always below the land-surface altitude. As hydraulic head declined throughout the simulation, 68 of these wells responded by ceasing to flow by the end of 2005. Total mean simulated discharge for the 571 flowing artesian wells was 55.1 cubic feet per second (ft^3/s), and the mean simulated flowing well discharge for individual wells was 0.118 ft^3/s. Simulated discharge to individual flowing artesian wells increased from 0.039 to 0.177 ft^3/s between 1961 and 1975 and decreased to 0.102 ft^3/s by 2005. The mean residual for 34 flowing wells with measured discharge was 0.014 ft^3/s, which indicates the transient model overestimated discharge to flowing artesian wells in the model area.

Model limitations arise from aspects of the conceptual model and from simplifications inherent in the construction and calibration of a regional-scale numerical groundwater-flow model. Simplifying assumptions in defining hydraulic parameters in space and hydrologic stresses and time-varying observational data in time can limit the capabilities of this tool to simulate how the groundwater-flow system responds to changes in hydrologic stresses, particularly at the local scale; nevertheless, the steady-state model adequately simulated flow in the uppermost principal aquifer systems in the Williston Basin based on the comparison between the simulated and estimated groundwater-flow budget, the comparison between simulated and estimated potentiometric surfaces, and the results of the calibration process.

Introduction

The U.S. Geological Survey (USGS) began a multi-year regional assessment of groundwater availability in the uppermost principal aquifer systems in the Williston Basin in the United States and Canada in 2011 as part of its ongoing regional assessments of groundwater availability of the principal aquifers of the Nation (Alley and others, 2013). The goals of this national assessment are to document effects of human activities on water levels and groundwater storage, to explore effects of climate variability on the regional water budget, and to provide consistent and integrated information that is useful to those who use and manage the groundwater resource. As part of this national assessment, the USGS evaluated available groundwater resources within the Williston Basin in the United States and Canada (fig. 1). The assessment was done because of the potential of increasing demands and stresses on groundwater associated with large-scale energy development in the area. As a part of this assessment, a three-dimensional numerical groundwater-flow model was developed as a tool that can be used to simulate how the groundwater-flow system responds to changes in hydrologic stresses at a regional scale.

The uppermost principal aquifer systems in the Williston Basin are the shallowest, the most accessible potable aquifers within the Northern Great Plains of the United States and Canada (fig. 1). They consist of the glacial, lower Tertiary, and Upper Cretaceous aquifer systems. The hydrogeologic framework and conceptual model of groundwater flow for most of the model area were described by Thamke and others (2014) and Long and others (2014), respectively, and provide a basis for the numerical model described in this report. The glacial aquifer system consists primarily of till and secondarily of sand and gravel from glacial outwash. The lower Tertiary and Upper Cretaceous aquifer systems are each defined by three hydrogeologic units (fig. 1) consisting primarily of shale, silt, sandstone, and coal and are described in detail in Thamke and others (2014).

Purpose and Scope

The purpose of this report is to describe the construction and calibration of an eight-layer, three-dimensional numerical groundwater-flow model for the three uppermost principal aquifer systems of the Northern Great Plains in the Williston Basin, which include the glacial, lower Tertiary, and Upper Cretaceous aquifer systems (fig. 1). The hydrogeologic framework and conceptual model of groundwater flow are described very briefly herein but are described in detail by Thamke and others (2014) and Long and others (2014), respectively. The hydrogeologic framework and conceptual model provided the basis for the vertical, spatial, and temporal range of the numerical model. The numerical model is intended to be used (1) to simulate hydrologic scenarios of interest to groundwater managers; (2) to advance the understanding of groundwater budgets and components

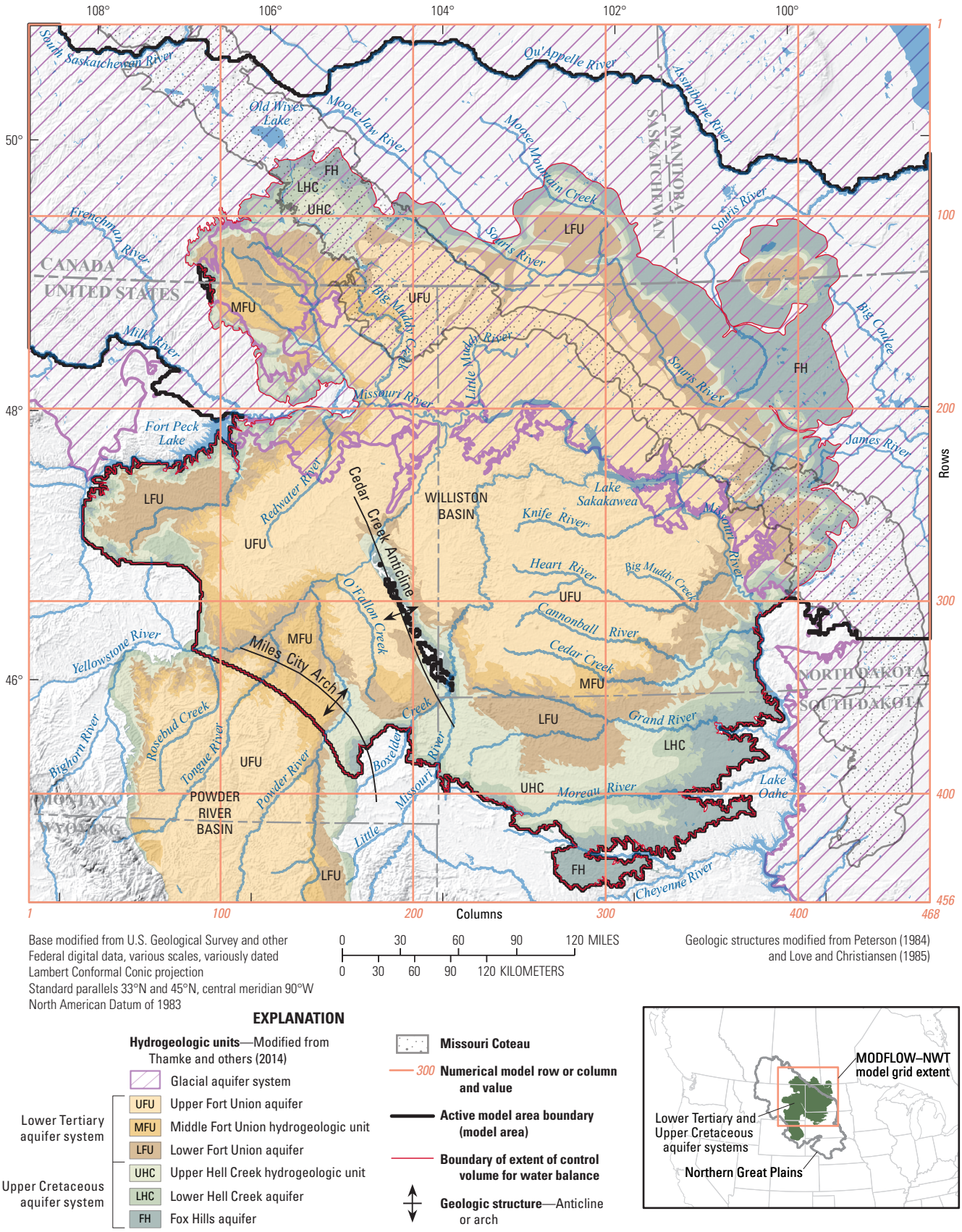

Figure 1. Structural basins, outcrops or subcrops (underling the glacial aquifer system) of hydrogeologic units of the principal aquifers in the Northern Great Plains, numerical model grid, and spatial extent of the active model area.

including recharge, discharge, and aquifer storage for the entire system; (3) to compute historical and projected system response to natural and anthropogenic stresses; and (4) to evaluate potential hydrologic monitoring programs at a scale relevant to basinwide water-management decisions.

Description of Model Area

The active model area (hereafter referred to as "model area") underlies about 143,000 square miles in parts of Montana, North Dakota, and South Dakota in the United States, and parts of Manitoba and Saskatchewan in Canada (fig. 1) and includes the three uppermost principal aquifer systems in the Williston Basin: the glacial, lower Tertiary, and Upper Cretaceous aquifer systems. In this report, the boundary of the Williston Basin is considered the outcrop and subcrop of the lower Tertiary and Upper Cretaceous aquifer systems inside the control volume shown on figure 1. The topography is characterized by low relief or gently rolling hills, except near large river channels with steep banks. The glacial aquifer system is characterized by surficial deposits in the northern part of the Williston Basin that primarily consist of glacial till and outwash. The Missouri Coteau, a narrow northwest and southeast trending plateau between the Missouri River and the Souris River, where the till is characterized by a hummocky knob-and-kettle topography, is characterized by an abundance of prairie potholes and lacks an integrated drainage pattern (Eisenlohr and Sloan, 1968). Underlying these glacial deposits, or exposed at the land surface where glacial deposits are absent, are sedimentary rocks that contain the lower Tertiary and Upper Cretaceous aquifer systems and are composed primarily of sandstone, coal, and shale (Long and others, 2014). Large rivers, such as the Missouri and Yellowstone Rivers, erode the semiconsolidated sedimentary rocks and create several hundred feet of local topographic relief. The climate is characterized as semiarid, and precipitation ranges from about 11 inches per year (in/yr) in the western part to 22 in/yr in the eastern part (Long and others, 2014). Pasture and hayland exist in 70 percent of the model area (Multi-Resolution Land Characteristics Consortium, 2011). Fort Peck Lake, Lake Sakakawea, and Lake Oahe are large reservoirs in the model area that control flow in the Missouri River (fig. 1).

In the active model area, the Missouri River flows toward the east and southeast, and the Yellowstone and Little Missouri Rivers enter from the south (fig. 1). Several other tributaries in the southeastern part of the Williston Basin flow toward the east and enter the Missouri River from the west. The South Saskatchewan River, Qu'Appelle River, and Assiniboine River make up the northern boundary of the model area. Streams south of the Missouri Coteau (fig. 1) flow into the Missouri River from the north. Streams north of the Missouri Coteau generally flow southeast, except for parts of the Souris River that flow to the north and the South Saskatchewan, Qu'Appelle, and Assiniboine Rivers that flow to the east. Few streams cross the Missouri Coteau because of its nonintegrated drainage pattern (fig. 1).

Previous Investigations

Previous model simulations for the model area (fig. 1) include Downey (1986), Anna (2011), and Fischer (2013). Downey (1986) simulated groundwater flow in the Upper Cretaceous aquifer system in the Williston and Powder River Basins. Anna (2011) simulated groundwater flow in the Fox Hills aquifer in the northwestern part of the Williston Basin. Groundwater-level declines for the Fox Hills and Hell Creek aquifers that resulted from flowing wells were simulated by Fischer (2013).

Hydraulic conductivity for the glacial, lower Tertiary, and Upper Cretaceous aquifers was estimated by Thamke and others (2014) by examining resistivity and lithologic logs in the Williston Basin. Storage properties including specific storage, storage coefficient, porosity, and specific yield for the glacial, lower Tertiary, and Upper Cretaceous aquifers were estimated by Anna (1981), Armstrong (1971), Bader and Radig (1991), Croft (1973, 1978, 1985), Croft and Wesolowski (1970), Fischer (2013), Klausing (1979), McWhorter (1984), Robson (1987), and Stoner (1981). Thamke and others (2014) and Long and others (2014) provide additional references for previous investigations related to this study.

Hydrogeologic Framework

The three uppermost principal aquifer systems in the Williston Basin are the glacial, lower Tertiary, and Upper Cretaceous aquifer systems (fig. 1). From these principal aquifers, eight separate hydrogeologic units were identified based on previously published information and digital data.

The glacial aquifer system consists of sand and gravel aquifers separated by till and other glacial deposits (Whitehead, 1996) and was subdivided into two hydrogeologic units: the upper part of the glacial aquifer system and the lower part of the glacial aquifer system. Hydrologic soil groups for glacial deposits (Long and others, 2014) were used to characterize permeability in the upper part of the glacial aquifer system as follows: high permeability is defined by glaciofluvial, loess, and eolian deposits; medium permeability is defined by glaciolacustrine and glaciotectonic deposits; and low permeability is defined by till. Buried sand and gravel valley-fill aquifers of high permeability and till or other glacial deposits of low permeability were assumed to be in the lower part of the glacial aquifer system. The glacial aquifer system has a wide range of hydraulic conductivities and is characterized by disconnected, local flow systems (Thamke and others, 2014).

The bedrock hydrogeologic units primarily consist of sandstone, coal, and shale and were subdivided into six hydrogeologic units based on a hydrogeologic framework developed by Thamke and others (2014). The six hydrogeologic units include the upper Fort Union aquifer, middle Fort

Union hydrogeologic unit, lower Fort Union aquifer, upper Hell Creek hydrogeologic unit, lower Hell Creek aquifer, and Fox Hills aquifer (fig. 1). The lower Tertiary and Upper Cretaceous aquifer systems are primarily under confined conditions, except along the basin margins and in the shallow aquifers in the uppermost part of the lower Tertiary hydrogeologic units where the lower Tertiary and Upper Cretaceous aquifer systems are characterized by local flow systems (Whitehead, 1996). Thamke and others (2014) provided detailed lithostratigraphic and hydrogeologic descriptions of these units.

Overview of Groundwater Flow

Long and others (2014) estimated a groundwater budget, or balance of groundwater inflows and outflows, for a control volume within the numerical model extent for 1981–2005. For this study, the control volume and estimated groundwater budget were modified from Long and others (2014) to correspond to the model boundary between the Williston and Powder River Basins, south of the Miles City Arch (fig. 1; table 1); this control volume, which is a subregion of the model area, was defined as a volume of the Earth consisting of the lower Tertiary and Upper Cretaceous aquifer systems and the overlying areas of the glacial aquifer system in the Williston Basin. Mean estimated annual recharge from precipitation for the model area for 1981–2005 ranges from 0 in the northwest to about 10 in/yr in the northeast, and the overall mean annual recharge is 0.18 in/yr (Long and others, 2014). The exchange of surface water and groundwater was estimated by Long and others (2014) for stream reaches in the model area. The long-term total stream infiltration and groundwater discharge to streams were estimated to be 5,860 and 6,660 cubic feet per second (ft^3/s), respectively, for all stream reaches where data were available in the model area. Long-term total stream infiltration and groundwater discharge to streams were estimated to be 3,302 and 4,477 ft^3/s, respectively, for the control volume (table 1). Estimated mean groundwater (well) withdrawal for 1981–2005 for the lower Tertiary, Upper Cretaceous, and overlying glacial aquifer systems was 126 ft^3/s. Estimated regional groundwater inflow from the Powder River Basin was 8 ft^3/s (fig. 1).

Groundwater flow in the lower Tertiary and Upper Cretaceous aquifer systems generally is from southwest to northeast in the Williston Basin (fig. 2). The Missouri Coteau (fig. 1) primarily consists of glacial till and outwash with densely spaced wetlands that lack an integrated drainage pattern (Eisenlohr and Sloan, 1968; Sloan, 1972; Van der Kamp and Hayashi, 1998). In other areas of the model area, the depth to water is smallest near streams and largest in upland areas, and groundwater typically flows toward streams in all hydrogeologic units (Long and others, 2014). Where unconfined, the potentiometric surface of the upper Fort Union aquifer is topographically controlled. In upland areas, the vertical

Table 1. Estimated mean groundwater recharge and discharge components for 1981–2005 for a control volume within the model area (modified from Long and others, 2014).

[Estimates for precipitation recharge, stream infiltration, and discharge to streams were increased by 1.28 percent compared to estimates from Long and others (2014) to account for the modified control volume in this report; ft^3/s, cubic foot per second; <, less than; --, not estimated]

Recharge or discharge component	Estimated		Simulated	
	ft^3/s	Percent[a]	ft^3/s	Percent
Groundwater recharge				
Precipitation recharge	1,205	26	1,723	35
Stream infiltration	3,302	72	815	16
Irrigation recharge[b]	98	2	98	2
Recharge from reservoirs	0	0	2,094	42
Groundwater inflow from the Powder River Basin	8	<1	84	2
Groundwater inflow from glacial deposits outside of subregion	--	--	134	3
Total recharge	4,613	100	4,948	100
Groundwater discharge				
Discharge to streams	4,477	97	2,633	52
Groundwater (well) withdrawal	126	3	86	2
Discharge to reservoirs	10	<1	2,128	42
Groundwater outflow to glacial deposits outside of subregion	--	--	185	4
Total discharge	4,613	100	5,032	100

[a]The percentage of total recharge or total discharge may not be equal to 100 because of rounding.

[b]Estimated recharge is assumed to represent simulated recharge.

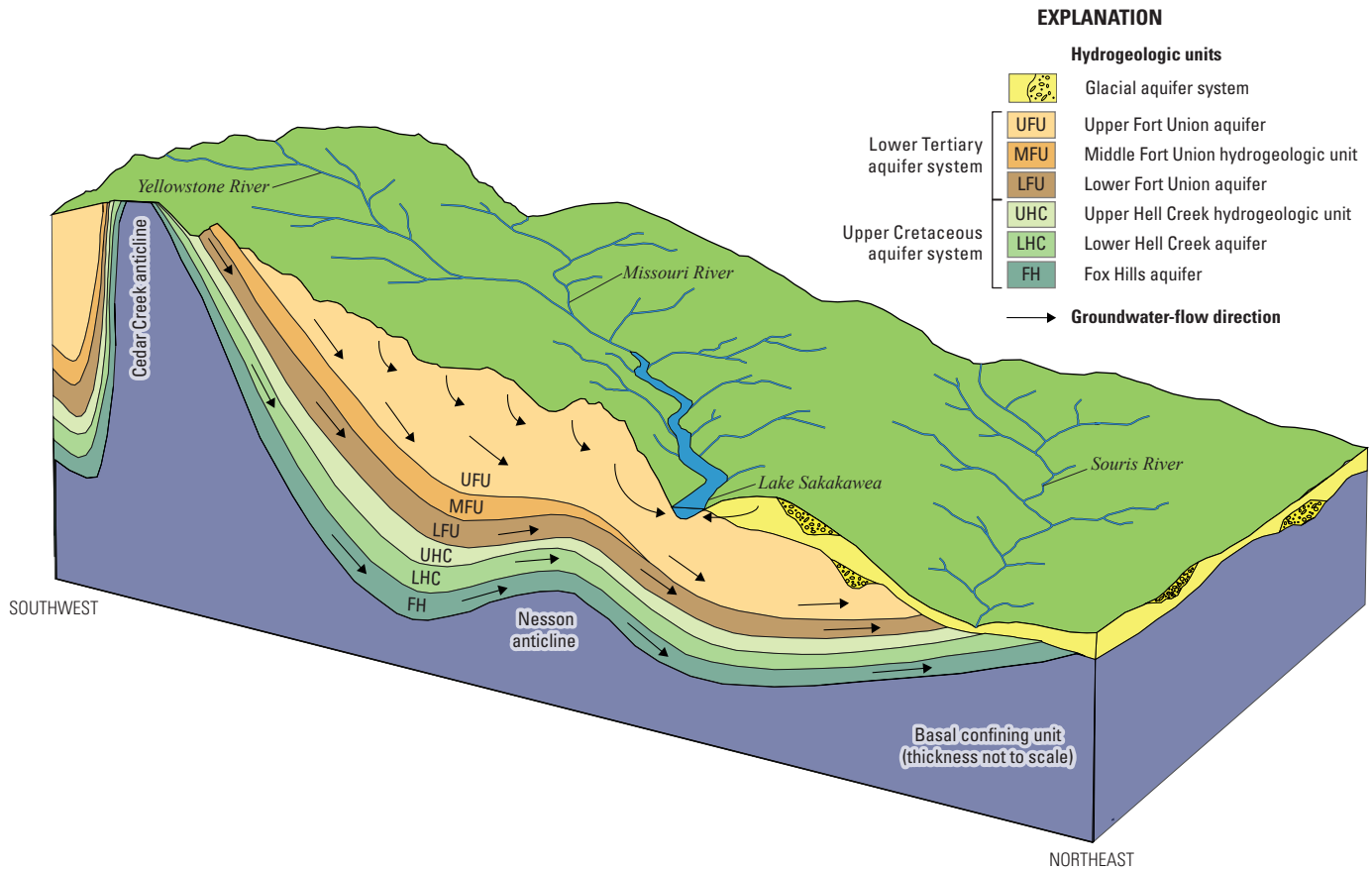

Figure 2. Conceptual block diagram of groundwater flow in the Williston Basin, as viewed from the southeast (from Long and others, 2014).

hydraulic gradient between the upper and lower Fort Union aquifers is downward; and near streams, this vertical hydraulic gradient is small and generally upward (fig. 2). Streams are the primary features where groundwater recharge and discharge exist (table 1). The potentiometric surface of the Upper Cretaceous aquifer system has less relief than the shallower aquifers (Long and others, 2014).

Groundwater levels have declined locally because of flowing artesian wells that were installed for domestic and livestock use; these wells flow continuously as a result of hydrostatic pressure (Montana Department of Natural Resources and Conservation, 2015; North Dakota State Water Commission, 2015). Fischer (2013) described 571 flowing artesian wells in North Dakota open to the Fox Hills and lower Hell Creek aquifers primarily near the Yellowstone, Little Missouri, and Knife Rivers (fig. 1). Collectively, these wells have a total flow rate of about 1.6 ft^3/s (Fischer, 2013). Near the Yellowstone River, flowing wells may have, in part, resulted in groundwater-level declines of about 1 foot per year since the 1970s in the Fox Hills and Hell Creek aquifers in this area (Smith and others, 2000; Fischer, 2013). Flowing artesian wells that discharge water from the Upper Cretaceous aquifer system might also allow leakage into the overlying lower Tertiary aquifer system because of inadequate sealing or corrosion of these wells (Fischer, 2013; Long and others, 2014); however, the exchange of water between aquifers through inadequate sealing or corrosion of well bores in the model area is beyond the scope of this study.

Methods Overview

This section provides a general description of the numerical methods that were used to simulate groundwater flow in the Williston Basin (fig. 1). An overview of MODFLOW–NWT, the U.S. Geological Survey's three-dimensional finite-difference groundwater model with the Newton-Rhapson solver, and its packages and the model calibration software, Parameter ESTimation (PEST), also are provided in this section.

The finite-difference model MODFLOW–2005 solves the groundwater-flow equation using linear and nonlinear numerical-solution methods (Harbaugh, 2005). MODFLOW–NWT is a Newton formulation variant of MODFLOW–2005 (Harbaugh, 2005), which is a numerical, three-dimensional, finite difference groundwater-flow model. The Newton formulation

extends the applicability of MODFLOW–2005, especially to those problems representing unconfined aquifers and surface-water/groundwater interaction (Niswonger and others, 2011).

MODFLOW–NWT (Niswonger and others, 2011) was used to simulate groundwater flow for the glacial, lower Tertiary, and Upper Cretaceous aquifer systems in the model area (fig. 1). MODFLOW–NWT uses several of the packages distributed with MODFLOW–2005. The MODFLOW–NWT packages that were incorporated into the model are documented in Niswonger and others (2011) and Harbaugh (2005) and included the Well (WEL), Drain (DRN), River (RIV), Recharge (RCH), and Upstream Weighting (UPW) Packages. Additional packages include an enhanced representation of groundwater and surface-water interactions using the Streamflow-Routing Package (SFR2) documented in Prudic and others (2004) and Niswonger and Prudic (2005) and the Multi-Node Well Package (MNW) (Halford and Hanson, 2002), which simulates groundwater interaction (injection, extraction, or exchange) among multiple aquifers in a single well.

The UPW Package is a new package that can be used in conjunction with the NWT solver in MODFLOW–NWT to provide a robust representation of dry (dewatered) cells in the model. The UPW Package smoothly reduces the conductance between a dry cell and an adjoining wetted cell to zero. This keeps a dry cell active and allows inflow to the cell from adjacent cells and from external sources while not allowing water to flow out of the cell (Niswonger and others, 2011). The MODFLOW–NWT WEL Package has the ability to smoothly reduce the pumping rate of a well in an unconfined cell as a function of the saturated thickness of the cell. The ability to reduce the pumping of a well prevents excess water from being removed from a cell as it becomes dewatered during a simulation.

Model calibration was completed by linking PEST (Doherty, 2010) software with MODFLOW–NWT (Niswonger and others, 2011). The PEST software is a model-independent calibration tool that applies statistical nonlinear parameter estimation techniques to optimize model parameters, such as aquifer storage properties, river conductance, hydraulic conductivity, and recharge. The PEST software systematically adjusts model input parameters based on the comparison between model-computed (simulated) variables and observed (measured or estimated) values, such as hydraulic head or stream base flow, until the best modeled fit to the observed data is mathematically determined.

Model Design and Construction

This section describes the spatial, vertical, and temporal model discretization, and simulated boundary conditions. This section also describes initial values for precipitation recharge that were adjusted during model calibration.

Spatial Discretization and Vertical Layering

The model grid consisted of square cells of uniform size that are about 1 mile (1,600 meters) on each side for each of the eight model layers (table 2). The map projection used for geospatial data management was USA Contiguous Lambert Conformal Conic. The model grid consisted of 468 columns (oriented north–south) and 456 rows (oriented east–west), with a total of about 657,000 active cells within the model area (fig. 1). The northwest corner of the model area was at latitude 50°50’52” N and longitude 108°48’5” W.

Vertically, the model consisted of eight layers: two layers represented the glacial aquifer system (layers 1 and 2), and six layers represented the underlying bedrock hydrogeologic units (layers 3–8, table 2). Where alluvium was present, it was lumped in with the uppermost hydrogeologic unit and included in the uppermost model layer in that area. Model layers were further subdivided into 12 hydraulic property zones (property zones) that correspond to the 8 hydrogeologic units but commonly occupy more than 1 model layer (fig. 3; table 2).

The glacial aquifer system was separated into two model layers, the upper part of the glacial aquifer system (layer 1) and the lower part of the glacial aquifer system (layer 2) (fig. 3), by multiplying the total thickness of the glacial aquifer system by one-half for all areas of the model. The thickness of the glacial aquifer system was estimated by Thamke and others (2014) for most of the model area. The thickness for the remaining part of the model area near the northern model boundary was estimated by the method used by Arihood (2009) with lithologic data from (1) the Groundwater Information Network for Manitoba and Saskatchewan (Groundwater Information Network, 2012a, b), (2) the Groundwater Information Center (Groundwater Information Center, 2013) for Montana, and (3) the North Dakota State Water Commission (North Dakota State Water Commission, 2013).

Glacial sand and gravel aquifers in the model area commonly are buried beneath till and other glacial or surficial deposits and typically are in preglacial valleys that exist on the buried bedrock surface (Kehew and Boettger, 1986; Cummings and others, 2012; Pugin and others, 2014). Locations of these valley-fill aquifers were available for North Dakota (North Dakota State Water Commission, 2010) but were not available for other areas of the model area; therefore, an estimated buried bedrock surface was used to estimate valley-fill aquifer locations for the extent of the glacial aquifer system (fig. 1). The buried bedrock surface from Thamke and others (2014) was used for the southern part of the glacial deposits, and the glacial-deposit thickness (previously described) was subtracted from the land surface generated from the National Elevation Dataset (NED) (U.S. Geological Survey, 2014a) for the remaining model area.

A process was developed to estimate the location and extent of unmapped buried glacial sand and gravel aquifers using available geographic information system (GIS) datasets and geoprocessing tools. This process was automated using a set of systematic scripts, written in the Python programming

Table 2. Relation of hydrogeologic units to numerical-model layers and hydraulic-property zones, description of zone properties, and mean simulated thickness.

[UGh, upper part of the glacial aquifer system-high; *K*, hydraulic conductivity; *S*, specific storage; *Sy*, specific yield; UGm, upper part of the glacial aquifer system-medium; UGl, upper part of the glacial aquifer system-low; UGu, upper part of the glacial aquifer system-unknown; LGh, lower part of the glacial aquifer system-high; LGl, lower part of the glacial aquifer system-low; UFU, upper Fort Union aquifer; MFU, middle Fort Union hydrogeologic unit; LFU, lower Fort Union aquifer; UHC, upper Hell Creek hydrogeologic unit; LHC, lower Hell Creek aquifer; FH, Fox Hills aquifer]

Aquifer system	Hydrogeologic unit name	Primary layer[a]	Property zone	Description	Model layers representing property zone	Mean simulated property zone thickness, in feet
Glacial	Upper part of the glacial aquifer system	1	UGh	High *K*, *S*, *Sy*: glaciofluvial, loess, and eolian deposits.	1	59.8
			UGm	Medium *K*, *S*, *Sy*: glaciolacustrine and glaciotectonic deposits.	1	63.7
			UGl	Low *K*, *S*, *Sy*: till.	1	77.25
			UGu	Unknown *K*, *S*, *Sy*: deposits of unknown origin.	1	80.2
	Lower part of glacial aquifer system	2	LGh	High *K*, *S*, *Sy*: sand and gravel outwash in bedrock valleys.	2	94.1
			LGl	Low *K*, *S*, *Sy*: till.	2	69.9
Lower Tertiary	Upper Fort Union aquifer	3	UFU	Variable *K*, *S*, *Sy*: sandstone, siltstone, shale, and coal originating from fluvial, deltaic, tidal, barrier-shoreface, and marine settings. Lithology includes complex interbedding of low-permeability layers of discontinuous lateral extent.[b]	2, 3	508.5
	Middle Fort Union hydrogeologic unit	4	MFU		2, 3, 4	160.5
	Lower Fort Union aquifer	5	LFU		2, 3, 4, 5	215.6
Upper Cretaceous	Upper Hell Creek hydrogeologic unit	6	UHC	Variable *K*, *S*, *Sy*: sandstone, siltstone, and shale.[b]	2, 3, 4, 5, 6	182.3
	Lower Hell Creek aquifer	7	LHC		2, 3, 4, 5, 6, 7	143.9
	Fox Hills aquifer	8	FH	Variable *K*, *S*, *Sy*: poorly-cemented to well-cemented sandstone, siltstone, and mudstone.[b]	8	155.3

[a]The hydrogeologic unit is represented primarily by this layer and secondarily by other layers because the property zones occupy more than one layer for bedrock units.

[b]Summarized from Thamke and others (2014) and Long and others (2014).

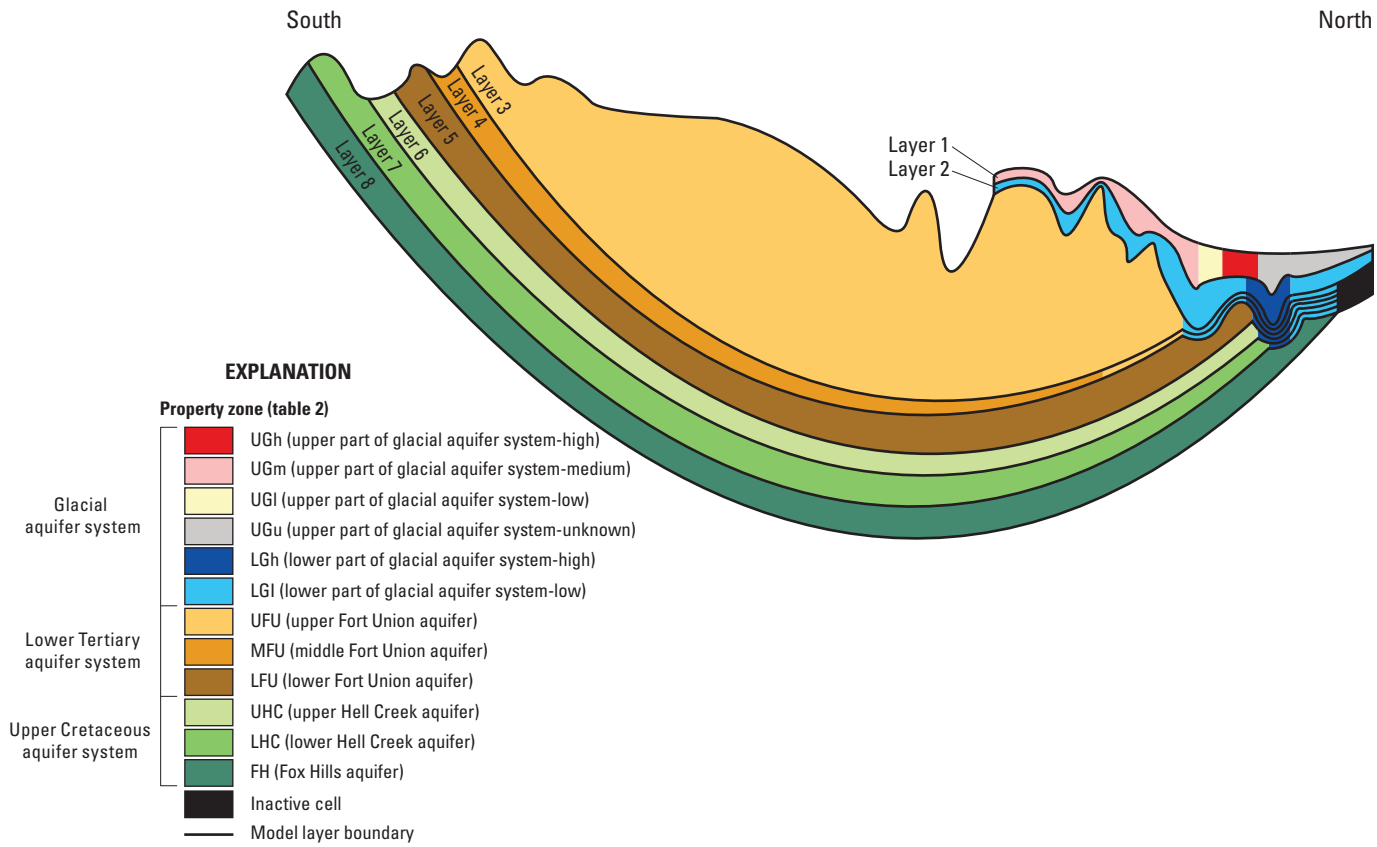

Figure 3. Example of the relation of aquifer systems and property zones to model layers, shown in vertical profile along a generalized south to north profile.

language (Rossum and Drake, 2011), and is hereafter referred to as the "valley-fill tool" (Davis and Long, 2018). For areas covered by glacial deposits, the valley-fill tool uses a digital elevation model (DEM) of the bedrock surface to create a potential subsurface flow network from which the extent of probable buried sand and gravel aquifers can be identified. The valley-fill tool was manually calibrated by adjusting various input parameters until the tool-generated aquifer extents matched those mapped for North Dakota as closely as possible. The tool-generated buried glacial aquifer extents for the entire model area then were used in the hydrogeologic framework for the glacial aquifer system.

A hydrogeologic framework developed by Thamke and others (2014) was used to construct the model layers that represented the six bedrock hydrogeologic units that compose the lower Tertiary and Upper Cretaceous aquifer systems in the model area (fig. 1). These bedrock units were separated into three layers for the lower Tertiary aquifer system, which includes the upper Fort Union aquifer (layer 3), the middle Fort Union hydrogeologic unit (layer 4), and the lower Fort Union aquifer (layer 5); and three layers for the Upper Cretaceous aquifer system, which includes the upper Hell Creek hydrogeologic unit (layer 6), the lower Hell Creek aquifer (layer 7), and the Fox Hills aquifer (layer 8) (fig. 3). Thamke and others (2014) constructed surface altitudes and hydrogeologic unit thicknesses based on existing publications and digital data. Data from Thamke and others (2014) were used directly in constructing the layer thicknesses and base altitudes for the bedrock hydrogeologic units represented by the model.

The outer horizontal extents of bedrock hydrogeologic units are buried beneath glacial deposits in subcrop areas north and east of the Missouri River (figs. 1 and 2); therefore, these bedrock hydrogeologic units are truncated horizontally (pinched) in the subsurface below glacial deposits. Additionally, the middle Fort Union hydrogeologic unit is pinched in the subsurface between the upper Fort Union aquifer and the lower Fort Union aquifer in the northeast part of the model area (fig. 2).

In a finite difference formulation of MODFLOW–NWT, model layers must extend throughout the vertical model area, even in areas where the corresponding hydrogeologic units do not exist. The cells in these areas cannot be inactive because this would place a vertical flow barrier between the overlying and underlying model layers; for example, in the northern part of the model area, the bedrock hydrogeologic units

subcrop below the glacial aquifer system where the intervening hydrogeologic units are not present; to simulate hydraulic connection between model layer 2 and the next underlying active layer, MODFLOW–NWT requires that the intervening layers are active. This problem was solved by setting model layers 3–7 to a minimum thickness of 0.5 foot (ft) where necessary and setting the hydraulic properties equal to those of the overlying layer (figs. 3 and 4). These areas are indicated in figures 4*C*–*G* where property zones LGh and LGl (table 2) exist in model layers 3–7. This approach allowed model layers 3–7 to effectively represent the lower part of the glacial aquifer system in areas where the bedrock hydrogeologic units are not beneath the glacial aquifer system. Additionally, model layer 4 was set to a minimum thickness of 0.5 ft where the middle Fort Union hydrogeologic unit is pinched between the upper and lower Fort Union aquifers in the central part of the model area (fig. 2). This area is indicated in figure 4*D* where property zone UFU (table 2) exists in model layer 4. In the southwest part of the model area, the upper Fort Union aquifer directly overlies the middle Fort Union hydrogeologic unit and is generally thin and unsaturated. Layer 4 in this area represents the upper and lower Fort Union aquifers to reduce the potential for simulated dry cells in the area and to keep the upper aquifer in the model.

Temporal Discretization

The model framework was used for two calibration periods and was created to represent different periods of groundwater development. The first model represents mean hydrological conditions for 1981–2005 and is executed in steady-state mode (Harbaugh, 2005), hereafter referred to as the “steady-state model,” and corresponds to the conceptual model developed by Long and others (2014). The second model represents mean hydrological conditions for 1981–2005 without groundwater withdrawal and temporally varying conditions for 1961–2005, hereafter referred to as the “transient model.” The transient model represents distinct blocks of time called “stress periods,” within which all hydrological stresses are constant, and model output applies to the end of each stress period. The transient model consisted of an initial simulation executed in steady-state mode representing the mean hydrological conditions for 1981–2005 without groundwater withdrawal, hereafter referred to as the “predevelopment period,” and was considered representative of steady-state conditions prior to 1961. The steady-state simulation without groundwater withdrawal was followed by a simulation executed in transient mode (Harbaugh, 2005) with four 5-year transient stress periods, representing the calendar years 1961–1965, 1966–1970, 1971–1975, 1976–1980 (stress periods 1–4), and 25 annual stress periods, representing the calendar years 1981–2005 (stress periods 5–29). The predevelopment period represents the period before 1960 when groundwater withdrawals were small (Long and others, 2014) and assumed negligible for purposes of numerical modeling. The steady-state model was calibrated to mean hydrological conditions for 1981–2005, and the transient model was calibrated to time-varying hydrological conditions for 1961–2005.

Hydraulic Properties

To allow for spatial and vertical differences in hydraulic properties within the model area, the model area was delineated into 12 property zones (table 2; figs. 3 and 4). Pilot points were used within each property zone (fig. 4) to allow a smooth spatial variation in horizontal and vertical hydraulic conductivity for the model area. Pilot points are discrete locations distributed throughout the model area that represent surrogate parameters from which horizontal and vertical hydraulic conductivity values are interpolated to the model grid using a Kriging process (Doherty and Hunt, 2010). Variogram models for each property zone were determined based on the distribution of hydraulic conductivity provided by Thamke and others (2014). Pilot points for the bedrock aquifers were co-located with resistivity and lithology wells used by Thamke and others (2014) to estimate aquifer hydraulic conductivity (fig. 4).

The initial values for the pilot points were set to the estimated values determined by Thamke and others (2014; table 3). Supplemental pilot points for the bedrock aquifers, layers 3–8, were added in areas where the pilot point separation was greater than the mean pilot point separation for that layer, and the initial values were set to the interpolated hydraulic property grid provided by Thamke and others (2014). Pilot points for the glacial aquifers were about 50 miles (mi) apart for each property zone (figs. 4*A*, *B*), and the initial values were based on literature values. The final horizontal and vertical hydraulic conductivity values and distributions for the model were determined through calibration of the steady-state model, described further in the “Model Calibration” section, and are listed in the parameter estimation files in the model archive (Davis and Long, 2018).

Storage properties, including specific storage and specific yield for the aquifers represented by the transient model, were set to uniform values for each property zone. Initial estimates were based on literature values (table 4) and were adjusted during transient model calibration.

All the aquifers represented by the model are both confined and unconfined within the model area except the upper part of the glacial aquifer system, which is unconfined throughout the model area. As a requirement of MODFLOW–NWT, model layers are simulated as either convertible or confined. Convertible layers are allowed to convert between unconfined and confined during a simulation, whereas confined layers do not change throughout the simulation. All layers except layers 2 and 8 were simulated as convertible for the steady-state model to provide stability to the numerical solutions calculated by MODFLOW–NWT; all layers were simulated as convertible for the transient model.

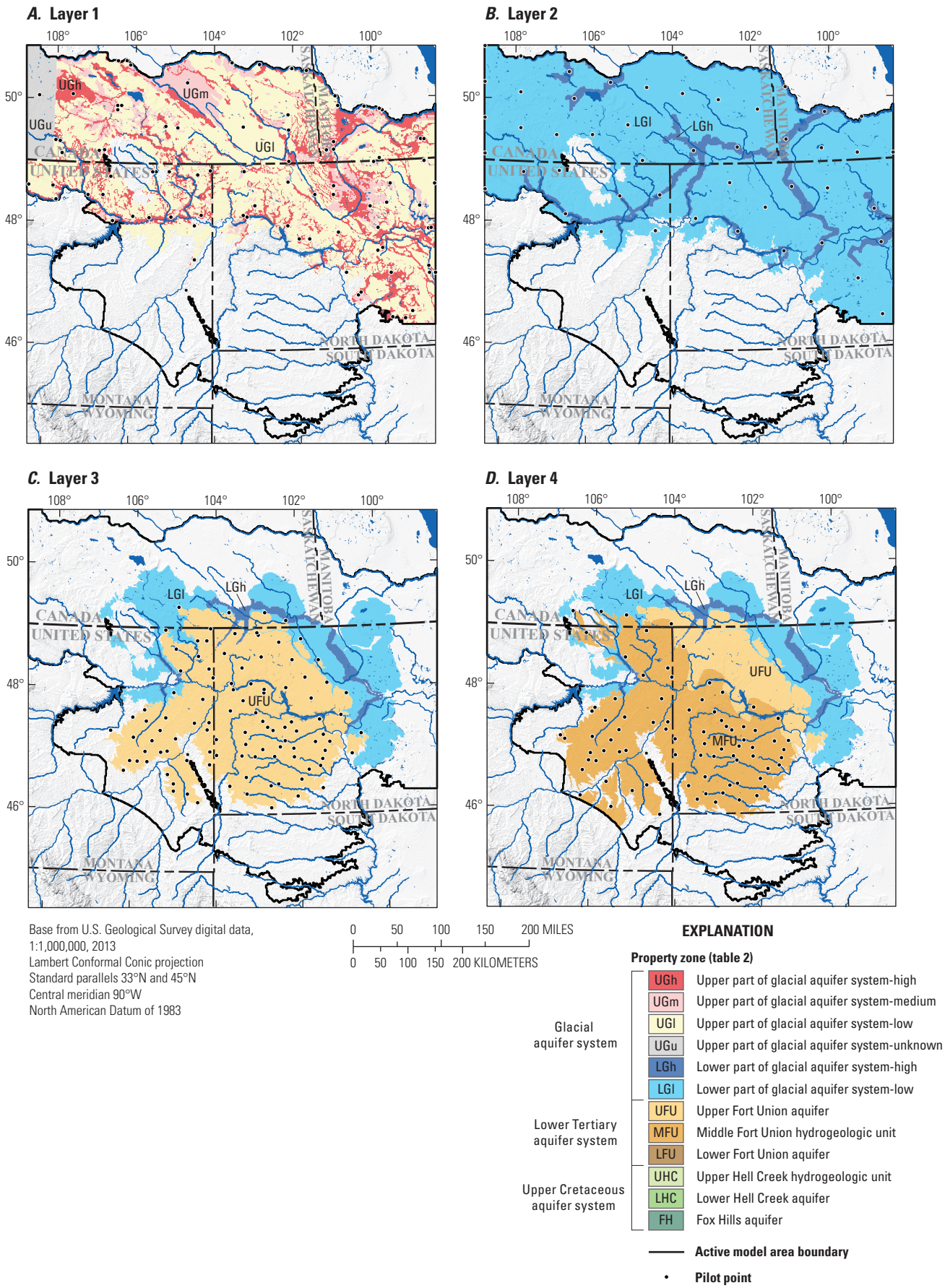

Figure 4. Property zones and pilot point locations for each model layer.

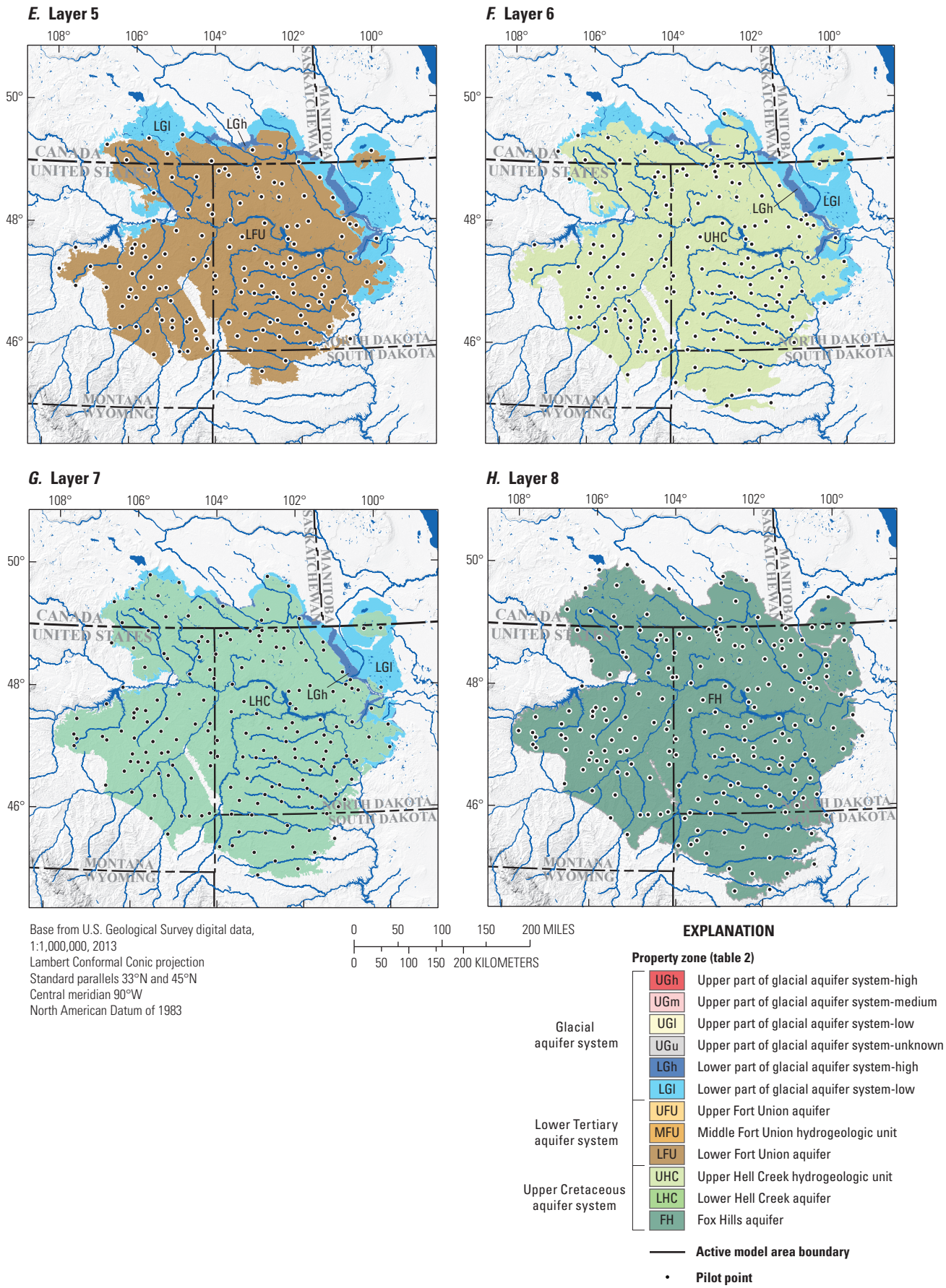

Figure 4. Property zones and pilot point locations for each model layer.—Continued

Table 3. Summary statistics of hydraulic properties from Thamke and others (2014).

[ft/d, foot per day; *n*, number of wells; UGh, upper part of the glacial aquifer system-high; UGm, upper part of the glacial aquifer system-medium; UGl, upper part of the glacial aquifer system-low; UGu, upper part of the glacial aquifer system-unknown; LGh, lower part of the glacial aquifer system-high; LGl, lower part of the glacial aquifer system-low; UFU, upper Fort Union aquifer; MFU, middle Fort Union hydrogeologic unit; LFU, lower Fort Union aquifer; UHC, upper Hell Creek hydrogeologic unit; LHC, lower Hell Creek aquifer; FH, Fox Hills aquifer]

Property zone (table 2)	Horizontal hydraulic conductivity				
	Minimum (ft/d)	Maximum (ft/d)	Median (ft/d)	Standard deviation	*n*
UGh, UGm, UGl, UGu, LGh, LGl	0.01	25.50	2.52	5.23	82
UFU	0.14	10.14	1.56	1.72	76
MFU	0.06	8.14	0.80	1.17	72
LFU	0.14	5.66	0.80	0.84	113
UHC	0.10	5.70	0.50	0.72	152
LHC	0.10	1.81	0.80	0.31	146
FH	0.06	0.90	0.44	0.19	168

Table 4. Previously published aquifer storage properties.

[UGh, upper part of the glacial aquifer system-high; UGm, upper part of the glacial aquifer system-medium; UGl, upper part of the glacial aquifer system-low; UGu, upper part of the glacial aquifer system-unknown; --, not available; LGh, lower part of the glacial aquifer system-high; LGl, lower part of the glacial aquifer system-low; UFU, upper Fort Union aquifer; MFU, middle Fort Union hydrogeologic unit; LFU, lower Fort Union aquifer; UHC, upper Hell Creek hydrogeologic unit; LHC, lower Hell Creek aquifer; FH, Fox Hills aquifer]

Property zone (table 2)	Specific storage	Storage coefficient	Specific yield	Porosity (*n*)	Source
UGh, UGm, UGl, UGu (undifferentiated)	--	0.0002–0.0006	0.20	--	Armstrong (1971), Croft (1985)
LGh, LGl (undifferentiated)	--	0.0001–0.14	0.15	--	Klausing (1974, 1979)
UFU	--	0.0002–0.007	--	0.27–0.37	Croft (1978, 1985), Klausing (1979)
MFU	--	--	--	--	
LFU	1.0×10^{-6}	0.0001–0.0008	--	0.26–0.37	Anna (1981), Croft (1973, 1978, 1985)
UHC	--	--	--	--	
LHC	--	--	--	--	
FH	--	0.0001–0.0004	0.048–0.38	--	Bader and Radig (1991), McWhorter (1984), Robson (1987)
UFU, MFU, LFU (undifferentiated)	--	0.00001–0.004	--	--	Bader and Radig (1991), Stoner (1981)
LFU, UHC (undifferentiated)	--	--	--	0.31–0.36	Croft (1978)
UHC, LHC, FH (undifferentiated)	3.52×10^{-7}–3.17×10^{-4}	2.9×10^{-6}–4.2×10^{-4}	--	0.29–0.40	Anna (1981), Croft (1973, 1978, 1985), Croft and Wesolowski (1970), Fischer (2013)

Boundary Conditions

Boundary conditions are specified in the model to allow simulated groundwater flux into or out of the groundwater system or to disallow this flux at the lateral and lower boundaries of the model area (no-flow boundaries). Boundary-condition categories consist of (1) lateral and lower boundaries, (2) precipitation recharge, (3) surface-water features, and (4) groundwater withdrawal.

Lateral and Lower Boundaries

The lateral and lower boundaries are at the horizontal and vertical periphery of the model area and were simulated as no-flow boundaries, specified-head boundaries, and stream boundaries (fig. 5). No-flow boundaries, used at the lateral extents of bedrock aquifers and the base of the model, do not allow horizontal flux into or out of the model. Specified-head boundaries are assigned a hydraulic head that remains constant throughout the simulation, and flux into or out of the model is determined by the hydraulic gradient between the simulated hydraulic head and the specified-head boundary. Specified-head cells were simulated using the Time-Variant Specified-Head Package (CHD) even though the specified hydraulic head values were invariant in the simulation (Harbaugh and others, 2000). Specified-head boundaries were assigned to model layers 1 and 2 along the eastern model edge and layer 2 along the western model edge to represent horizontal flux into and out of the model (fig. 5). Specified-head boundaries were assigned to layers 5–8 at the model edge about 10 mi southwest of the Miles City Arch to represent inflow from the Powder River Basin (fig. 5).

Where applicable, values for specified-head cells were assigned based on published potentiometric surfaces (Thamke and others, 2014). In general, published values of specified-head applied to layers 5–8 southwest of the Miles City Arch (fig. 5). Values for specified-head cells for layers 5 and 6 were assigned based on the potentiometric surface for the lower Fort Union aquifer (Thamke and others, 2014). Values for specified-head cells for layers 7 and 8 were assigned based on the potentiometric surface for the Fox Hills aquifer (Thamke and others, 2014). Potentiometric surfaces were not available for the glacial aquifer system represented by layers 1 and 2; therefore, values for specified-head cells for layer 1 along the eastern model boundary were assigned to the midpoint altitude of the cell based on the cell thickness, and values for specified-head cells for layer 2 along the western and eastern model boundary were assigned to the top of the layer.

The northern model boundary corresponds to the South Saskatchewan, Qu'Appelle, and Assiniboine Rivers and was simulated with the RIV Package (Harbaugh, 2005) to allow groundwater flux exchange with the river, as described further in the section "Surface-Water Features;" underlying layers had a no-flow boundary at the outer edge. Near the western edge of the model, most of the glacial deposits south of the Milk River (fig. 1) were not included in the model, and the Milk River was used as a model boundary (figs. 1 and 5) simulated using the Streamflow-Routing Package (SFR2) (Niswonger and Prudic, 2005). The underlying layers had a no-flow boundary at the outer edge.

Precipitation Recharge

Recharge to the groundwater system that results from deep percolation of precipitation and water used for irrigation that exceeds evapotranspiration (irrigation recharge) was represented with the RCH Package (Harbaugh, 2005). Annual precipitation recharge for 1981–2011 was estimated by Long and others (2014) using the Soil-Water-Balance (SWB) model (Westenbroek and others, 2010) and is hereafter referred to as "SWB-estimated recharge." Recharge was calculated by subtracting evapotranspiration from precipitation using the SWB model; therefore, evapotranspiration was not explicitly simulated in the MODFLOW model. The SWB-estimated recharge distribution was available at a 0.621 mi (1-kilometer) spatial resolution but had a different map projection than that used for the MODFLOW model (1,600-m resolution). The resolution of the recharge estimated from the SWB model was converted with GIS geoprocessing tools to the resolution of the MODFLOW model by accounting for differences in spatial resolution and map projections. Annual SWB-estimated recharge ranged from 0.00 to 0.96 in/yr (0.002 and 11.0 percent of precipitation for 1988 and 2009, respectively) and had a 30-year mean of 0.27 in/yr (1.5 percent of precipitation) for 1981–2011 (Long and others, 2014).

The mean annual recharge distribution for the steady-state model was determined based on SWB-estimated recharge for the model area (fig. 5) (Long and others, 2014), and the annual recharge distributions for 1981–2005 were used in the transient model and corresponded to stress periods 5–29. Long and others (2014) used two different methods to estimate soil properties for two areas: one that was covered by glacial deposits (fig. 1) and another that was not covered by these deposits. Two corresponding recharge zones were delineated for the groundwater-flow model to adjust for possible inconsistencies in the recharge estimates between these two areas, and a scalar multiplier was applied to each of the two zones. These two scalar multipliers were estimated during calibration of the steady-state model, and the estimated values then were applied to all stress periods of the transient model without further calibration.

Spatially variable recharge estimates were not available for 1961–1980; therefore, temporal recharge multipliers were calculated for stress periods 1–4 of the transient model and applied to the steady-state recharge distribution to produce spatially varied 5-year recharge estimates for 1961–1980. Recharge multipliers for stress periods 1–4 of the transient model were calculated by dividing the 5-year mean precipitation for 1961–1965, 1966–1970, 1971–1975, and 1976–1980 by the mean precipitation for 1981–2005 using precipitation records from a long-term National Oceanic and Atmospheric Administration (NOAA) climate station at Williston Sloulin

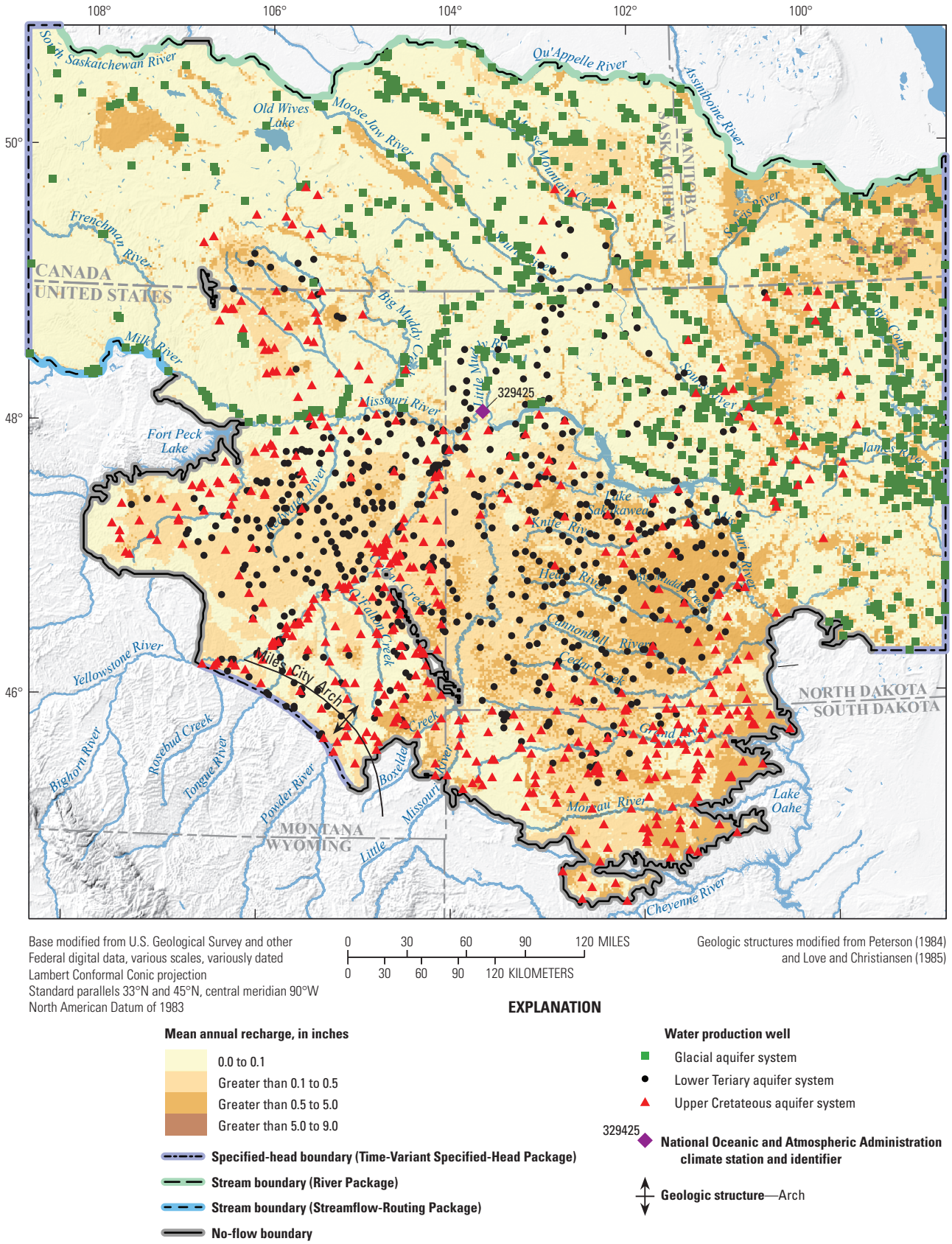

Figure 5. Active-extent boundaries for the steady-state and transient models, and recharge and pumping wells for the steady-state model.

Field International Airport, North Dakota (station 329425; fig. 5) (National Oceanic and Atmospheric Administration, 2014). Recharge for stress periods 1–4 was calculated by multiplying the calculated 5-year recharge multipliers by the mean annual recharge distribution from the steady-state model. The calculated temporal recharge multipliers for stress periods 1, 2, 3, and 4 were 1.08, 0.88, 1.09, and 0.83, respectively.

Surface-Water Features

Streams in the model area were represented by the RIV, DRN, and SFR2 Packages in the model (fig. 6). Stream networks used to develop the RIV, DRN, and SFR2 Packages used in the model are from the National Hydrography Dataset (NHDPlus v2) (McKay and others, 2012) for the United States and from the National Hydro Network for Canada (Natural Resources Canada, 2012). For the United States, groundwater interaction with streams was simulated using the SFR2 Package (Niswonger and Prudic, 2005) (fig. 6), which requires streamflow-routing data. The RIV and DRN Packages (Harbaugh, 2005) were used to represent streams in Canada (fig. 6) because routing data were not available for these streams. The flux rate between the streams and the groundwater (or the difference of stream infiltration and groundwater discharge to streams), hereafter referred to as "stream flux," is simulated by Darcy's Law based on the difference between the stream stage and groundwater level and streambed hydraulic conductivity, length, thickness, and width. The spatial distribution of RIV, DRN, and SFR2 Packages was identical for the steady-state and transient models.

Streambed hydraulic conductivity, in addition to the river geometry, is a direct input for the SFR2 Package, whereas streambed conductance is needed for the RIV and DRN Packages. The hydraulic conductance between the streambed and aquifer (streambed conductance) is defined as hydraulic conductivity of the streambed material multiplied by the cross-sectional area of the stream reach divided by the streambed thickness (McDonald and Harbaugh, 1988). The streambed conductance for the RIV and DRN Packages was calculated on a cellular basis by multiplying the streambed hydraulic conductivity by the width and length of the stream in the cell divided by the thickness of the streambed material.

The SFR2 Package, used to represent streams in the United States (fig. 6), simulates the routing of water through the stream network and calculates the stream stage based on the accumulated stream flux upstream from a stream cell in addition to external inflows to and outflows from the cell. External inflows could include precipitation on the stream and accumulated land-surface runoff to the stream. External outflows could include evapotranspiration or specified diversion from the stream. For this model, stream stage and accumulated stream flux calculated by the SFR2 Package represents values associated with stream base flow because only the accumulated stream flux was considered. Although the SFR2 Package had the ability to simulate total accumulated streamflow, the package inputs were limited to those necessary to calculate accumulated base flow for streams in the model area. The stream stage and accumulated stream flux simulated by the SFR2 Package were calculated by representing streams as wide, rectangular shaped channels. Streams simulated by the SFR2 Package were assigned a uniform Manning's roughness coefficient of 0.037, which is representative of stable channels and flood plains with cobble bed material (Arcement and Schneider, 1989).

Input for the SFR2 Package, including routing information, stream geometry, and altitudes for each modeled stream, was developed from the GIS information in NHDPlus v2 (McKay and others, 2012) using an automated Python program. The general approach for developing the SFR2 Package and description of the Python program is outlined in Leaf and others (2015). Streams of a second order or higher as identified by the NHDPlus v2 were used in the analysis. A uniform streambed thickness of 1 ft was used for streams represented by the SFR2 Package. The SFR2 Package requires stream input at two scales, reaches and segments. Reaches represent sections of streams that allow stream flux to be calculated at the scale of a single model cell. Segments are groups of one or more sequentially numbered reaches from a single stream that contain required streamflow routing information. Streamflow routing information for segments may include segment inflow rates (for segments at the model boundary to where base flow would have been routed from an upstream segment) and the segment number of the next downstream segment to which accumulated stream flux is routed. Other required segment information includes upstream segment width, downstream segment width, and the channel roughness coefficient.

The SFR2 Package allows multiple stream reaches to exist in a single model cell; however, cells with multiple stream reaches may not accurately account for the stream flux within that cell, resulting in large discrepancies in the overall simulated model budget. A representative streambed hydraulic conductivity was calculated for cells with multiple stream reaches and was assigned to the stream reach with the lowest altitude in the cell. The representative streambed hydraulic conductivity was determined by calculating the sum of the individual streambed conductances in a cell and back-calculating the representative streambed hydraulic conductivity based on the geometry of the stream with the lowest altitude. The remaining stream reaches were assigned a streambed hydraulic conductivity of 0 feet per day (ft/d). This method allowed the streamflow-routing network to have full connectivity, stream flux to exist in only one stream reach within each cell, and stream flux to be accurately represented in the overall simulated model budget.

Streams that cross the model boundary and received upstream inflow were assigned an inflow rate based on the estimated base-flow values at streamgages within the model area for each stress period. Daily base flow for 1961–2005 was estimated using the PART hydrograph separation method (Rutledge, 1998) for streamgages described by Long and others (2014). Streams typically crossed the model boundary between streamgages; therefore, inflow was adjusted based on the

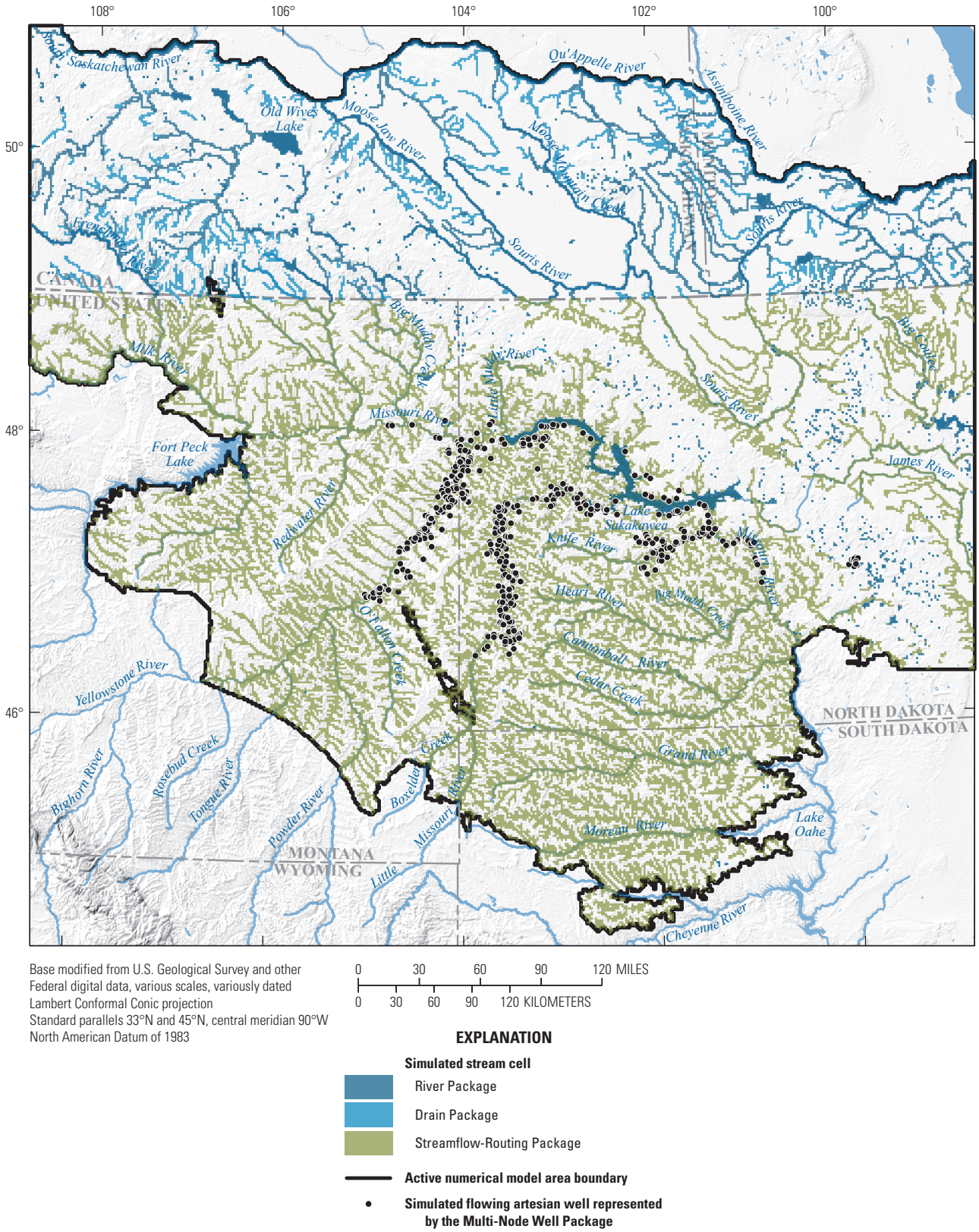

Figure 6. Simulated stream cells used in the River, Drain, and Streamflow-Routing Packages, and simulated flowing wells represented by the Multi-Node Well Package.

percentage of the length of the main stem stream within the model upstream from a streamgage used to estimate base flow.

In the Canadian part of the model area (fig. 1), the RIV and DRN Packages were used to simulate stream flux for perennial and ephemeral streams, respectively (fig. 6). Perennial and ephemeral streams in Canada were determined from GIS information contained in the National Hydro Network (NHN) (Natural Resources Canada, 2012). Named streams from the NHN were assumed to represent perennial streams, and streams with a Horton Order of greater than two generally were used to represent ephemeral streams. This method produced a stream network in Canada that visually matched the distribution of simulated streams in the United States indicated by NHDPlus v2 (McKay and others, 2012).

The RIV and DRN Packages (Harbaugh, 2005) simulated stream flux like the SFR2 Package simulated stream flux, except the stream stage was specified for the RIV Package rather than simulated by streamflow-routing as in the SFR2 Package. The stream flux simulated by the RIV and DRN Packages depends on the groundwater level in the cell and the water level altitude (stream stage) in the river for the RIV package and the streambed altitude for DRN Package. The RIV Package allows stream flux into and out of the groundwater system, whereas the DRN Package only allows stream flux out of the groundwater system and only where the groundwater level in the cell is higher than the altitude of the streambed (drain altitude). The stream stage for each model cell represented by the RIV Package (RIV cells) was determined by finding the most downstream point of a stream within a cell and extracting the altitude of that point from the NED (U.S. Geological Survey, 2014a). In some RIV cells, this method produced a stream stage that was below the bottom of the model. For these RIV cells, the stream stage was assumed to be 0.5 ft above the bottom of the model, and the streambed altitude was set equal to the bottom of the model. The streambed altitude for the remaining RIV cells was set equal to 1 ft below the stream stage. This method produced some RIV cells with a streambed altitude below the bottom of the model. For these RIV cells, the streambed altitude was set equal to the bottom of the model. This procedure produced RIV cells with streambed altitudes that ranged from 0.02 to 1 ft below the stream stage. The drain altitude for each model cell represented by the DRN Package (DRN cells) was determined by finding the most downstream point of a stream within a cell and extracting the altitude of that point from the NED (U.S. Geological Survey, 2014a). Properties for the RIV and DRN Packages were simulated as constants for the steady-state and transient models.

Groundwater interaction with wetlands, lakes, and Lake Sakakawea, hereafter referred to as “lake flux,” was simulated using the RIV Package (fig. 6). Using the RIV Package for lakes allowed for simulation of inflow and outflow of groundwater based on the lake stage and groundwater level in the cell. The NHDPlus v2 (McKay and others, 2012) contains the locations wetlands and lakes. The RIV Package was applied to cells that contain wetlands or lakes in at least 12 percent of the cell area and is suitable for this application because, unlike the SFR2 Package, the RIV Package cells operate independently and do not simulate the routing of water. The RIV Package cells were assigned to the area of Lake Sakakawea, and SFR2 cells were set to route streamflow through the lake area without groundwater interaction. The riverbed hydraulic conductivity was set to 0 ft/d for SFR2 cells underlying Lake Sakakawea. Setting the riverbed hydraulic conductivity to 0 ft/d for SFR2 cells underlying Lake Sakakawea allowed full connectivity of the streamflow-routing network and allows Lake Sakakawea to be simulated by the same method as the other lakes. For wetlands and lakes, the lake stage in each cell was assumed to be equal to the land surface from the NED (Gesch, 2007; Gesch and others, 2002). The lake or wetland bottom was specified for the RIV Package and was assumed to be 2 ft below the lake stage. The stage for Lake Sakakawea was assigned based on the mean recorded stage for each stress period (U.S. Army Corps of Engineers, 2013). The mean stage for each stress period was calculated based on the reported monthly mean daily midnight altitude for 1967–2005.

Groundwater Withdrawal

Groundwater withdrawals for the numerical model were simulated using the WEL and MNW Packages. The WEL Package was used to simulate specified withdrawals for the steady-state and transient models at pumping wells (fig. 5), and the MNW Package was used to simulate flowing artesian wells in the transient model (fig. 6). Groundwater withdrawals were estimated by Long and others (2014) for the control volume (fig. 1). The estimates were provided for each United States county or Canadian census division within the model area for each hydrogeologic unit for 5-year periods during 1981–2005 and represented combined rates from public and nonpublic supplies. Groundwater withdrawals were estimated for the glacial aquifer system outside of the control volume by extrapolating water use from the wells within the control volume to wells outside of the control volume. Wells in the area not estimated by Long and others (2014) were assigned withdrawal rates equivalent to the nearest well in the glacial area estimated by Long and others (2014).

Withdrawal information for the model area was available at the county level and not for individual wells; therefore, for nonpublic supplies, well locations in the model were selected from those provided by the U.S. Geological Survey (2014b) for the United States and by the Groundwater Information Network (2012a) for Canada. Public-supply well locations were selected from those provided by the Montana Department of Environmental Quality (2012), North Dakota Information Technology Department (2012), and South Dakota Department of Environment and Natural Resources (2013) for the United States and by the Groundwater Information Network (2012a) for Canada. Public-supply groundwater use was the second largest groundwater withdrawal category in the model area between 1981 and 2005 (Long and others,

2014), and public-supply withdrawal locations were available; therefore, public-supply estimates were subtracted from total water-use estimates to obtain nonpublic-supply estimates. Public-supply withdrawal estimates were obtained from Solley and others (1988, 1993, 1998), Hutson and others (2004), Kenny and others (2009), and Saskatchewan Water Security Agency (2012).

Where data were available, wells were assigned to specific model layers according to aquifer completion information. For all other wells, a model layer was assigned by assuming that each well is open to the aquifer that holds the bottom of the screened interval or the bottom of the well. A subset of these wells for each model layer was selected for the steady-state model using methods described by Scott (1990). The selection method provides a random subset of geospatially distributed points using various user-defined selection mechanisms (Scott, 1990). The selection method was completed using trial and error to obtain a spatial distribution of wells that visually represented the distribution of wells from U.S. Geological Survey (2014b) and Groundwater Information Network (2012a). The selection method was allowed to select as many as 1,200 wells per model layer, where available, based on a user-defined number of subareas distributed throughout each layer to reach this representation.

Mean pumping rates for 1981–2005 for each well were specified in the steady-state model. The water-use estimates by county and census division for nonpublic supply wells (Long and others, 2014) were distributed uniformly to the simulated wells; therefore, the pumping rate from each well increases by reducing the total number of simulated wells. In some areas of the model, large drawdowns of hydraulic head were present as a result of sparsely spaced wells with unrealistic withdrawal rates; in these areas, all well locations from the original databases were used as pumping wells in the model to prevent excessive withdrawal from individual wells. All well locations from the database previously described were included for the purpose of spatially distributing the pumping rates within the transient model to reduce numerical instability potentially created by unrealistic pumping values. Withdrawal from all available public supplies was simulated in the steady-state and transient models.

Numerous flowing artesian wells were constructed between 1960 and 1990 near the Yellowstone, Little Missouri, and Knife Rivers (fig. 6) (Fischer, 2013). Long and others (2014) did not estimate discharge from flowing wells separately from total groundwater withdrawals, and, for this reason, the discharge from flowing wells was not simulated separately in the steady-state model. Flowing wells were included in the distribution of specified withdrawals in the WEL Package for the steady-state model; however, flowing wells were simulated in layers 7 and 8 for the transient model using the MNW Package (Halford and Hanson, 2002). The locations of 571 flowing wells simulated in the transient model (fig. 6) were identified by Wanek (2009).

The well skin, which is the alteration of the hydraulic conductivity near a well screen because of the construction and operation of a well (Wilson and Moore, 1998), is a unitless parameter in the MNW Package that was used to calibrate the transient model. The value of skin for a model cell depends on the hydraulic conductivity of the model cell, the hydraulic conductivity of the skin, the length of the borehole, and the thickness of the skin (Konikow and others, 2009). A negative well-skin parameter indicates that the hydraulic conductivity of the well skin is larger than the hydraulic conductivity of the media composing the finite-difference cell that holds the well. Flowing wells were assigned to two well skin parameter groups. Flowing wells with estimated discharge data were assigned to well-skin group 1, and flowing wells with no available discharge data were assigned to well-skin group 2. Values of well skin for each group were adjusted during the calibration of the transient model.

The MODFLOW–NWT options for the WEL Package were selected to automatically reduce the pumping rate from a well when the saturated thickness of the cell that holds the well decreases to less than 20 percent of the cell thickness. When the saturated thickness of a cell that holds a well reduces to less than 20 percent of the cell thickness, the reduction in pumping is linearly proportional to the decrease in saturated thickness (Niswonger and others, 2011). The original specified pumping rate resumes when the saturated thickness exceeds this threshold. The purpose of this reduction is to simulate the inability of a well to continue to produce water when the aquifer has become dewatered. These simulated changes in pumping rates happen during solver iterations as the saturated thickness changes, which adds nonlinearity to the groundwater-flow equations being solved and leads to numerical instability. Because these pumping reductions caused solver instability, the pumping rates for these wells were set to zero for the steady-state and transient models. Well withdrawals were reduced by 32 percent for the steady-state model and between 46 and 54 percent for the transient model. Although these reductions to pumping seem substantial, when compared to the other water budget components, they are only a small part of the overall water budget.

Model Calibration

Model calibration is the process of estimating model parameters to minimize the differences, or residuals, between observed (measured or estimated) data and simulated values. The observed data that are used in model calibration are hereafter referred to as calibration targets. The PEST software (Doherty, 2010) was used for model calibration. The PEST process identifies an optimum set of parameters that minimizes the sum of the squared and weighted residuals (hereafter referred to as the objective-function value), where constraints can be placed on the ranges of parameter values and the relations among different parameters (Doherty, 2010). Guidelines by Doherty and Hunt (2010) for using PEST to calibrate groundwater models were used for the parameter estimation

approach in this study. Hydraulic properties estimated by PEST included horizontal hydraulic conductivity, vertical hydraulic conductivity, aquifer storage, and streambed hydraulic conductivity. Groundwater recharge also was estimated using PEST.

PEST implements the Gauss-Levenberg-Marquardt algorithm (Doherty, 2010, 2014; Doherty and Hunt, 2010) and the singular-value decomposition (SVD)-based parameter estimation methodology (Tonkin and Doherty, 2005). The Gauss-Levenberg-Marquardt algorithm is a gradient-based search method that adjusts parameters by attempting to minimize the sum of the squared and weighted residuals.

PEST's implementation of Tikhonov regularization and use of pilot points for estimation of spatial hydraulic properties allow for a large number of parameters to be optimized and estimated simultaneously. Regularization is the name given to a broad class of mathematical techniques that can be used to bring numerical stability to an otherwise overparameterized inverse problem through the introduction of an appropriate smoothness or other constraint on parameter values (Tikhonov 1963a, 1963b; Barbosa and Silva, 1994). Using regularization in conjunction with pilot points is a benefit because it allows many more parameters to be estimated compared to the number of observations used to calibrate against (Doherty, 2003). The method of pilot points (Doherty, 2003), in which hydraulic conductivity is estimated for a set of point locations within the model area, was used to estimate vertical and horizontal hydraulic conductivity in the model area. The method of pilot points was used to interpolate a smooth hydraulic-conductivity field and apply the resulting spatially variable distribution of hydraulic conductivity to the model grid.

The first step in model calibration was the construction of a steady-state model calibrated to mean conditions for 1981–2005. Parameters optimized during calibration of the steady-state model are grouped into four categories consisting of horizontal hydraulic conductivity, vertical hydraulic conductivity, streambed hydraulic conductivity (SFR2 Package, RIV Package, and DRN Package), and recharge (RCH Package). These parameters were fixed at the values estimated from the steady-state model during calibration of the transient model. Additional parameters of specific-storage, specific-yield, and well skin (MNW Package) values were adjusted during the transient calibration (table 5). All calibration targets and settings, including observation weights, parameter bounds, and regularization constraints, are available in the parameter estimation files in the model archive (Davis and Long, 2018).

Calibration Targets

Calibration targets are observed values (measured or estimated) from which model simulated values are compared against, and generally consist of measured groundwater levels, estimated exchange rates between surface water and groundwater, and measured discharge from flowing wells. The steady-state calibration targets consisted of (1) measured hydraulic head, (2) estimated hydraulic head differences between model layers, (3) estimated stream infiltration, and (4) estimated groundwater discharge to streams. Calibration targets for the transient model consisted of temporally distributed values used for steady-state calibration; however; hydraulic head differences were not used as calibration targets

Table 5. Summary of parameters estimated during model calibration.

[ft/d, foot per day; --, not applicable; ft, foot]

Parameter category	MODFLOW package	Model that parameter was applied to	Number of parameters applied in model	Number of independent values estimated	Units	Comments
Horizontal hydraulic conductivity	Upstream Weighting	Steady-state	1,025	1,025	ft/d	Pilot points
Vertical hydraulic conductivity	Upstream Weighting	Steady-state	1,025	1,025	ft/d	Pilot points
Streambed hydraulic conductivity	Streamflow Routing	Steady-state	92	92	ft/d	--
Streambed hydraulic conductivity	River	Steady-state	59	12	ft/d	Tied parameters
Drain hydraulic conductivity	Drain	Steady-state	24	0	ft/d	Tied parameters
Recharge	Recharge	Steady-state	2	2	Dimensionless	Recharge multipliers applied to previous estimates
Well skin	Multi-Node Well	Transient	2	2	Dimensionless	Proportional to the hydraulic conductivity of the well skin
Specific storage	Upstream Weighting	Transient	13	13	per ft	Zones
Specific yield	Upstream Weighting	Transient	13	13	Dimensionless	Zones

in the transient model. Additionally, groundwater discharge from flowing wells was used as a calibration target for the transient model. Calibration target information used for model calibration is available in appendix 1.

Groundwater Levels

Calibration targets for groundwater levels for bedrock aquifers were developed from table 3–1 in Thamke and others (2014), a dataset of groundwater levels assembled from State and Federal agencies. From this dataset, Thamke and others (2014) selected a subset of wells with high-quality measurements for estimating potentiometric surfaces for the upper Fort Union and lower Fort Union aquifers and the Upper Cretaceous aquifer system. All water levels from this dataset, including those not used in creating potentiometric surfaces, were used as groundwater-level calibration targets and assigned weights as described in appendix 2. Groundwater-level data from the glacial aquifer system were obtained from the U.S. Geological Survey (2014b), Saskatchewan Water Security Agency (2014), and Groundwater Information Network (2012a, b) for use as calibration targets.

Groundwater-level measurements from 2,735 wells were used for calibration targets (layers 1 and 2 in appendix table 1–1) for the glacial aquifer system. Groundwater levels measured from wells in till-dominated areas were excluded for layers 1 and 2. No attempt was made to calibrate the model to water levels in till-dominated areas because of the possibility of perched groundwater or poor hydraulic connection with the regional flow system.

Water levels were grouped into six categories, A through F, that were differentiated by data quality, in which observation group A is considered to contain the highest quality data (appendix 2). In general, weights were assigned so that the precalibration sum of squared weighted observations for the glacial and bedrock aquifers was highest for group A and lowest for group F. Weights for observations are available in table 2–4, and a comprehensive description of the observation weighting scheme is available in appendix 2. Groundwater-level calibration targets for the steady-state and transient models are summarized in appendix tables 1–1 and 1–2, respectively.

Single measurements were used for calibration targets for steady-state calibration but were given a low weight (appendix 2), and the mean of all measurements was used for wells with multiple measurements. The dataset from Thamke and others (2014) did not differentiate water levels for the Upper Cretaceous aquifer system into the three hydrogeologic units (Upper Hell Creek hydrogeologic unit, Lower Hell Creek aquifer, and Fox Hills aquifer). In general, the water-bearing units of the Upper Cretaceous aquifer system are the lower Hell Creek and Fox Hills aquifers (Thamke and others, 2014); therefore, these water-levels were assigned to model layers 7 and 8 as calibration targets. For steady-state calibration, 11,109 hydraulic head observation targets were used (table 1–1).

The transient model was calibrated to groundwater-level changes (table 1–2), rather than absolute water-level values, because the transient model was considered to be most useful for assessing changes in groundwater level and storage. The absolute water levels were assumed to be optimized as much as possible during steady-state calibration; therefore, they were not used as calibration targets in the transient model. The mean water-level change for each stress period was used for calibration targets in the transient model. Groundwater-level change calibration targets were calculated for 1,006 observation locations.

Differences in hydraulic heads among model layers 1, 2, 3, 5, and 7 also were used as calibration targets in the steady-state model (table 1–3). Vertical hydraulic head difference targets were calculated with layers 3, 5, 7, and 8 because estimated potentiometric surfaces were available for the hydrogeologic units represented by these layers (Thamke and others, 2014). Thamke and others (2014) estimated one potentiometric surface for the Upper Cretaceous aquifer system (layers 7 and 8); therefore, the hydraulic head was considered to be equivalent where the layers overlapped, and hydraulic head differences between upper layers and layer 8 were only calculated where layer 7 was absent. Vertical hydraulic head difference targets were included because the vertical component of groundwater flow between model layers was considered an important process to represent in the groundwater-flow model. Vertical hydraulic head difference targets for layers 1 and 2 were calculated as the difference between the measured hydraulic head in glacial wells and the estimated potentiometric surfaces for the bedrock hydrogeologic units represented by layers 3, 5, 7, and 8. A set of uniformly distributed points was generated for the model area at the center of every 20 model cells for the bedrock layers, and the potentiometric surface differences for layers 3, 5, 7, and 8 were calculated for each point and used as vertical hydraulic head difference targets for the steady-state model. Vertical hydraulic head difference calibration targets for the steady-state model are available in table 1–3.

Exchanges Between Groundwater and Surface Water

Exchanges between groundwater and surface water were used as calibration targets for the steady-state and transient models. Groundwater discharge into streams and lakes is defined as negative stream flux and lake flux, respectively; groundwater recharge from these features is defined as positive flux. The PART-estimated base flow at a streamgage was assumed to represent the net stream flux upstream from that specific streamgage. The PART-estimated mean daily base-flow values that correspond to model stress periods were computed for streamgages described by Long and others (2014). The PART-estimated base-flow values were compared with simulated values through the Gage Package (Prudic and others, 2004) for streams represented with the SFR2 Package

(Niswonger and Prudic, 2005). Calibration targets from streams represented with the RIV Package were determined for the total stream flux within reaches between streamgages by subtracting the mean base flows for the upstream streamgage from the mean base flows for the downstream streamgage for relevant stress periods.

The mean values for all relevant stress periods for each streamgage were used as calibration targets for the steady-state model. PART-estimated base flows for available stress periods were used as calibration targets for the transient model. Long and others (2014) estimated the long-term mean (1903–2011) stream flux by reach using a combination of PART-estimated base flow and September and October observed streamflow values. These estimates differed from the steady-state calibration targets by only 0.21 percent for all heavily weighted (greater importance) calibration targets (see appendix 2 for details on observation weights). Base-flow calibration targets were separated into three groups (table 1–4; table 2–4): (1) base-flow targets for streamgages in the glacial aquifer system (model layers 1 and 2) that had an estimated base flow less than 1,000 ft^3/s, (2) base-flow targets for streamgages in the lower Tertiary and Upper Cretaceous aquifer systems (model layers 3–8) that had an estimated base flow less than 1,000 ft^3/s, and (3) base-flow targets that had an estimated base flow greater than 1,000 ft^3/s (large rivers, Missouri and Yellowstone). Base-flow and stream flux calibration targets for the steady-state and transient models are shown in table 1–4.

Discharge From Flowing Artesian Wells

Discharge rates for 38 flowing artesian wells, measured periodically between 1968 and 2010 (Honeyman, 2007a, b, c), and 37 flowing well discharge rates identified by Wanek (2009) were used to develop transient calibration targets for flowing wells represented by the model (table 1–5). Wanek (2009) provided the locations of 571 wells in North Dakota and Montana that, at some point during the model simulation period, were potentially flowing artesian wells (fig. 6). Wanek (2009) designated wells in Montana as flowing by comparing the land-surface altitude to the estimated pressure head of the Fox Hills-Hell Creek (FH–HC) aquifer. Wells in North Dakota were determined to be flowing wells based on well completion logs and site visits. Decreases in the pressure head between 1968 and 2010 have resulted in overall decreases in discharge from flowing artesian wells in the model area (Honeyman, 2007a, b, c).

Calibration Results

Calibration results are described through optimal parameter estimates for horizontal and vertical hydraulic conductivity, specific storage, specific yield, recharge, streambed hydraulic conductivity, and well skin; and through an assessment of model fit using potentiometric surfaces, calibration targets, groundwater flow, and flowing artesian wells. The evaluation of parameter sensitivity and identifiability is also discussed.

Optimal Parameter Estimates

The final calibrated parameter values for horizontal and vertical hydraulic conductivity, specific storage, specific yield, recharge, streambed hydraulic conductivity, and well skin were considered reasonable for the hydrogeologic materials and conditions of uppermost principle aquifers of the Williston Basin (fig. 1). The calibrated parameter values, in general, were within the ranges of previously published values.

Generally, model-estimated (calibrated) values for horizontal and vertical hydraulic conductivity for the bedrock aquifers (figs. 7 and 8, respectively) were lower than the initial estimated values at pilot point locations based on Thamke and others (2014) (tables 3 and 6). The minimum calibrated horizontal hydraulic conductivity values were lower than previously published values, the maximum calibrated values were higher than previously published values, and the median calibrated values were lower than previously published values for each hydraulic property zone (with the exception of the Fox Hills aquifer). Calibrated specific storage and specific yield (table 6) were typically within range of previously estimated values (table 4).

Calibrated horizontal hydraulic conductivity for the glacial aquifer system was highest in property zone UGh, which represents glaciofluvial, loess, and eolian deposits, and was lowest in property zone LGl, which represents buried glacial till (table 6). Property zone LHC, which represents the lower Hell Creek aquifer, typically had the highest horizontal hydraulic conductivity of the bedrock aquifers. Hydraulic conductivity for property zones UFU (representing upper Fort Union aquifer), LFU (representing lower Fort Union aquifer), and UHC (representing upper Hell Creek hydrogeologic unit) was highest where the aquifers were near outcrop areas. Property zones MFU (representing middle Fort Union hydrogeologic unit), LHC (representing the lower Hell Creek aquifer), and FH (representing Fox Hills aquifer) had the highest horizontal hydraulic conductivity where the aquifers were buried. Property zone LHC had a zone of high horizontal hydraulic conductivity in the center of the basin near an area where flowing artesian wells exist.

The calibrated horizontal hydraulic conductivity for the bedrock aquifer systems was generally lower compared to the glacial aquifer system. Calibrated horizontal hydraulic conductivity for the glacial aquifer system ranged from 2.14×10^{-4} to 864 ft/d. Calibrated horizontal hydraulic conductivity ranged from 8.20×10^{-4} to 45.4 ft/d for the lower Tertiary aquifer system and from 2.99×10^{-4} to 89.0 ft/d for the Upper Cretaceous aquifer system.

Calibrated vertical hydraulic conductivity in the basin was lower than the horizontal hydraulic conductivity for all simulated aquifers (figs. 7 and 8). Calibrated vertical hydraulic conductivity ranged from 2.14×10^{-4} to 320 ft/d for the glacial aquifer system, from 8.70×10^{-7} to 2.99 ft/d for the

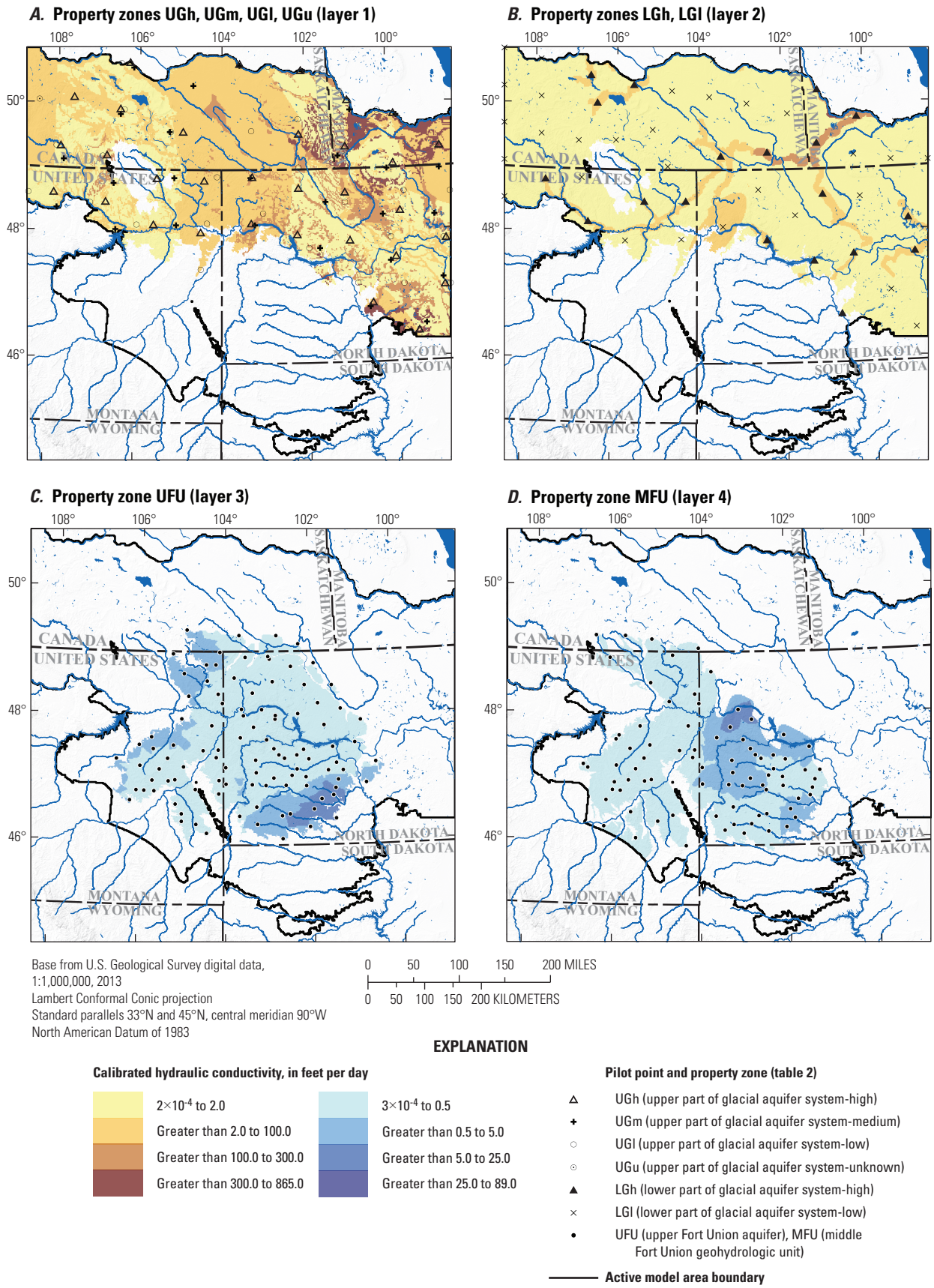

Figure 7. Horizontal hydraulic conductivity and pilot points for *A*, layer 1; *B*, layer 2; *C*, layer 3; *D*, layer 4; *E*, layer 5; *F*, layer 6; *G*, layer 7; and *H*, layer 8, estimated by model calibration.

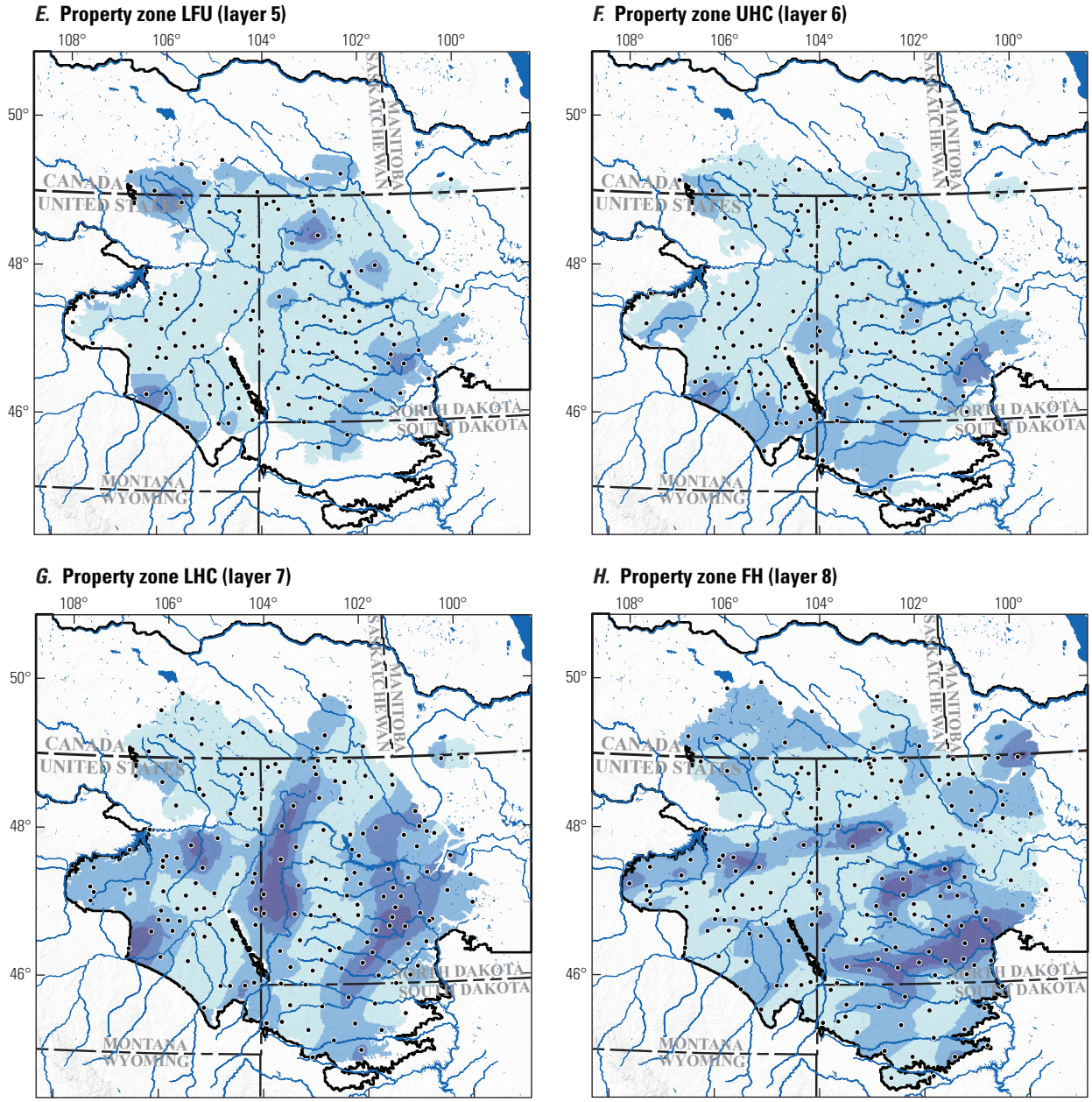

Base from U.S. Geological Survey digital data, 1:1,000,000, 2013
Lambert Conformal Conic projection
Standard parallels 33°N and 45°N, central meridian 90°W
North American Datum of 1983

0 50 100 150 200 MILES
0 50 100 150 200 KILOMETERS

EXPLANATION

Calibrated hydraulic conductivity, in feet per day

- 3×10^{-4} to 0.5
- Greater than 0.5 to 5.0
- Greater than 5.0 to 25.0
- Greater than 25 .0- 89.0

Active model area

Pilot point

Property zone (table 2)—LFU, lower Fort Union aquifer; UHC, upper Hell Creek hydrogeologic unit; LHC, lower Hell Creek aquifer; FH, Fox Hills aquifer

Figure 7. Horizontal hydraulic conductivity and pilot points for *A*, layer 1; *B*, layer 2; *C*, layer 3; *D*, layer 4; *E*, layer 5; *F*, layer 6; *G*, layer 7; and *H*, layer 8, estimated by model calibration.—Continued

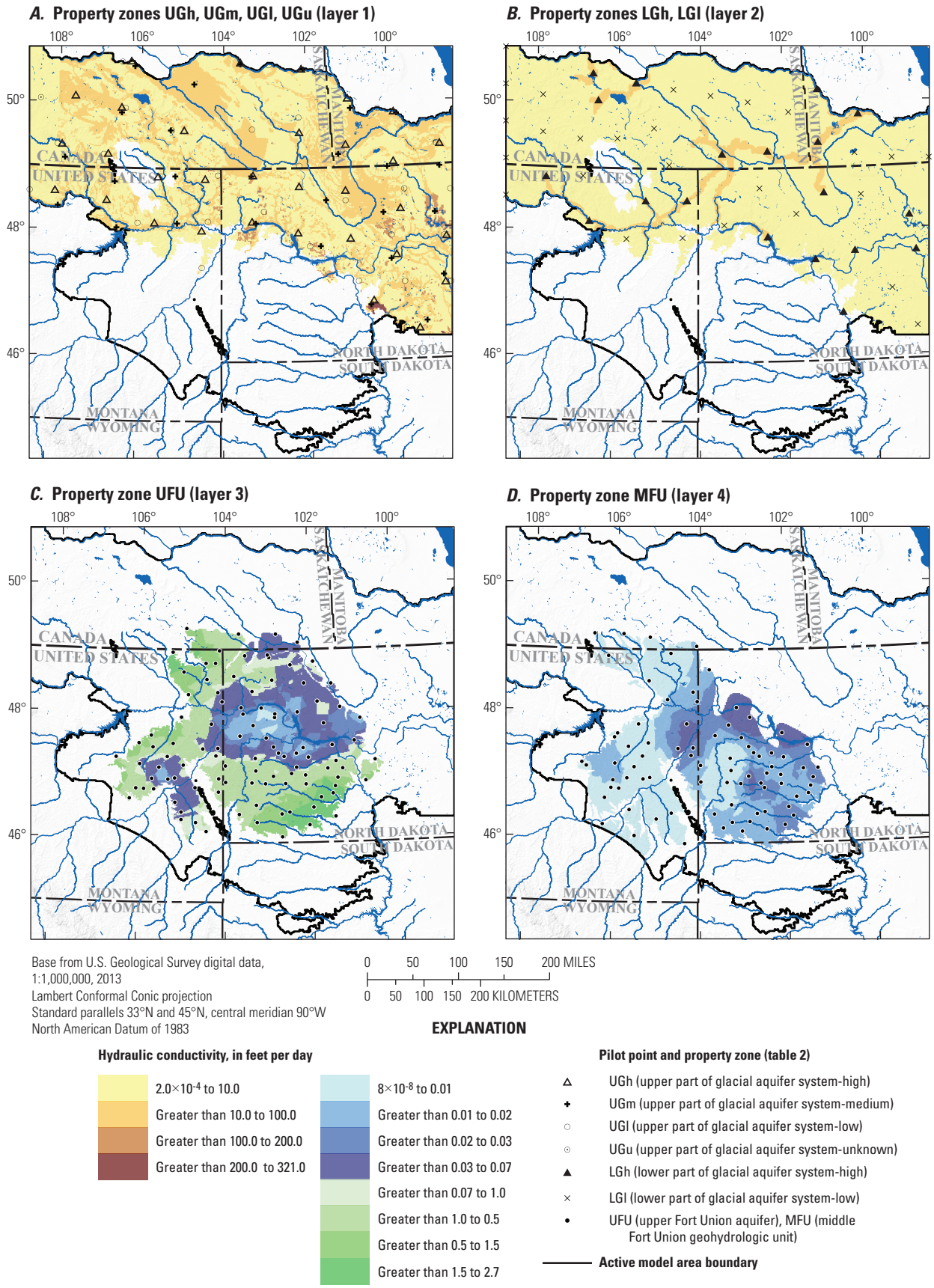

Figure 8. Vertical hydraulic conductivity and pilot points for *A*, layer 1; *B*, layer 2; *C*, layer 3; *D*, layer 4; *E*, layer 5; *F*, layer 6; *G*, layer 7; and *H*, layer 8, estimated by model calibration.

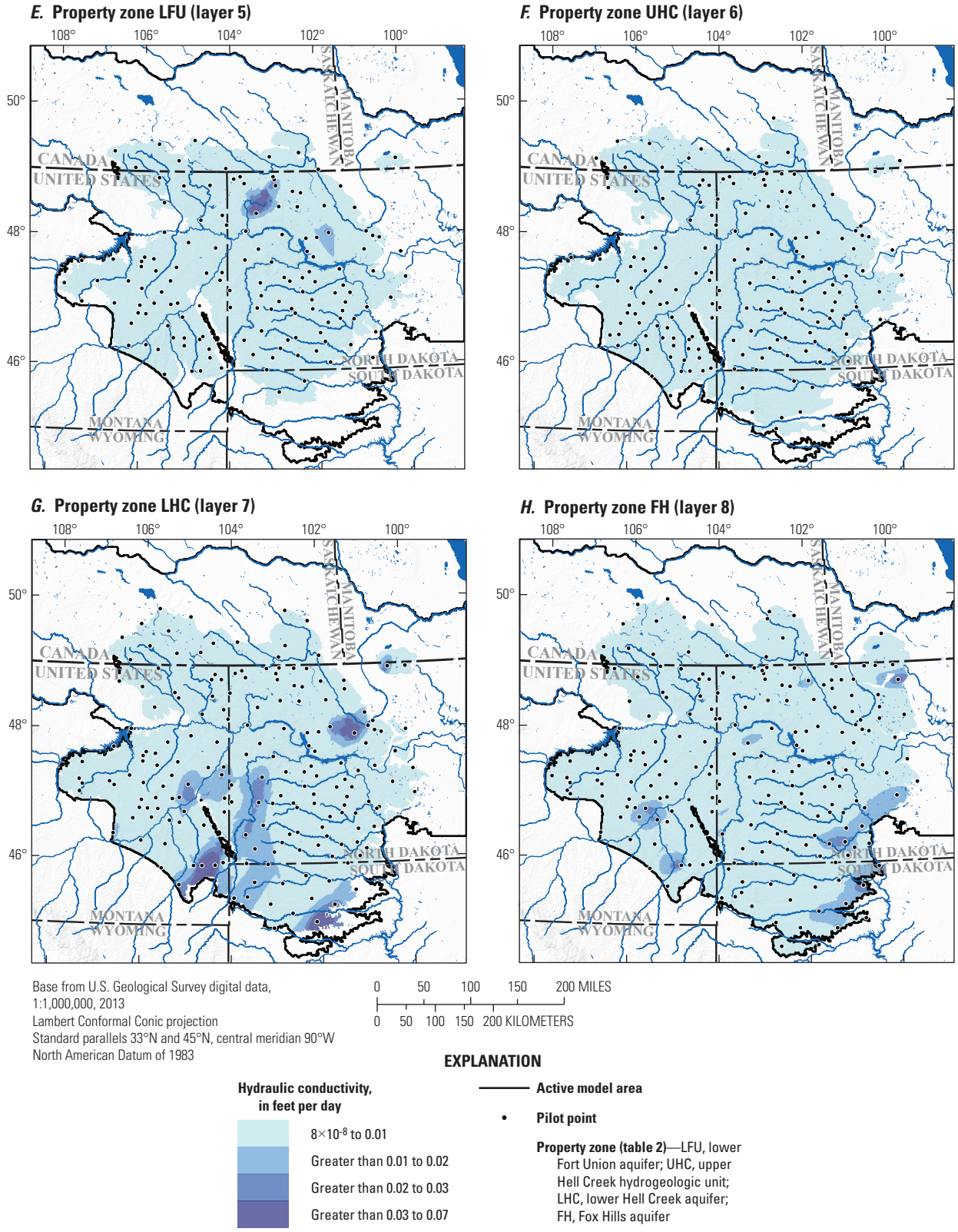

Figure 8. Vertical hydraulic conductivity and pilot points for *A*, layer 1; *B*, layer 2; *C*, layer 3; *D*, layer 4; *E*, layer 5; *F*, layer 6; *G*, layer 7; and *H*, layer 8, estimated by model calibration.—Continued

Table 6. Summary statistics of model-estimated (calibrated) aquifer properties by hydraulic property zone.

[ft/d, foot per day; *n*, number of model cells; UGh, upper part of the glacial aquifer system-high; UGm, upper part of the glacial aquifer system-medium; UGl, upper part of the glacial aquifer system-low; UGu, upper part of the glacial aquifer system-unknown; --, not available; LGh, lower part of the glacial aquifer system-high; LGl, lower part of the glacial aquifer system-low; UFU, upper Fort Union aquifer; MFU, middle Fort Union hydrogeologic unit; LFU, lower Fort Union aquifer; UHC, upper Hell Creek hydrogeologic unit; LHC, lower Hell Creek aquifer; FH, Fox Hills aquifer]

Aquifer system	Property zone (table 2)	Horizontal hydraulic conductivity					Vertical hydraulic conductivity					Specific storage (unitless)	Specific yield (percent)
		Minimum (ft/d)	Maximum (ft/d)	Median (ft/d)	Standard deviation (ft/d)	*n*	Minimum (ft/d)	Maximum (ft/d)	Median (ft/d)	Standard deviation (ft/d)	*n*		
Glacial	UGh	8.43	637	102	143	22,918	8.43	136	58.3	17.7	22,918	1.49×10^{-7}	0.30
	UGm	18.1	864	79.4	57.6	10,033	18.1	320	71.2	32.6	10,033	1.30×10^{-7}	0.30
	UGl	0.26	42	1.48	6.35	53,454	0.26	15.4	1.26	2.7	53,454	1.30×10^{-7}	0.10
	UGu	23.9	23.9	23.9	--	4,070	9.03	9.03	9.03	--	4,070	8.57×10^{-7}	0.05
	LGh	1.68	327	29.9	69.7	19,344	1.68	92.7	28.2	23.3	19,344	9.95×10^{-7}	0.30
	LGl	2.14×10^{-4}	56.3	0.18	0.5	151,083	2.14×10^{-4}	7.19	0.14	0.22	151,083	4.81×10^{-7}	0.10
Lower Tertiary	UFU	4.28×10^{-3}	17.9	0.10	1.79	50,407	3.59×10^{-3}	2.99	0.08	0.46	50,407	5.38×10^{-7}	0.30
	MFU	6.74×10^{-3}	6.1	0.06	1.01	34,763	1.38×10^{-3}	5.78×10^{-2}	1.14×10^{-2}	9.87×10^{-3}	34,763	3.67×10^{-6}	0.05
	LFU	8.20×10^{-4}	45.4	0.13	2.15	62,927	8.90×10^{-7}	6.03×10^{-2}	5.32×10^{-4}	3.85×10^{-3}	62,927	1.73×10^{-5}	0.30
Upper Cretaceous	UHC	2.99×10^{-4}	15.9	0.15	1.28	73,783	8.64×10^{-8}	2.74×10^{-3}	6.10×10^{-5}	2.52×10^{-4}	73,783	1.38×10^{-7}	0.05
	LHC	2.88×10^{-3}	70.2	0.70	9.21	80,670	2.62×10^{-5}	0.10	2.98×10^{-3}	7.94×10^{-3}	80,670	1.30×10^{-7}	0.11
	FH	4.19×10^{-4}	89.0	0.62	10.2	93,535	7.33×10^{-5}	4.19×10^{-2}	2.37×10^{-3}	3.86×10^{-3}	93,535	5.97×10^{-6}	0.30

lower Tertiary aquifer system, and from 8.64×10^{-8} to 0.10 ft/d for the Upper Cretaceous aquifer system. Calibrated vertical hydraulic conductivity is higher for property zone UFU than for the other bedrock zones. Property zone UFU represents the upper Fort Union aquifer and is the uppermost bedrock aquifer simulated by the model. The upper Fort Union aquifer contains the greatest thicknesses of sand (Thamke and others, 2014) when compared to the other bedrock hydrogeologic units, and sequences of well-sorted sand and gravel commonly have higher vertical hydraulic conductivities than sequences that contain substantial amounts of clay, silt, or cemented materials (Harrill, 1986).

Long and others (2014) estimated annual recharge for 1981–2011 using the SWB model. The two scalar multipliers for precipitation recharge, described in the "Model Design" section of this report, were estimated during calibration of the steady-state model, and the estimated values then were applied to all stress periods of the transient model without additional calibration. The calibrated recharge multipliers for glacial and nonglacial areas were 1.35 and 0.86, respectively. The calibrated recharge multipliers may indicate that the SWB-calculated recharge underestimated recharge in glaciated areas and overestimated recharge in nonglaciated areas. Irrigation recharge was not simulated explicitly (table 1); rather, the adjustment in recharge multipliers was assumed to account for additional recharge in the model from irrigation return, and estimated values for irrigation recharge are assumed to represent simulated values for the control-volume water budget.

Two calibrated well-skin values of 100 and 1.24 were applied to flowing artesian wells. Wells with estimated flow data were assigned to well-skin group 1 with a skin of 100, and wells with no available flow data were assigned to well-skin group 2 with a skin of 1.24 (see "Groundwater Withdrawal" section for description of groups).

Calibrated streambed hydraulic conductivity for the SFR2, RIV, and DRN Packages ranged from 1.59×10^{-3} to 25.2 ft/d (table 1–4). Previous estimates of riverbed hydraulic conductivity were not available for the model area for comparison.

Assessment of Model Fit

The ability of the model to accurately simulate groundwater flow in the Williston Basin was assessed primarily by the ability of the model to match calibration targets for hydraulic head, stream base flow, and flowing artesian well discharge. The steady-state model also was assessed, in part, by its ability to replicate the potentiometric surfaces and hydraulic gradients from Thamke and others (2014) for the upper Fort Union aquifer (layer 3, fig. 9), lower Fort Union aquifer (layer 5, fig. 10), and Fox Hills aquifer (layer 8, fig. 11). An additional metric used to assess model performance was the comparison of the conceptual groundwater budget (Long and others, 2014) to the simulated groundwater model budget for a control volume within the model area (fig. 1; table 1) for the steady-state model. Regional potentiometric surfaces for the glacial aquifer system were not available for comparison.

Potentiometric Surfaces

Thamke and others (2014) estimated potentiometric surfaces for the upper Fort Union aquifer, the lower Fort Union aquifer, and the Fox Hills aquifer (figs. 9–11). These potentiometric surfaces were visually compared with the steady-state modeled potentiometric surfaces for model layers 3, 5, and 8, respectively. The simulated potentiometric surfaces (represented in figs. 9–11 as shaded hydraulic head ranges) and hydraulic gradients for the upper Fort Union aquifer, lower Fort Union aquifer, and Fox Hills aquifer generally matched well with the estimated potentiometric surfaces. Based on potential flow paths drawn at approximate 90 degree angles to the potentiometric contours (not shown in figures), the estimated potentiometric surfaces typically indicated localized groundwater-flow gradients that were topographically controlled in outcrop areas and more generalized gradients where the aquifers were confined. The simulated potentiometric surfaces follow the same general trend as the estimated potentiometric surfaces: localized, topographically controlled groundwater-flow gradients existed in outcrop areas, and more generalized gradients existed where the aquifers were confined (figs. 9, 10, and 11). Groundwater highs and lows and overall potentiometric surfaces correspond reasonably well for the simulated potentiometric surfaces compared with the estimated potentiometric surfaces.

Although some discrepancies exist between the estimated and simulated potentiometric surfaces, the discrepancies are not unreasonable given the difficulties in mapping and modeling groundwater flow in large, complex, regional aquifer systems. The simulated and estimated potentiometric contours for the upper Fort Union aquifer are topographically affected south of the Missouri River where the aquifer is under confined conditions and are more generalized north of the Missouri River where the aquifer is under unconfined conditions (fig. 9); however, the simulated potentiometric contours are much more generalized when compared to the estimated contours to the south of the Missouri River (fig. 9). The simulated and estimated potentiometric contours for the lower Fort Union aquifer (fig. 10) are less typographically affected compared to those for the upper Fort Union aquifer (fig. 9), which is expected because the lower Fort Union aquifer is mainly confined in the model area. Potential groundwater flow paths based on potentiometric contours for the lower Fort Union aquifer (not shown in figures) indicate general groundwater flow from southwest to northeast but also from areas of higher topographic relief toward major streams. Simulated and estimated potentiometric contours for the Fox Hills aquifer (fig. 11) are much more generalized compared to those in the upper and lower Fort Union aquifers (figs. 9 and 10). Groundwater flow in the Fox Hills aquifer is much

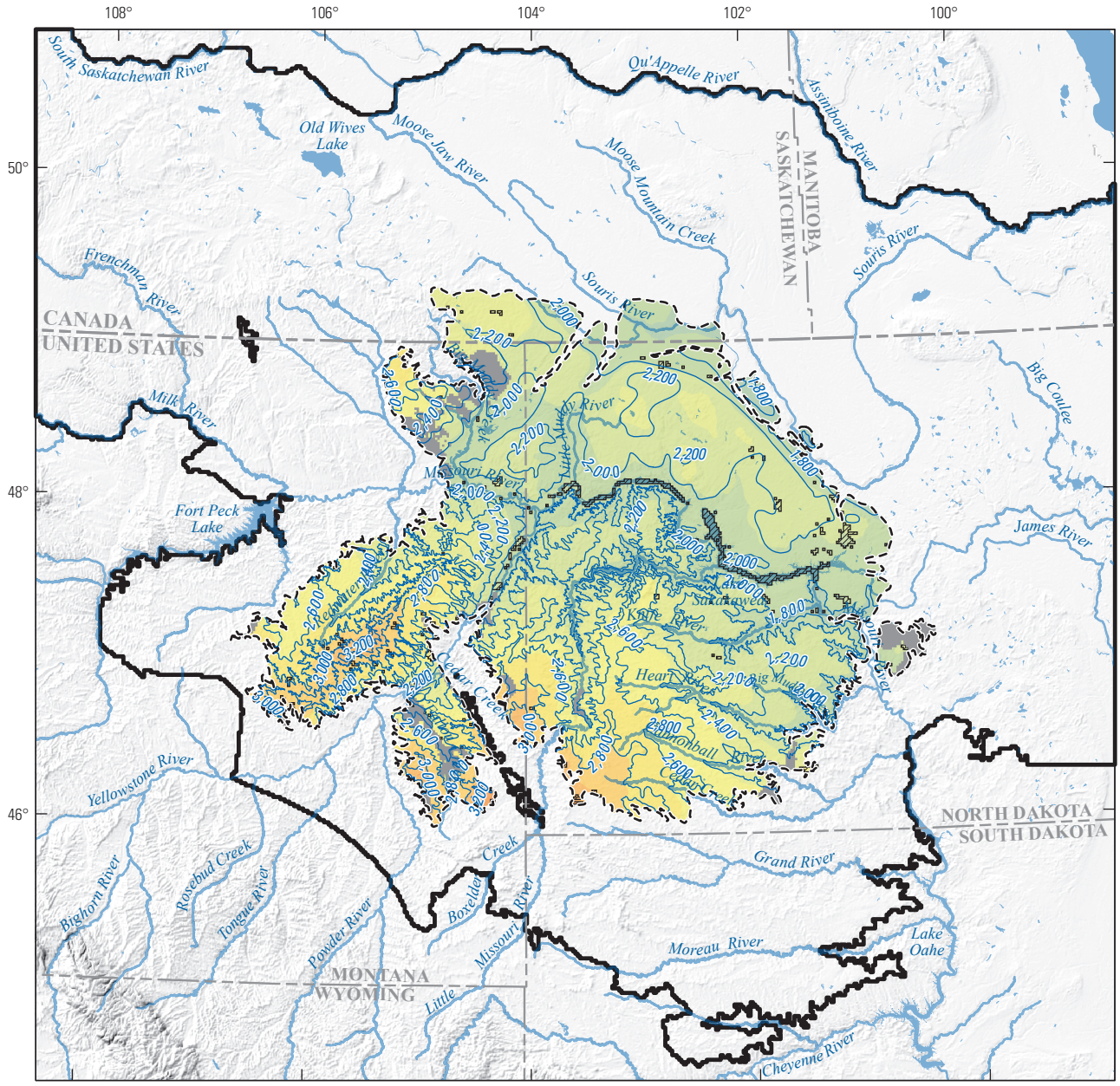

Base modified from U.S. Geological Survey and other Federal digital data, various scales, variously dated
Lambert Conformal Conic projection
Standard parallels 33°N and 45°N, central meridian 90°W
North American Datum of 1983

0 30 60 90 120 MILES
0 30 60 90 120 KILOMETERS

EXPLANATION

Simulated dry cells

Simulated flooded cells

Simulated hydraulic head, in feet above North American Vertical Datum of 1988

- Greater than 1,600 to 1,800
- Greater than 1,800 to 2,000
- Greater than 2,000 to 2,200
- Greater than 2,200 to 2,400
- Greater than 2,400 to 2,600
- Greater than 2,600 to 2,800
- Greater than 2,800 to 3,000
- Greater than 3,000 to 3,200
- Greater than 3,200 to 3,400
- Greater than 3,400 to 3,600

Extent of the upper Fort Union (UFU) aquifer—Property zone UFU (table 2)

Active model area boundary

—2,600— **Potentiometric contour and value**—Shows altitude at which water level would have stood in tightly cased wells. Contour interval 200 feet. Datum is North American Vertical Datum of 1988. Modified from Thamke and others (2014)

Figure 9. Comparison of observed (estimated) and simulated steady-state potentiometric surfaces for the upper Fort Union aquifer (model layer 3).

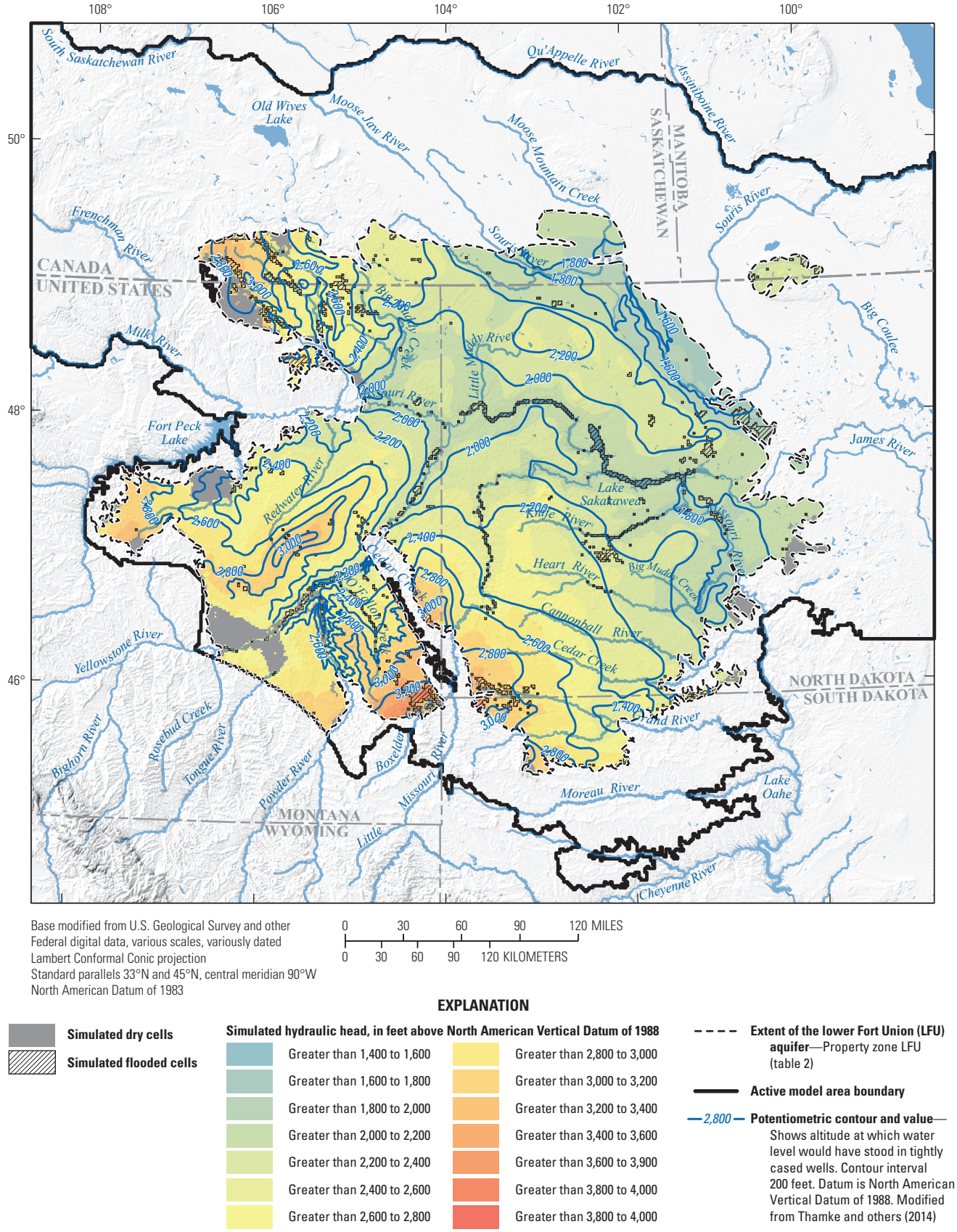

Figure 10. Comparison of observed (estimated) and simulated steady-state potentiometric surfaces for the lower Fort Union aquifer (model layer 5).

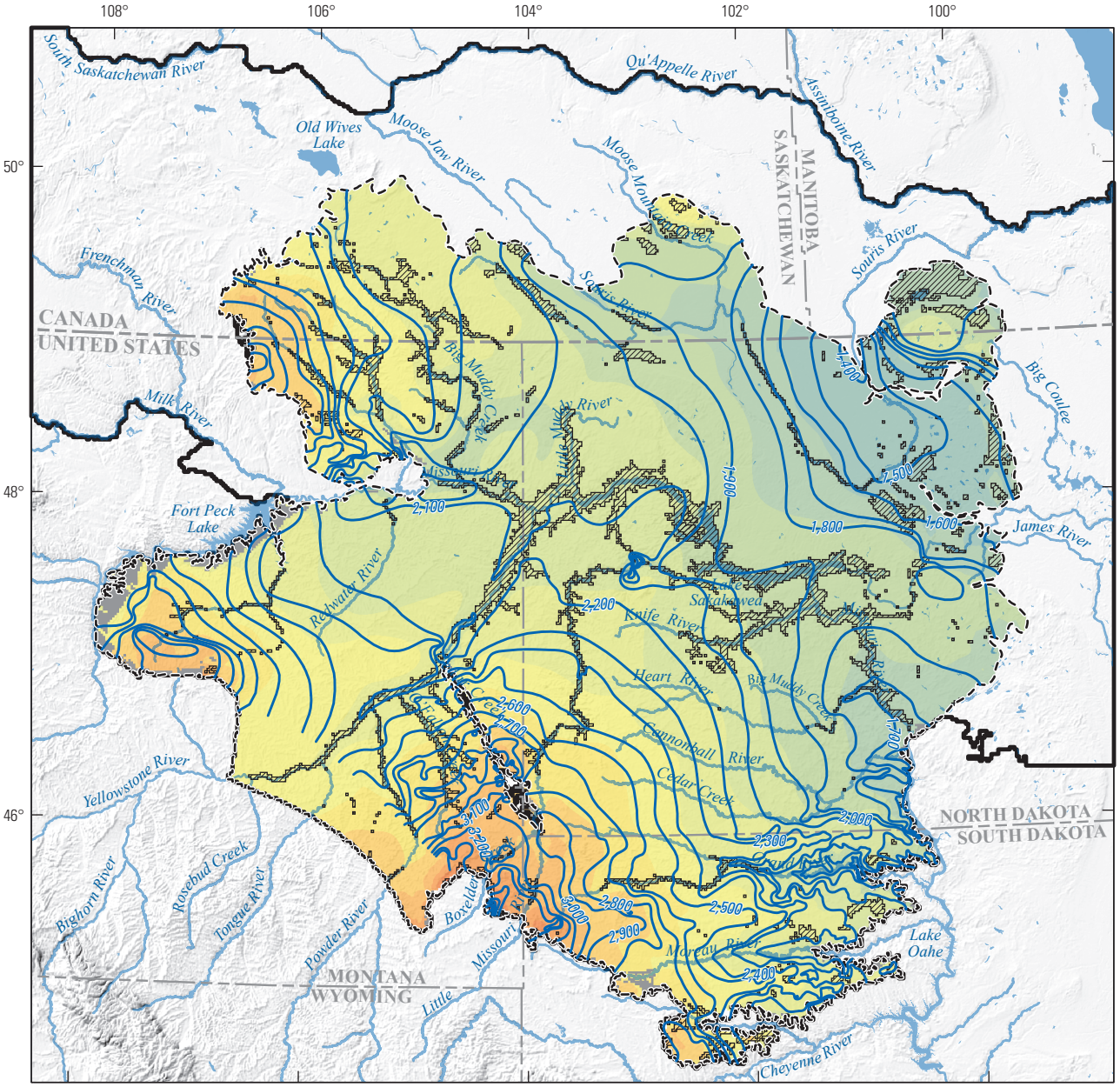

Base modified from U.S. Geological Survey and other Federal digital data, various scales, variously dated
Lambert Conformal Conic projection
Standard parallels 33°N and 45°N, central meridian 90°W
North American Datum of 1983

0 30 60 90 120 MILES
0 30 60 90 120 KILOMETERS

EXPLANATION

Simulated dry cells

Simulated flooded cells

Simulated hydraulic head, in feet above North American Vertical Datum of 1988

- Greater than 1,400 to 1,600
- Greater than 1,600 to 1,800
- Greater than 1,800 to 2,000
- Greater than 2,000 to 2,200
- Greater than 2,200 to 2,400
- Greater than 2,400 to 2,600
- Greater than 2,600 to 2,800
- Greater than 2,800 to 3,000
- Greater than 3,000 to 3,200
- Greater than 3,200 to 3,400
- Greater than 3,400 to 3,600
- Greater than 3,600 to 3,900
- Greater than 3,800 to 4,000
- Greater than 4,000

Extent of the FoxHills (FH) aquifer—Property zone FH (table 2)

Active model area boundary

2,400 **Potentiometric contour and value**—Shows altitude at which water level would have stood in tightly cased wells. Contour interval 100 feet. Datum is North American Vertical Datum of 1988. Modified from Thamke and others (2014)

Figure 11. Comparison of observed (estimated) and simulated steady-state potentiometric surfaces for the Fox Hills aquifer (model layer 8).

more regionalized when compared to the other hydrogeologic units and is typically from the southwest to northeast with some discharge in major stream valleys.

Calibration Targets

Hydraulic head residuals (observed minus simulated values) were calculated for 11,109 observation locations using the steady-state model (table 1–1). Simulated hydraulic heads for the steady-state model matched those at observed hydraulic head locations reasonably well (figs. 12 and 13). Simulated hydraulic heads from observation groups A, B, and C more closely matched the observed values when compared to observations in groups D, E, and F (fig. 12). The hydraulic head residual data in comparison to the 1:1 perfect-fit line shown in figure 12 indicate a slight underestimation bias for hydraulic heads for all layers simulated by the steady-state model. In general, the model underestimates hydraulic head in the model area, and this is indicated by the positive mean residual for all calibration targets of 11.2 ft. The steady-state model underestimates hydraulic head for all property zones except property zone LHC, which is indicated by the negative mean residual in table 7. The positive residuals shown in figure 13 indicate simulated hydraulic heads that were lower than the observed values, and the negative residuals indicate simulated hydraulic heads that were higher than the observed values. Simulated hydraulic heads for the glacial aquifers (figs. 13*A*, *B*) generally were lower than observed values across the model area. Simulated hydraulic heads for the lower Tertiary aquifers (figs. 13*C*, *D*) generally were lower than observed values except in larger stream valleys. Simulated hydraulic heads for the Upper Cretaceous aquifers (figs. 13*E*, *F*) generally were lower than observed values near outcrop areas and higher than observed values where the aquifers were confined.

Groundwater-level change residuals were calculated for 1,006 observation locations using the transient model (table 1–2). Simulated groundwater-level changes for the

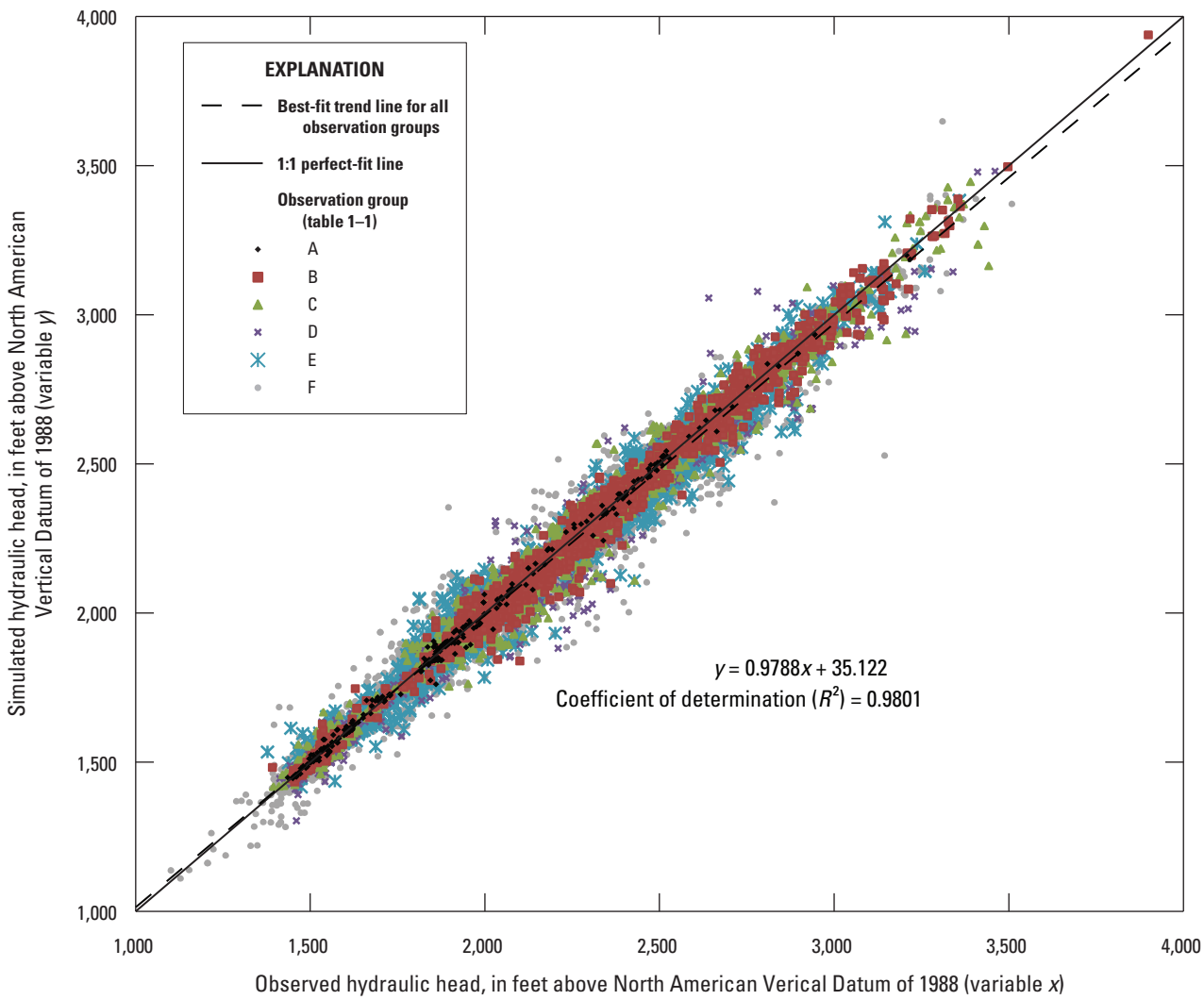

Figure 12. Relation between observed and simulated hydraulic heads for the steady-state (1981–2005) model. The 1:1 perfect fit line also is shown for reference to visualize bias.

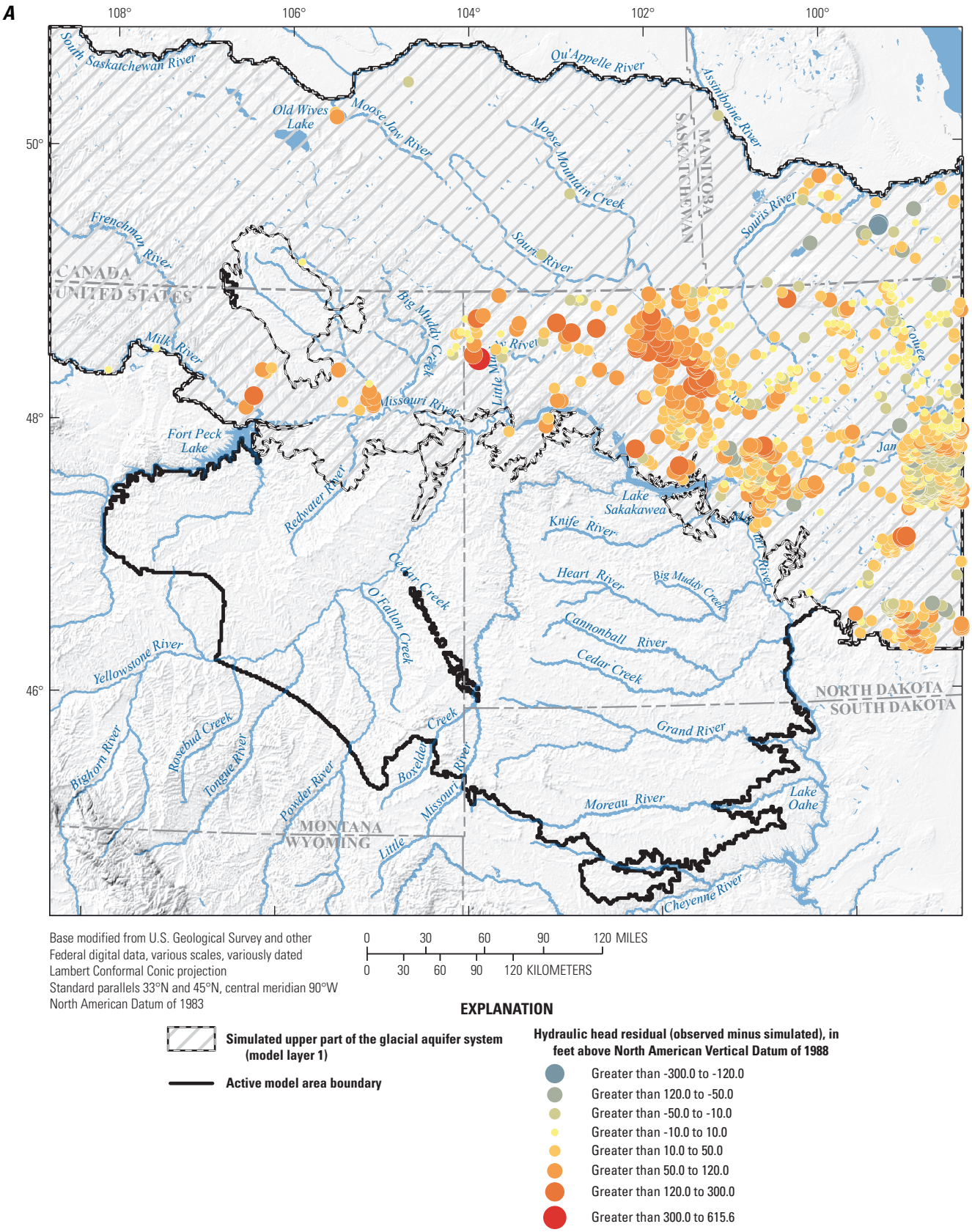

Figure 13. Hydraulic head residuals (observed minus simulated values) for the steady-state (1981–2005) model for the *A*, upper part of the glacial aquifer system; *B*, lower part of the glacial aquifer system; *C*, upper Fort Union aquifer; *D*, lower Fort Union aquifer; *E*, lower Hell Creek aquifer; and *F*, Fox Hills aquifer.

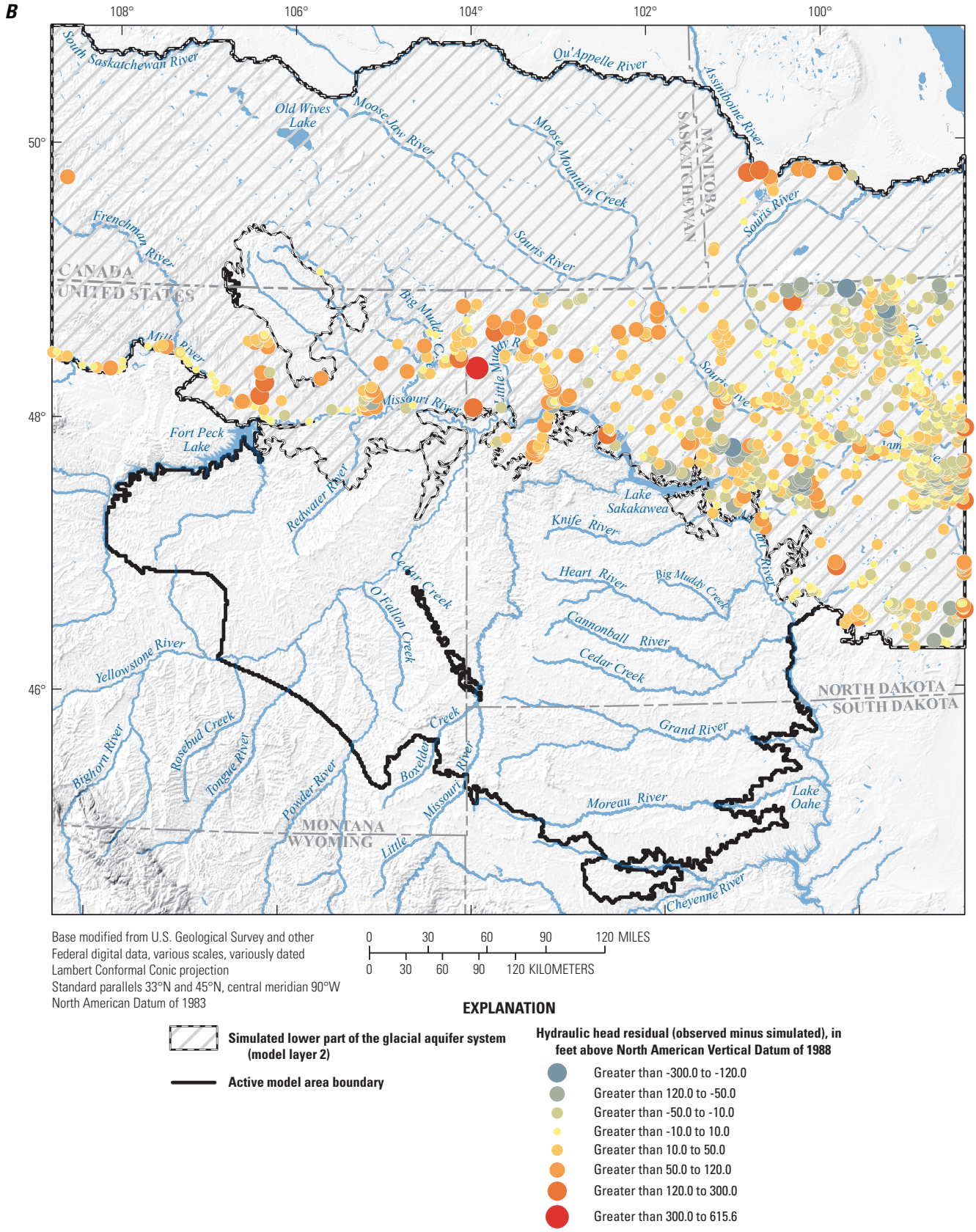

Figure 13. Hydraulic head residuals (observed minus simulated values) for the steady-state (1981–2005) model for the *A*, upper part of the glacial aquifer system; *B*, lower part of the glacial aquifer system; *C*, upper Fort Union aquifer; *D*, lower Fort Union aquifer; *E*, lower Hell Creek aquifer; and *F*, Fox Hills aquifer.—Continued

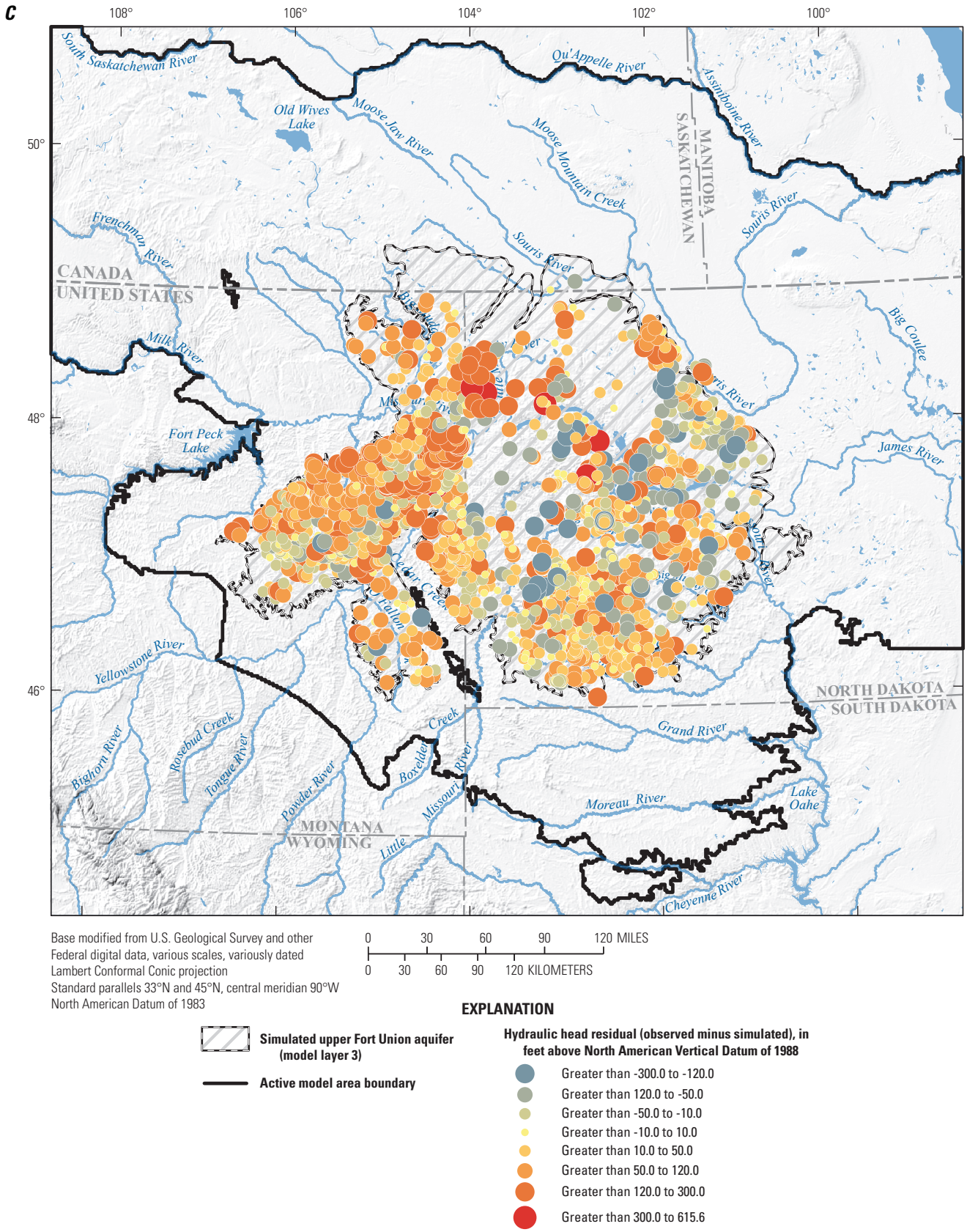

Figure 13. Hydraulic head residuals (observed minus simulated values) for the steady-state (1981–2005) model for the *A*, upper part of the glacial aquifer system; *B*, lower part of the glacial aquifer system; *C*, upper Fort Union aquifer; *D*, lower Fort Union aquifer; *E*, lower Hell Creek aquifer; and *F*, Fox Hills aquifer.—Continued

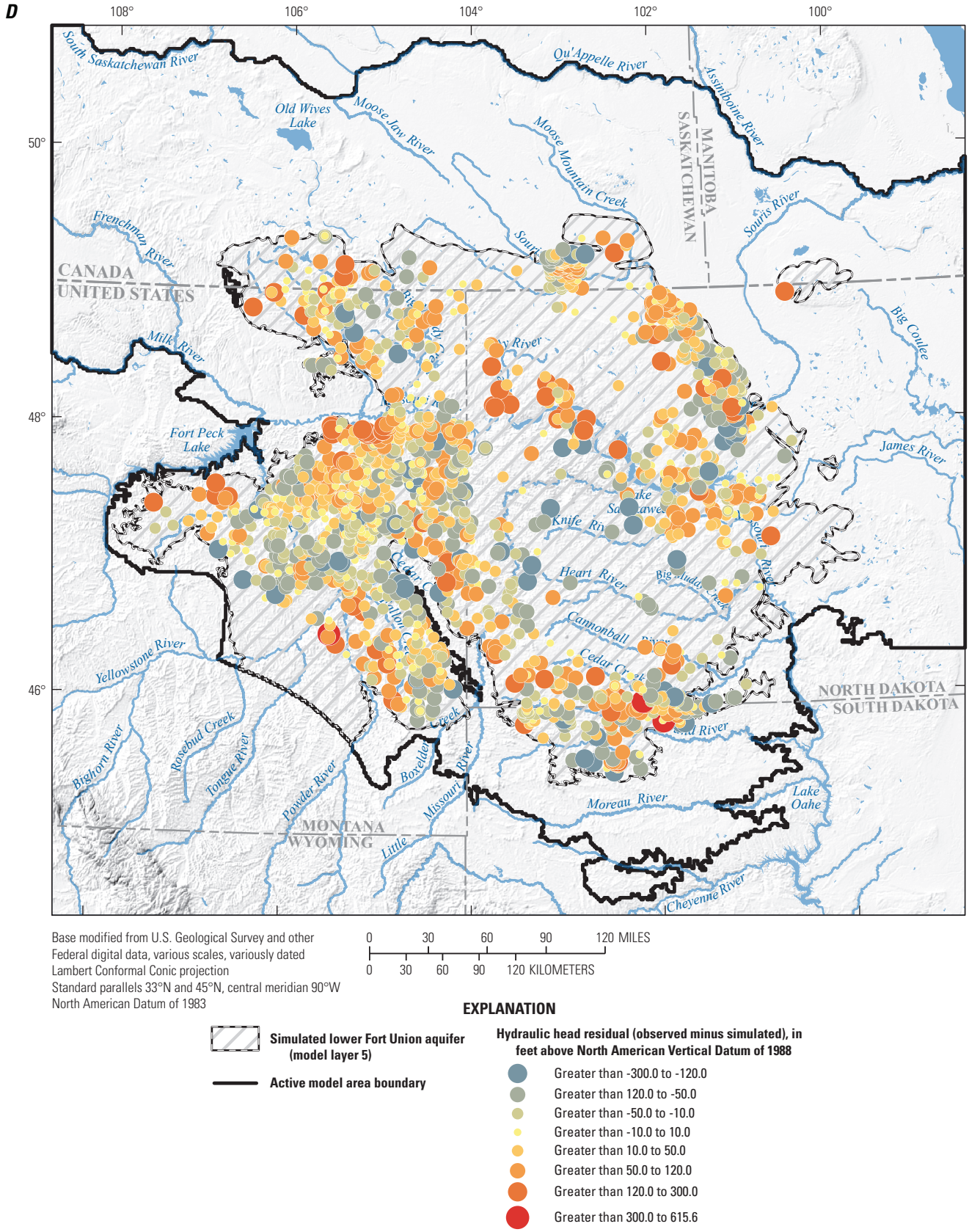

Figure 13. Hydraulic head residuals (observed minus simulated values) for the steady-state (1981–2005) model for the *A*, upper part of the glacial aquifer system; *B*, lower part of the glacial aquifer system; *C*, upper Fort Union aquifer; *D*, lower Fort Union aquifer; *E*, lower Hell Creek aquifer; and *F*, Fox Hills aquifer.—Continued

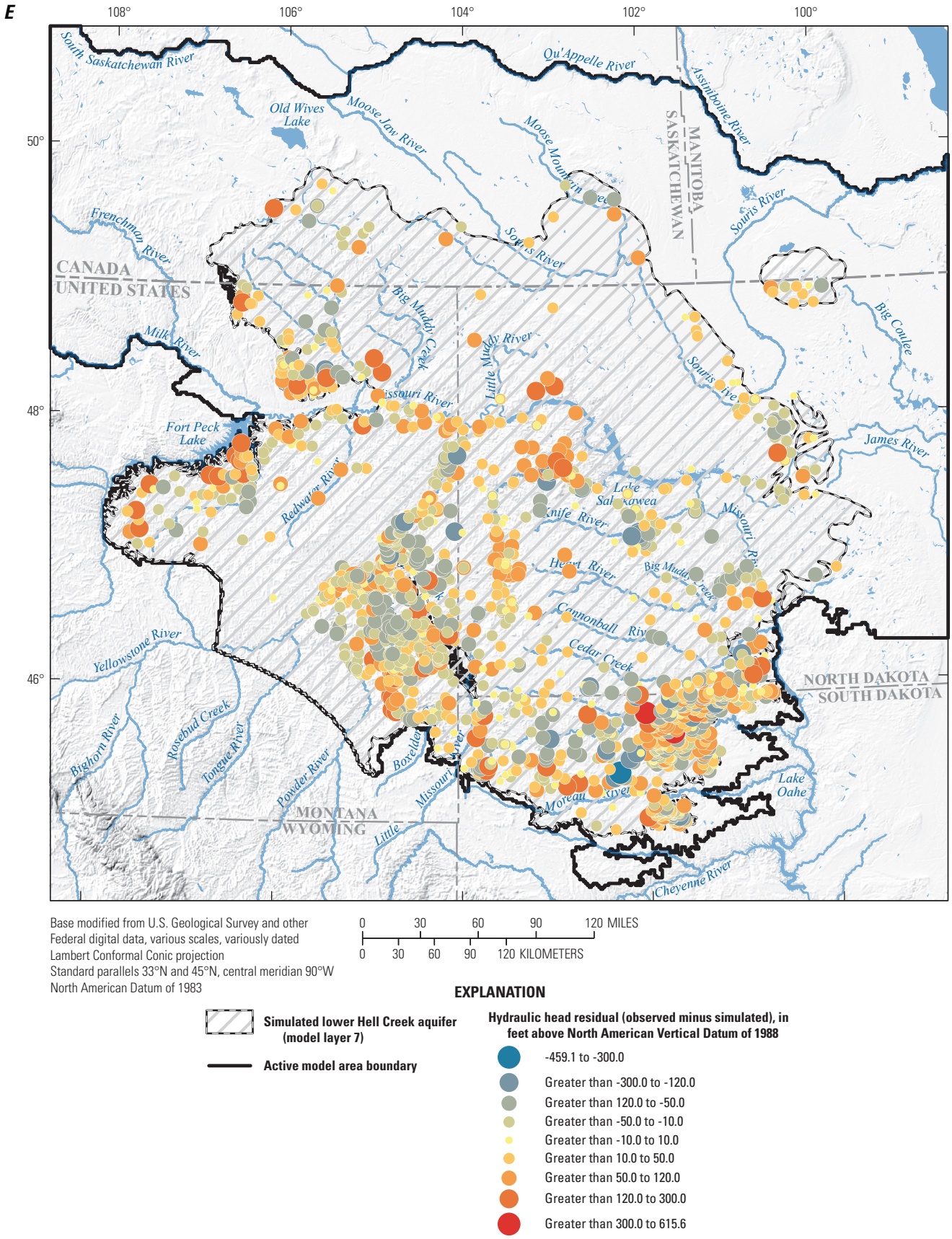

Base modified from U.S. Geological Survey and other Federal digital data, various scales, variously dated
Lambert Conformal Conic projection
Standard parallels 33°N and 45°N, central meridian 90°W
North American Datum of 1983

0 30 60 90 120 MILES
0 30 60 90 120 KILOMETERS

EXPLANATION

Simulated lower Hell Creek aquifer (model layer 7)

Active model area boundary

Hydraulic head residual (observed minus simulated), in feet above North American Vertical Datum of 1988

- -459.1 to -300.0
- Greater than -300.0 to -120.0
- Greater than 120.0 to -50.0
- Greater than -50.0 to -10.0
- Greater than -10.0 to 10.0
- Greater than 10.0 to 50.0
- Greater than 50.0 to 120.0
- Greater than 120.0 to 300.0
- Greater than 300.0 to 615.6

Figure 13. Hydraulic head residuals (observed minus simulated values) for the steady-state (1981–2005) model for the *A*, upper part of the glacial aquifer system; *B*, lower part of the glacial aquifer system; *C*, upper Fort Union aquifer; *D*, lower Fort Union aquifer; *E*, lower Hell Creek aquifer; and *F*, Fox Hills aquifer.—Continued

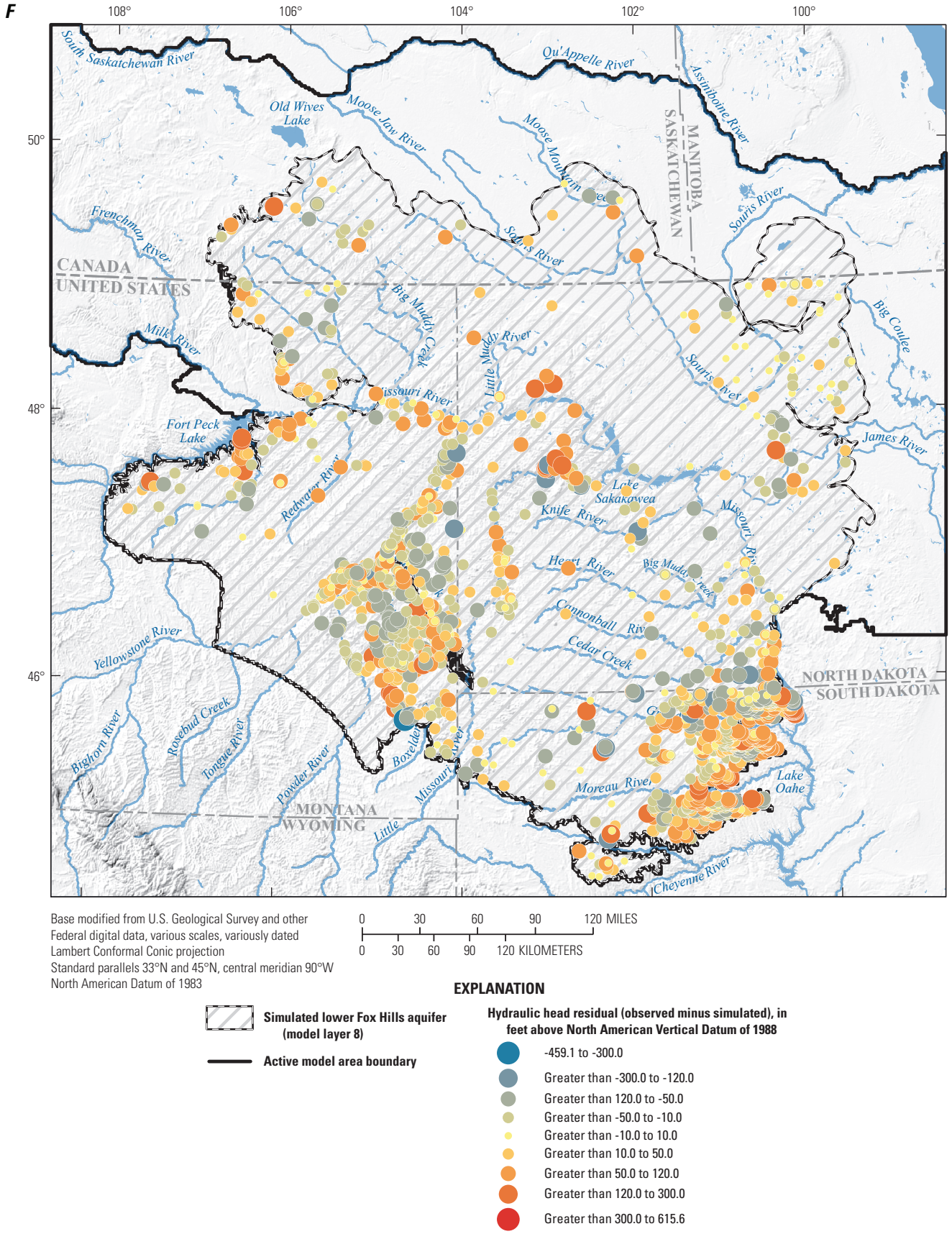

Base modified from U.S. Geological Survey and other Federal digital data, various scales, variously dated
Lambert Conformal Conic projection
Standard parallels 33°N and 45°N, central meridian 90°W
North American Datum of 1983

0 30 60 90 120 MILES
0 30 60 90 120 KILOMETERS

EXPLANATION

Simulated lower Fox Hills aquifer (model layer 8)

Active model area boundary

Hydraulic head residual (observed minus simulated), in feet above North American Vertical Datum of 1988

- -459.1 to -300.0
- Greater than -300.0 to -120.0
- Greater than 120.0 to -50.0
- Greater than -50.0 to -10.0
- Greater than -10.0 to 10.0
- Greater than 10.0 to 50.0
- Greater than 50.0 to 120.0
- Greater than 120.0 to 300.0
- Greater than 300.0 to 615.6

Figure 13. Hydraulic head residuals (observed minus simulated values) for the steady-state (1981–2005) model for the *A*, upper part of the glacial aquifer system; *B*, lower part of the glacial aquifer system; *C*, upper Fort Union aquifer; *D*, lower Fort Union aquifer; *E*, lower Hell Creek aquifer; and *F*, Fox Hills aquifer.—Continued

Table 7. Summary statistics of simulated hydraulic head for the steady-state (1981–2005) model.

[Residuals calculated as observed minus simulated values; ft, foot; *n*, number of observations; UGh, upper part of the glacial aquifer system-high; UGm, upper part of the glacial aquifer system-medium; UGl, upper part of the glacial aquifer system-low; UGu, upper part of the glacial aquifer system-unknown; LGh, lower part of the glacial aquifer system-high; LGl, lower part of the glacial aquifer system-low; UFU, upper Fort Union aquifer; MFU, middle Fort Union hydrogeologic unit; LFU, lower Fort Union aquifer; UHC, upper Hell Creek hydrogeologic unit; --, not available; LHC, lower Hell Creek aquifer; FH, Fox Hills aquifer]

Property zone (table 2)	Hydraulic-head residual				
	Minimum (ft)	Maximum (ft)	Mean (ft)	Standard deviation (ft)	*n*
UGh, UGm, UGl, UGu	-273.6	371.7	18.3	41.9	1,253
LGh, LGl	-128.1	408.3	2.7	37.2	1,482
UFU	-253.4	360.5	36.7	76.5	2,427
MFU	-248.3	214.1	50.8	126.4	18
LFU	-459.1	615.6	4.2	67.1	2,289
UHC	--	--	--	--	--
LHC	-305.7	360.8	-1.9	59.7	1,806
FH	-338.5	279.5	0.6	53.0	1,834
All	-459.1	615.6	11.2	62.2	11,109

transient model matched well when compared with the observed values. A histogram of groundwater-level change residuals indicated that the minimum and maximum groundwater-level change residuals were -275.0 and 170.7 ft, respectively; however, more than 60 percent of simulated groundwater-level changes were within plus or minus 2.5 ft of the observed values, and 95 percent were within plus or minus 17.5 ft of the observed values (fig. 14). The different magnitudes of the minimum and maximum residuals indicated that the distribution of groundwater-level change residuals is somewhat negatively skewed. The negative skew indicates that the transient model has a slight tendency to underestimate groundwater-level changes. Hydrographs for selected wells comparing observed and simulated groundwater-level changes also indicate that the transient model underestimated groundwater-level changes in the model area for all simulated hydrogeologic units (fig. 15).

Stream flux residuals were calculated using the steady-state and transient models (table 1–4). Comparison of simulated and observed (estimated) base flow (figs. 16*A*, *B*, and 17) indicated that the model had a tendency to overestimate base flow in streams, particularly for lower flows; however, selected base-flow hydrographs indicate that the model generally underestimated the magnitude of annual fluctuations in base flow when compared to estimated values (fig. 18). The hydrographs shown in figure 18 were selected for streamgages that had a record of at least 10 years and a contributing drainage area that was fully contained within the model area; therefore, this selection of hydrographs does not exhibit bias from user-specified inflow in the SFR2 Package along the model boundary.

Groundwater Flow

Comparing the simulated groundwater-flow budgets with previously estimated groundwater-flow budgets is a useful metric for evaluating model performance; therefore, simulated groundwater-recharge and groundwater-discharge components for steady-state and transient conditions were compared with published estimates of recharge and discharge for the control volume (fig. 1) within the model area. Simulated groundwater flow for the upper Fort Union, lower Fort Union, and Fox Hills aquifers also is summarized in this section because these aquifers are the primary bedrock aquifers in the model area (Thamke and others, 2014; Long and others, 2014). The estimated and simulated steady-state recharge and discharge components for the control volume are summarized in table 1, and the simulated steady-state and transient model budgets are shown in figure 19.

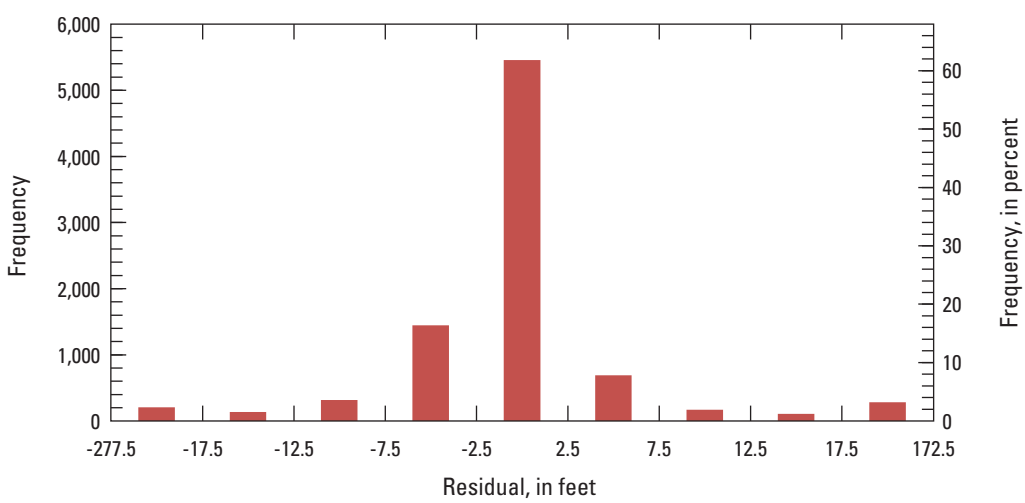

Figure 14. Histogram of hydraulic head residuals (observed minus simulated values) for the transient model.

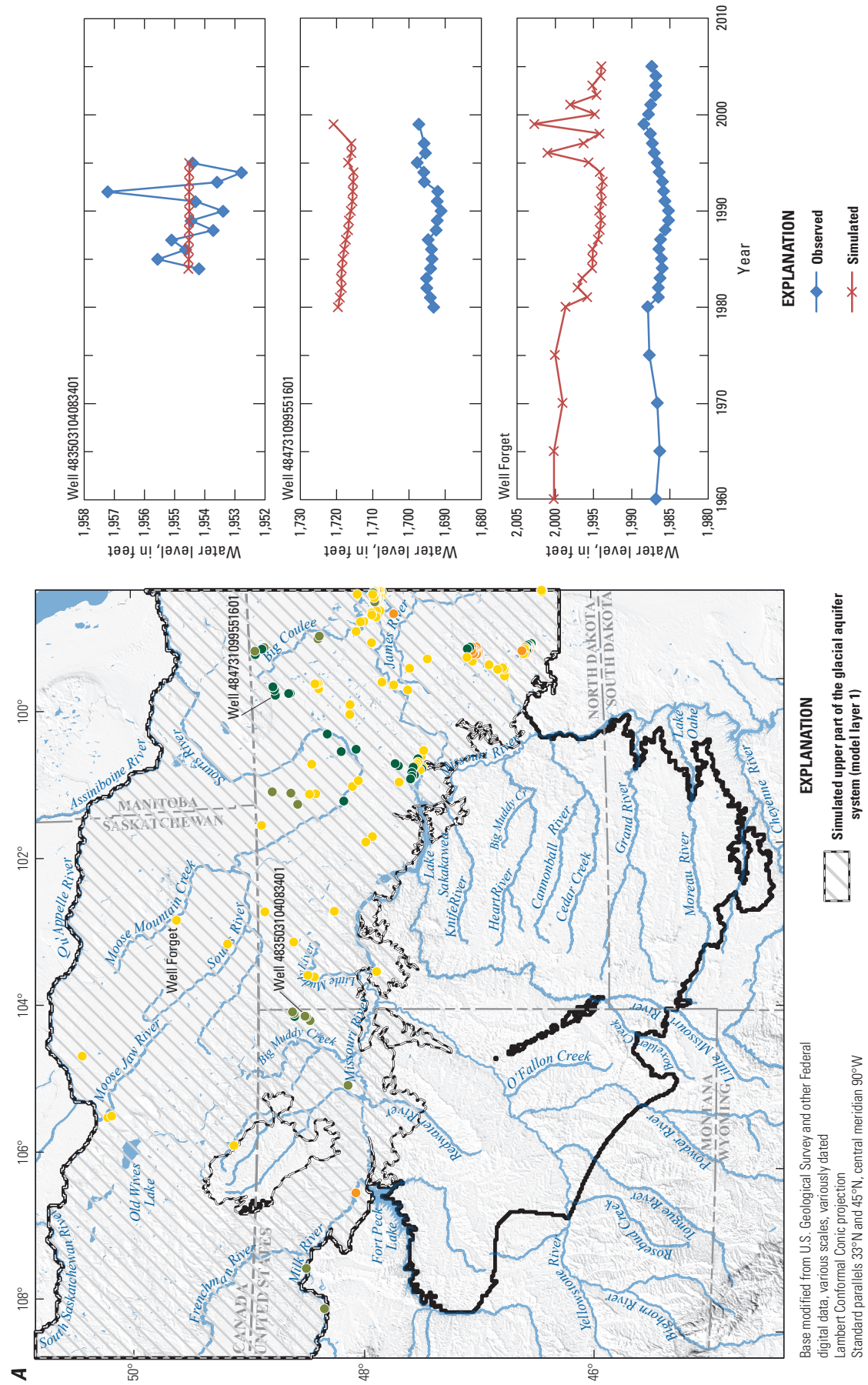

Figure 15. Maps and selected hydrographs showing observed and simulated hydraulic head for the transient model for the *A*, upper part of the glacial aquifer system; *B*, lower part of the glacial aquifer system; *C*, upper Fort Union aquifer; *D*, lower Fort Union aquifer; *E*, lower Hell Creek aquifer; and *F*, Fox Hills aquifer.

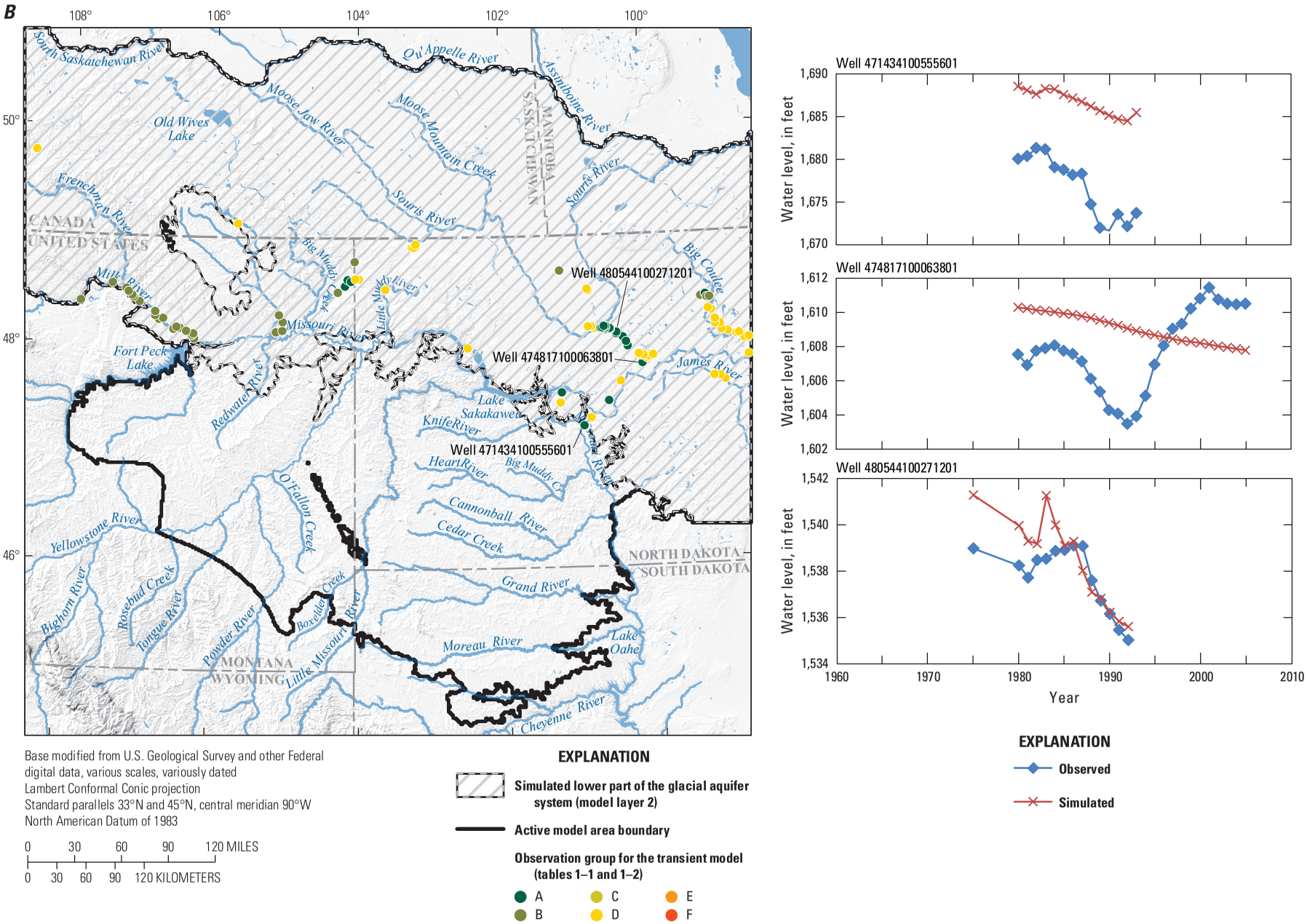

Figure 15. Maps and selected hydrographs showing observed and simulated hydraulic head for the transient model for the *A*, upper part of the glacial aquifer system; *B*, lower part of the glacial aquifer system; *C*, upper Fort Union aquifer; *D*, lower Fort Union aquifer; *E*, lower Hell Creek aquifer; and *F*, Fox Hills aquifer.—Continued

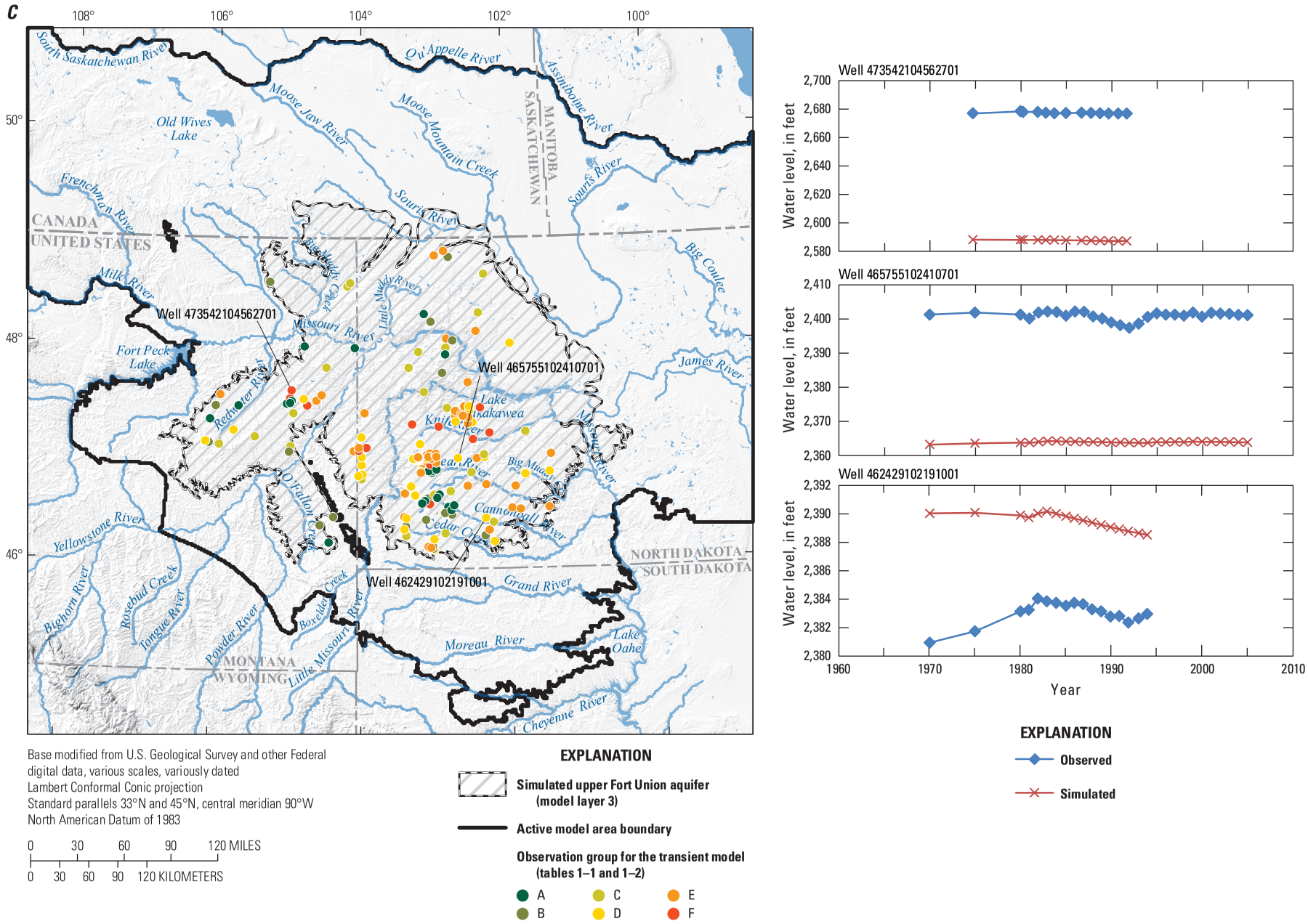

Figure 15. Maps and selected hydrographs showing observed and simulated hydraulic head for the transient model for the *A*, upper part of the glacial aquifer system; *B*, lower part of the glacial aquifer system; *C*, upper Fort Union aquifer; *D*, lower Fort Union aquifer; *E*, lower Hell Creek aquifer; and *F*, Fox Hills aquifer.—Continued

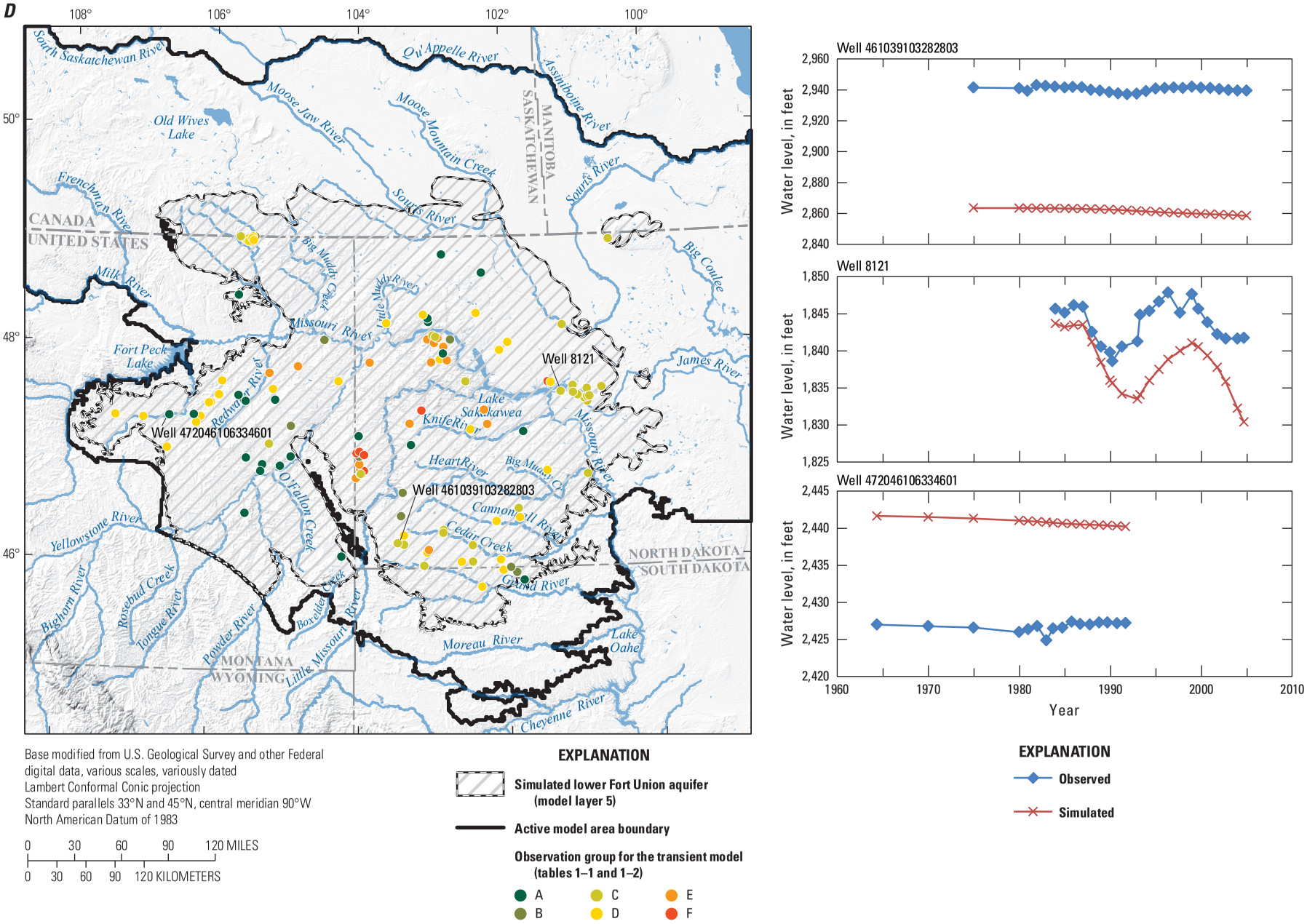

Figure 15. Maps and selected hydrographs showing observed and simulated hydraulic head for the transient model for the *A*, upper part of the glacial aquifer system; *B*, lower part of the glacial aquifer system; *C*, upper Fort Union aquifer; *D*, lower Fort Union aquifer; *E*, lower Hell Creek aquifer; and *F*, Fox Hills aquifer.—Continued

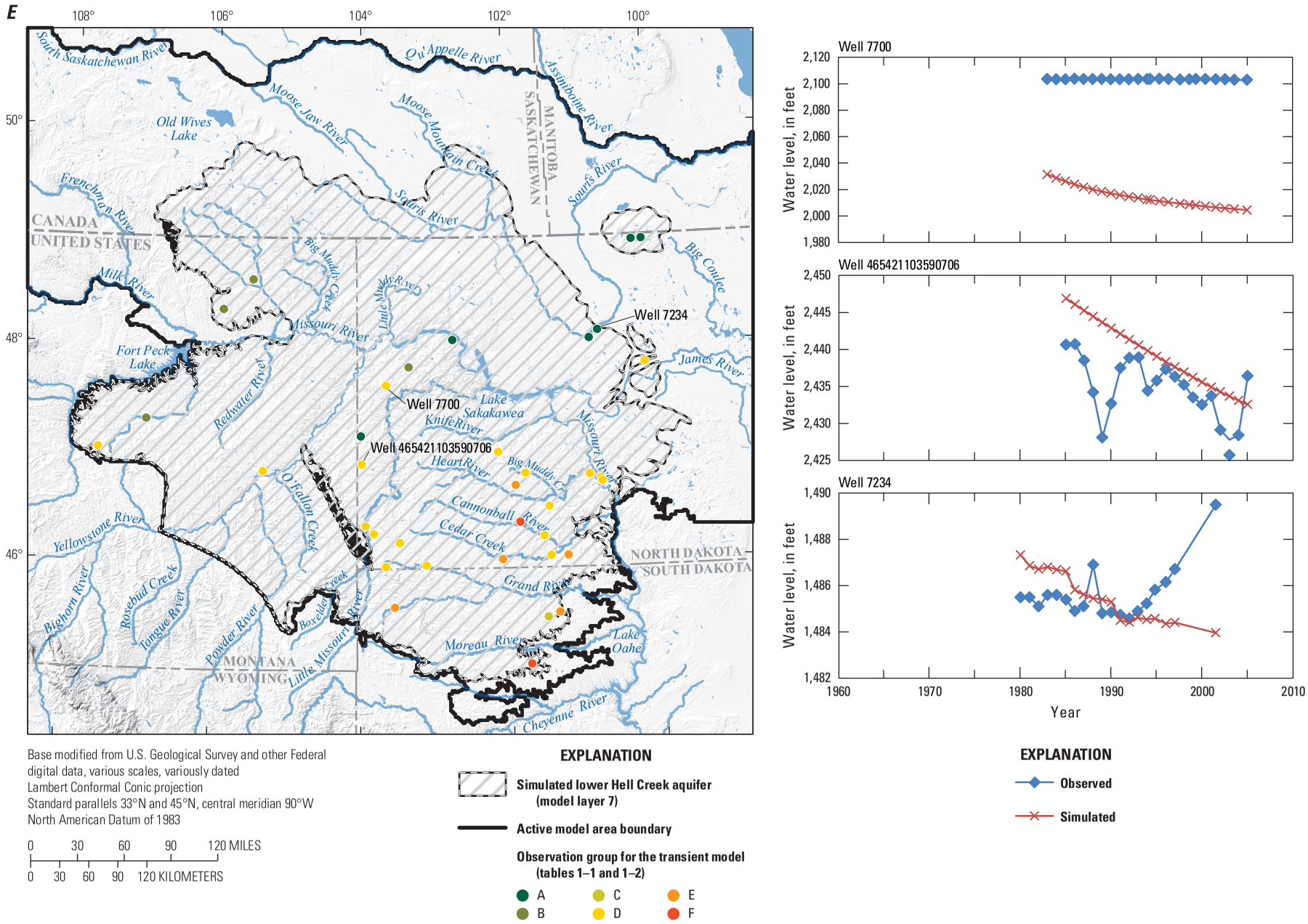

Figure 15. Maps and selected hydrographs showing observed and simulated hydraulic head for the transient model for the *A*, upper part of the glacial aquifer system; *B*, lower part of the glacial aquifer system; *C*, upper Fort Union aquifer; *D*, lower Fort Union aquifer; *E*, lower Hell Creek aquifer; and *F*, Fox Hills aquifer.—Continued

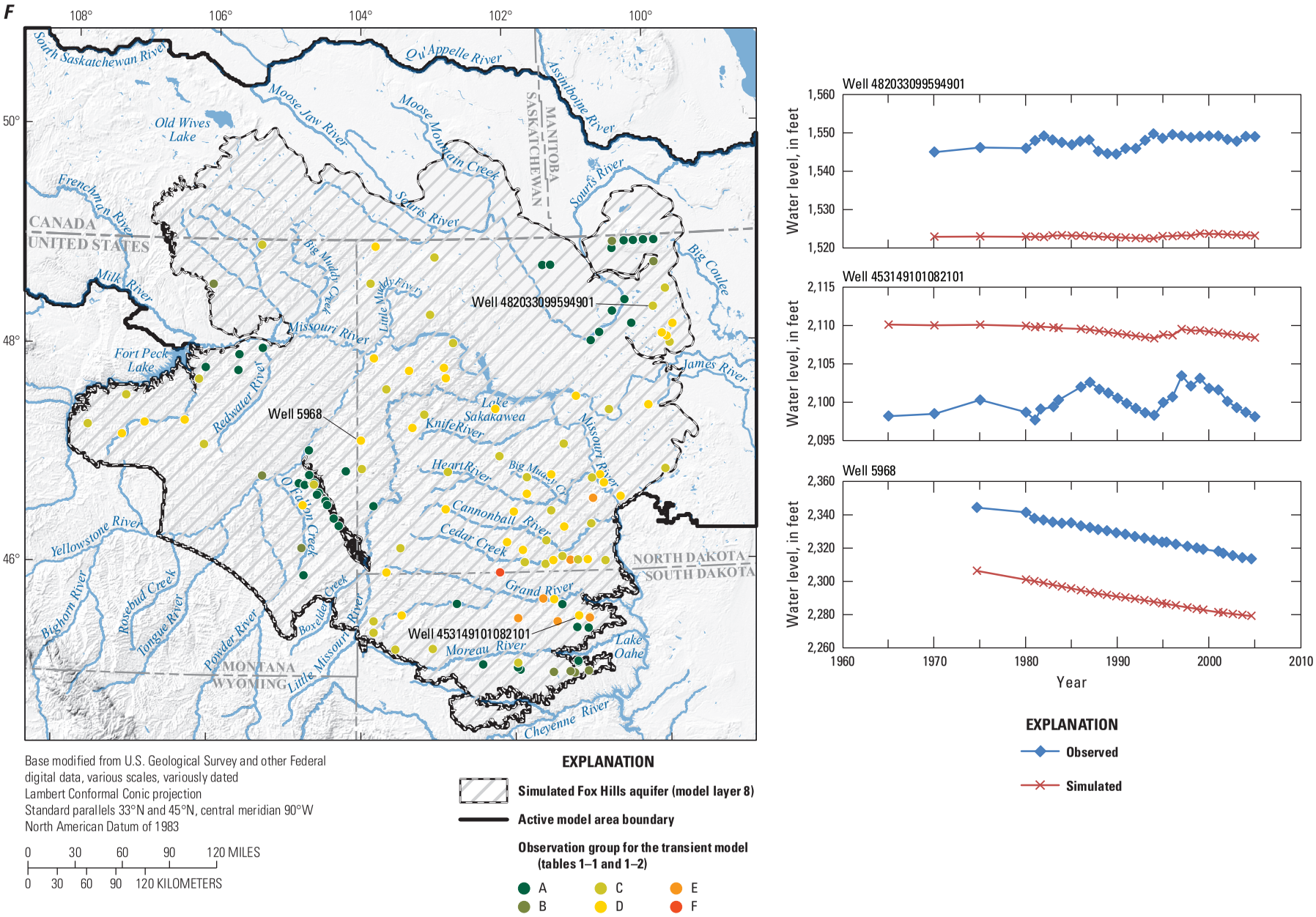

Figure 15. Maps and selected hydrographs showing observed and simulated hydraulic head for the transient model for the *A*, upper part of the glacial aquifer system; *B*, lower part of the glacial aquifer system; *C*, upper Fort Union aquifer; *D*, lower Fort Union aquifer; *E*, lower Hell Creek aquifer; and *F*, Fox Hills aquifer.—Continued

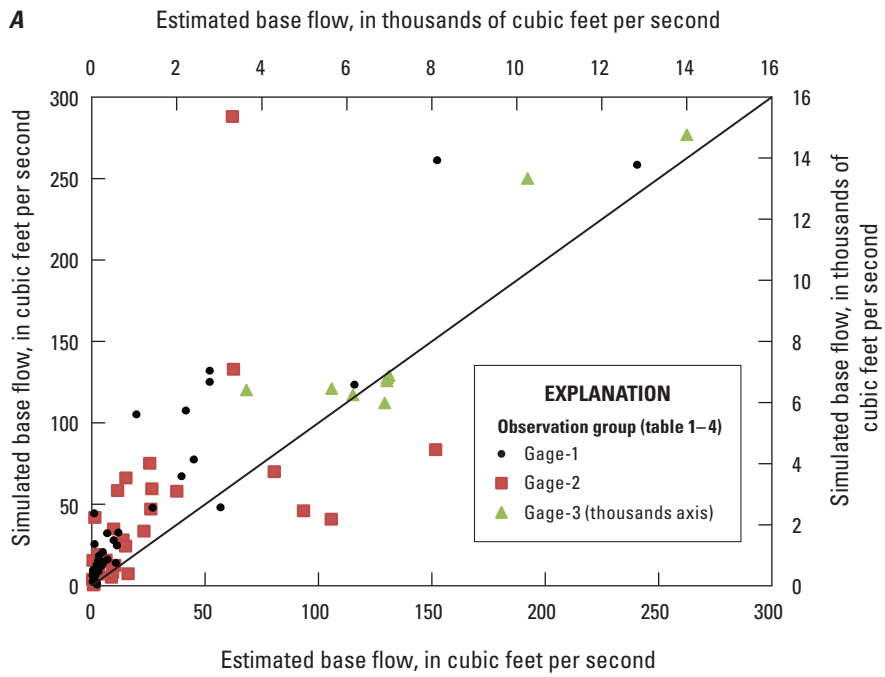

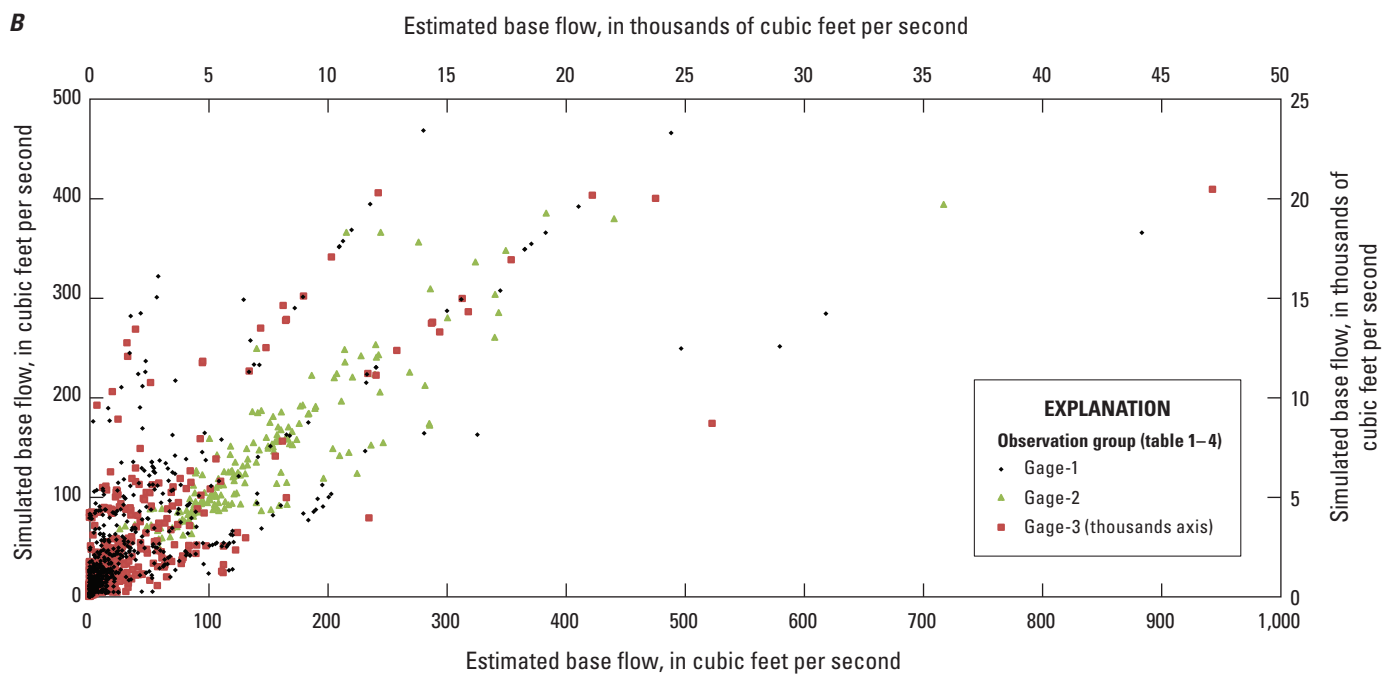

Figure 16. Comparison of observed (estimated) and simulated base flow for the *A*, steady-state (1981–2005) model and *B*, transient model. The 1:1 perfect fit line also is shown for reference to visualize bias. [See table 2–4 for descriptions of Gage-1, Gage-2, and Gage-3].

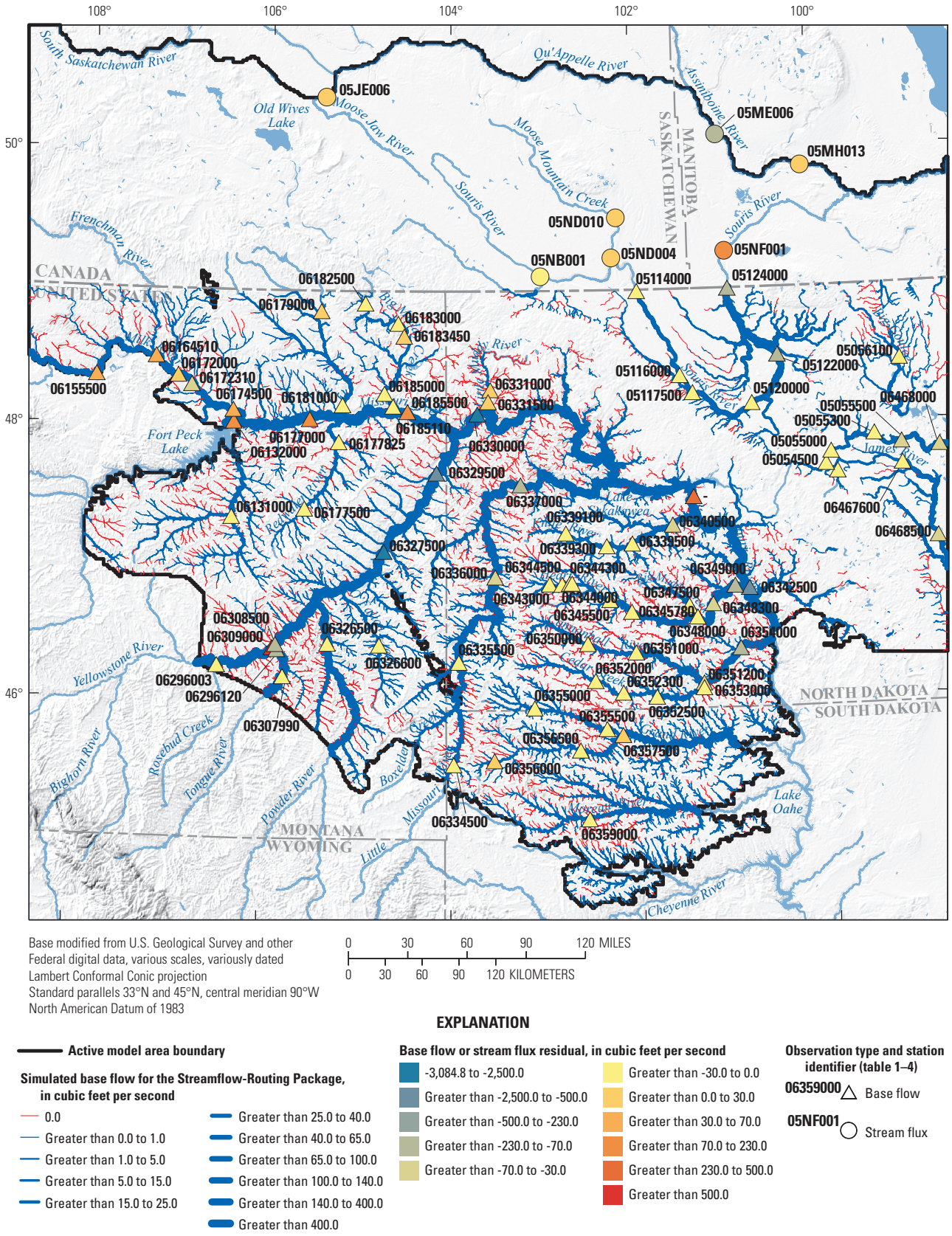

Base modified from U.S. Geological Survey and other Federal digital data, various scales, variously dated
Lambert Conformal Conic projection
Standard parallels 33°N and 45°N, central meridian 90°W
North American Datum of 1983

0 30 60 90 120 MILES
0 30 60 90 120 KILOMETERS

EXPLANATION

Active model area boundary

Simulated base flow for the Streamflow-Routing Package, in cubic feet per second

- 0.0
- Greater than 0.0 to 1.0
- Greater than 1.0 to 5.0
- Greater than 5.0 to 15.0
- Greater than 15.0 to 25.0
- Greater than 25.0 to 40.0
- Greater than 40.0 to 65.0
- Greater than 65.0 to 100.0
- Greater than 100.0 to 140.0
- Greater than 140.0 to 400.0
- Greater than 400.0

Base flow or stream flux residual, in cubic feet per second

- -3,084.8 to -2,500.0
- Greater than -2,500.0 to -500.0
- Greater than -500.0 to -230.0
- Greater than -230.0 to -70.0
- Greater than -70.0 to -30.0
- Greater than -30.0 to 0.0
- Greater than 0.0 to 30.0
- Greater than 30.0 to 70.0
- Greater than 70.0 to 230.0
- Greater than 230.0 to 500.0
- Greater than 500.0

Observation type and station identifier (table 1–4)

- 06359000 △ Base flow
- 05NF001 ○ Stream flux

Figure 17. Base-flow or stream-flux residuals (observed minus simulated values) for the Gage Package and base flow from the Streamflow-Routing (SFR2) Package for the steady-state (1981–2005) model.

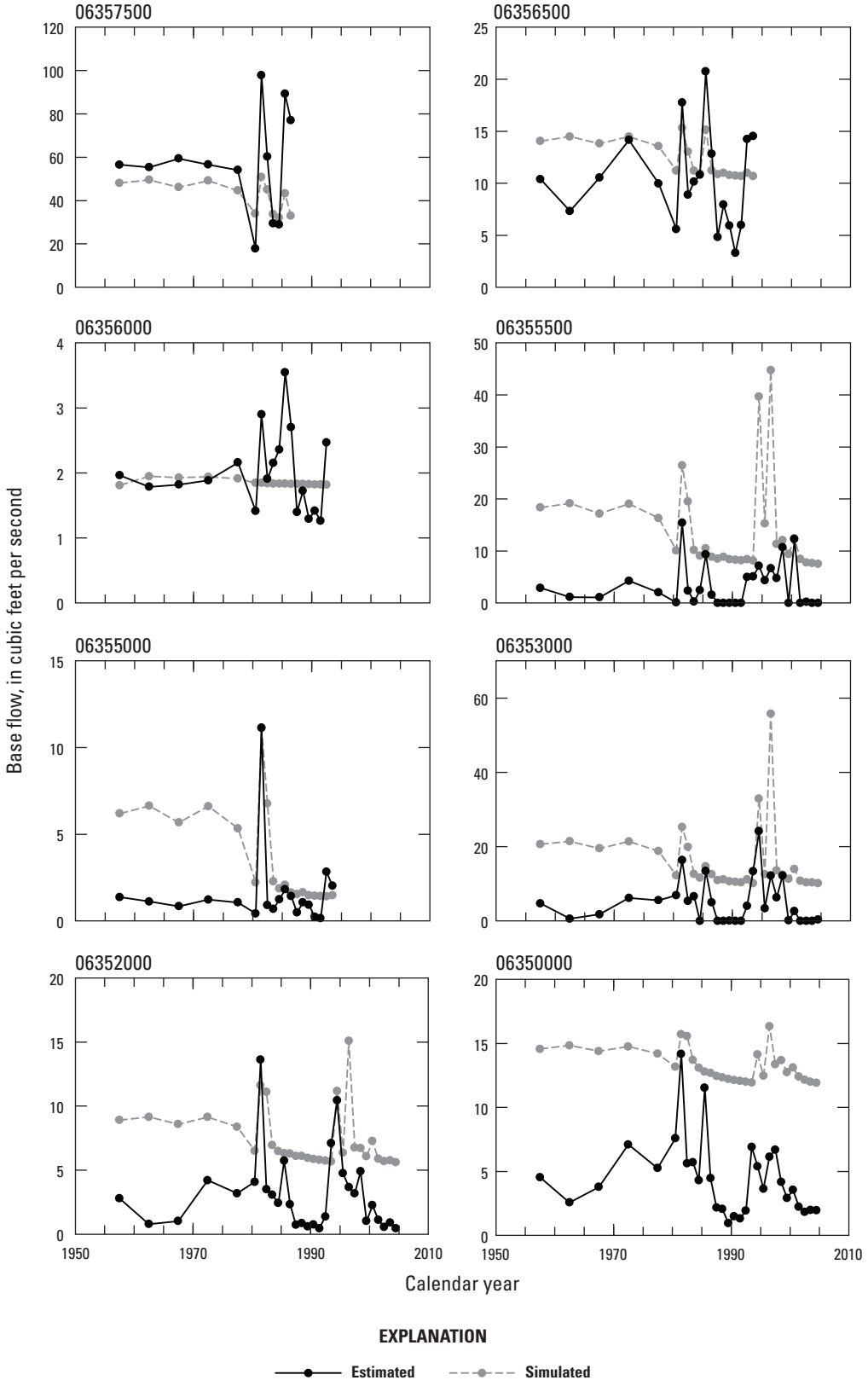

Figure 18. Observed (estimated) hydrographs and simulated hydrographs using the transient model for streamgages with 10 or more years of streamflow record and contributing drainage area entirely within the model area.

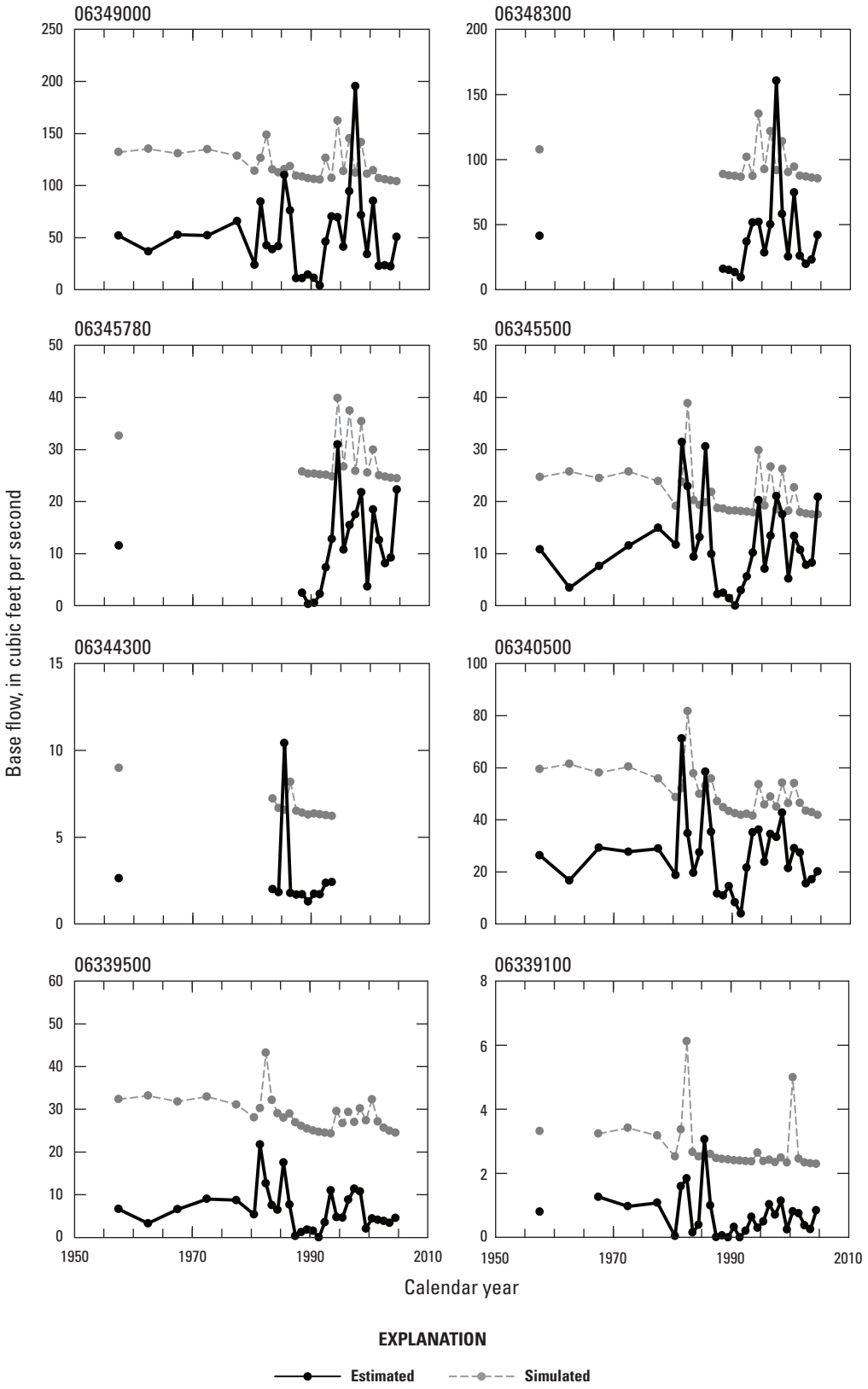

Figure 18. Observed (estimated) hydrographs and simulated hydrographs using the transient model for streamgages with 10 or more years of streamflow record and contributing drainage area entirely within the model area.—Continued

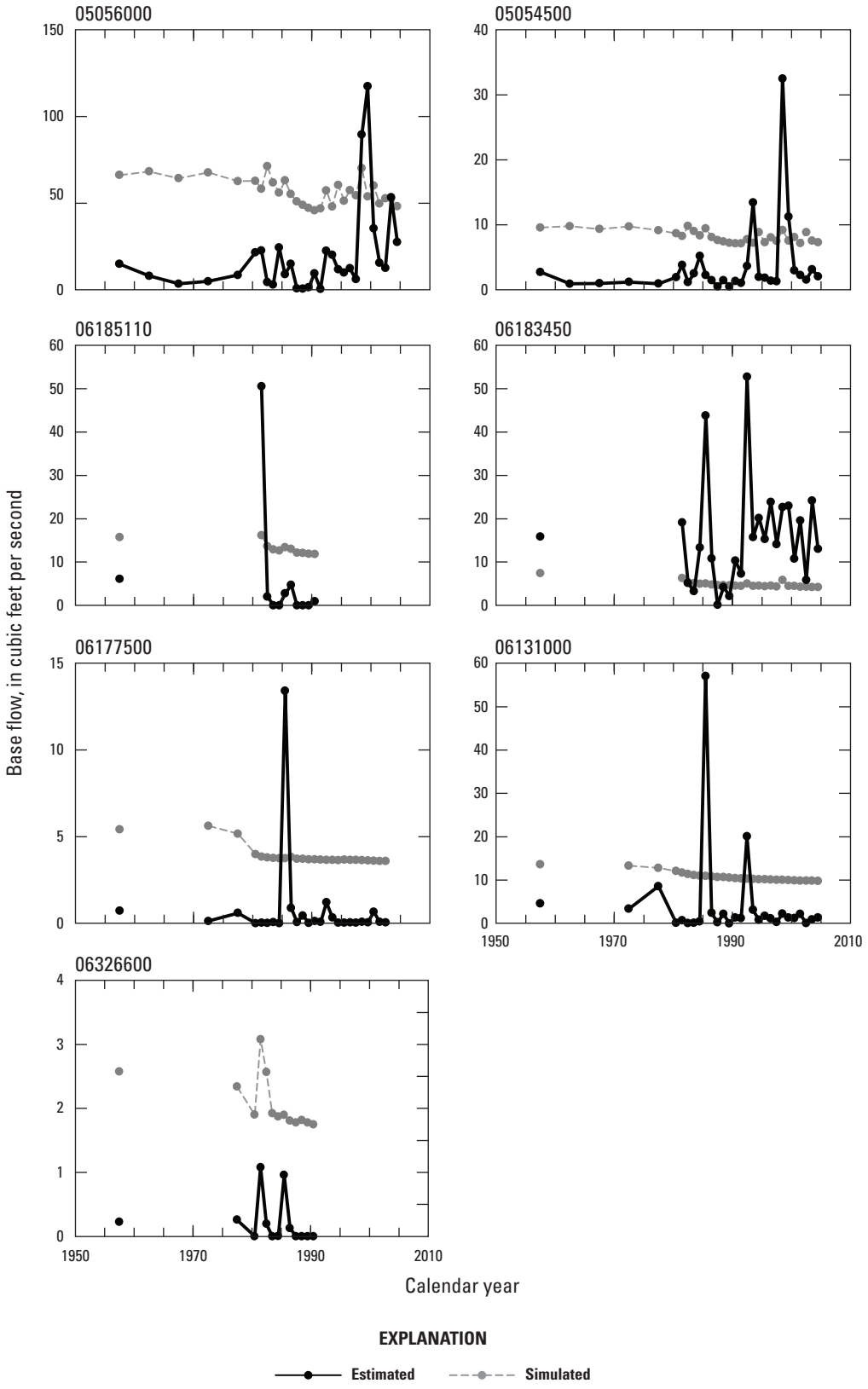

Figure 18. Observed (estimated) hydrographs and simulated hydrographs using the transient model for streamgages with 10 or more years of streamflow record and contributing drainage area entirely within the model area.—Continued

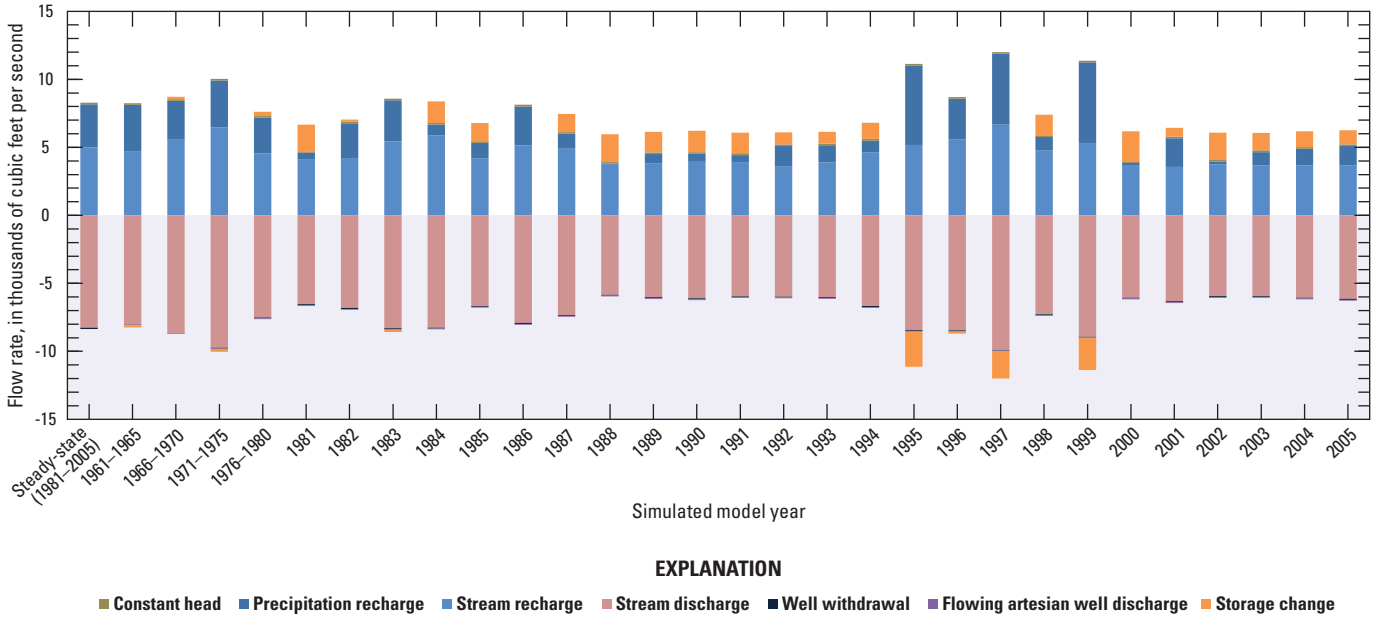

Figure 19. Simulated groundwater budgets for the steady-state (1981–2005) and transient models.

The estimated and simulated groundwater budgets indicate that the model area received a substantial amount of recharge from precipitation, stream infiltration, and recharge from reservoirs. Simulated reservoir seepage (recharge from reservoirs) was a larger component of recharge in the Williston Basin compared to the estimated value (table 1). Irrigation recharge, groundwater inflow from the Powder River Basin, and groundwater inflow from the glacial aquifer system outside the control volume accounted for a relatively small part of the total groundwater recharge in the Williston Basin. The sum of these components of groundwater recharge accounted for less than 3 percent of estimated total groundwater recharge, and the simulated values account for less than 7 percent of total groundwater recharge (table 1). Simulated discharge components match well with estimated values. Estimated and simulated groundwater discharge to streams in the numerical model area accounted for about 97 and 52 percent of the total groundwater discharge, respectively. The model simulated less groundwater withdrawal and a greater discharge to reservoirs when compared to published estimates (table 1). Groundwater outflow to the glacial aquifer system outside the control volume was not estimated by Thamke and others (2014) but accounted for about 4 percent of total simulated groundwater discharge. Groundwater flow was typically from outcrop areas (where the aquifers receive recharge from precipitation) toward streams (where the aquifers discharge).

Streams flowing into Lake Sakakawea were simulated with the SFR2 Package (Niswonger and Prudic, 2005), whereas the reservoir was simulated with the RIV Package (Harbaugh, 2005). At reservoir edges, these stream cells interact directly with reservoir cells. Simulated groundwater recharge from and discharge to reservoirs (table 1) was obtained from model output by isolating the reservoir area and calculating the groundwater budget for that area. To minimize potential artificial boundary effects at the transition from stream cells to reservoir cells that might result from differences in how the SFR2 and RIV Packages calculate groundwater flows, the area used for the reservoir water budget was slightly larger than the surface area of the reservoir. This area included two stream cells directly upstream from the reservoir for each inflowing stream. This assured a smooth transition of groundwater flow across the boundary of the reservoir water-budget area. On this basis, the numerical model simulated large values for recharge from and discharge to reservoirs (table 1) compared to the estimated values; however, the updated reservoir area equates to a net groundwater discharge into the reservoir of 34 ft^3/s, which is similar the estimated value.

The simulated groundwater budget for the upper Fort Union aquifer indicates that this aquifer typically receives recharge from precipitation and stream infiltration, with the largest recharge component being from reservoirs, and groundwater discharge is primarily to nearby streams (table 8). Groundwater inflow from the overlying glacial aquifer system and inflow from the underlying middle Fort Union hydrogeologic unit and lower Fort Union aquifer accounted for a much smaller component of overall recharge compared to precipitations and stream infiltration to the upper Fort Union aquifer. Groundwater discharge to streams was the largest component of aquifer discharge. Well withdrawal and groundwater outflow to the overlying glacial aquifer system and underlying middle Fort Union hydrogeologic unit and lower Fort Union aquifer accounted for a smaller component of total discharge compared to discharge to streams from the aquifer.

Table 8. Simulated steady-state groundwater recharge and discharge components for 1981–2005 for the upper Fort Union aquifer.

[ft³/s, cubic foot per second; --, not simulated]

Recharge or discharge component	Simulated	
	ft³/s	Percent[a]
Groundwater recharge		
Precipitation recharge	536	24
Stream infiltration	340	15
Recharge from reservoirs	1,101	48
Groundwater inflow from the Powder River Basin[b]	--	0
Groundwater inflow from the glacial aquifer system	116	5
Groundwater inflow from the middle Fort Union hydrogeologic unit	138	6
Groundwater inflow from the lower Fort Union aquifer	44	2
Total recharge	2,275	100
Groundwater discharge		
Discharge to streams	1,575	69
Discharge to reservoirs	321	14
Groundwater (well) withdrawal	22	1
Groundwater outflow to the glacial aquifer system	58	3
Groundwater outflow to the middle Fort Union hydrogeologic unit	233	10
Groundwater outflow to the lower Fort Union aquifer	65	3
Total discharge	2,274	100

[a]The percentage of total recharge or total discharge.

[b]Calculated as the difference between recharge and discharge.

Table 9. Simulated steady-state groundwater recharge and discharge components for 1981–2005 for the lower Fort Union aquifer.

[ft³/s, cubic foot per second; <, less than]

Recharge or discharge component	Simulated	
	ft³/s	Percent[a]
Groundwater recharge		
Precipitation recharge	214	36
Stream infiltration	16	3
Groundwater inflow from the Powder River Basin[b]	2	<1
Groundwater inflow from the glacial aquifer system	51	8
Groundwater inflow from the upper Fort Union aquifer	65	11
Groundwater inflow from the middle Fort Union hydrogeologic unit	177	29
Groundwater inflow from the upper Hell Creek hydrogeologic unit	76	13
Total recharge	601	100
Groundwater discharge		
Discharge to streams	235	37
Groundwater (well) withdrawal	4	1
Groundwater outflow to the glacial aquifer system	21	3
Groundwater outflow to the upper Fort Union aquifer	44	7
Groundwater outflow to the middle Fort Union hydrogeologic unit	56	9
Groundwater outflow to the upper Hell Creek hydrogeologic unit	267	43
Total discharge	627	100

[a]The percentage of total recharge or total discharge; may not equal 100 because of rounding.

[b]Calculated as the difference between recharge and discharge.

The simulated groundwater budget for the lower Fort Union aquifer indicates that it primarily received recharge from precipitation and groundwater inflow from the overlying middle Fort Union hydrogeologic unit (table 9). Smaller components of simulated recharge for the lower Fort Union aquifer are groundwater inflow from the overlying glacial and upper Fort Union aquifers and inflow from the underlying upper Hell Creek hydrogeologic unit. The primary discharge component for the lower Fort Union aquifer was groundwater outflow to the underlying upper Hell Creek hydrogeologic unit. The remaining discharge components from the lower Fort Union aquifer were groundwater withdrawals, discharge to streams, and groundwater outflow to the overlying glacial aquifer system, upper Fort Union aquifer, and middle Fort Union hydrogeologic unit. Groundwater discharge in major stream valleys was indicated by vertical head gradients in those areas.

Simulated recharge to the Fox Hills aquifer was primarily from precipitation recharge and groundwater inflow from the overlying lower Hell Creek aquifer (table 10). Minor simulated recharge components were stream infiltration and groundwater inflow from the Powder River Basin and the overlying glacial aquifer system. Primary discharge components for the Fox Hills aquifer were discharge to streams and groundwater outflow to the overlying lower Hell Creek aquifer. Minor discharge components are groundwater withdrawals and groundwater outflow to the glacial aquifer system. Groundwater flow in the Fox Hills aquifer was much more regionalized than the overlying aquifers; however, local discharge was to major streams including the Yellowstone River, Little Missouri River, and Missouri River (fig. 11). The simulated potentiometric surface for the Fox Hills aquifer was above the land surface in the major stream valleys, which produced vertical upward groundwater-flow gradients in these areas.

Table 10. Simulated steady-state groundwater recharge and discharge components for 1981–2005 for the Fox Hills aquifer.

[ft³/s, cubic foot per second]

Recharge or discharge component	Simulated	
	ft³/s	Percent[a]
Groundwater recharge		
Precipitation recharge	119	27
Stream infiltration	10	2
Groundwater inflow from the Powder River Basin[b]	11	3
Groundwater inflow from the glacial aquifer system	48	11
Groundwater inflow from the lower Hell Creek aquifer	252	57
Total recharge	440	100
Groundwater discharge		
Discharge to streams	256	57
Groundwater (well) withdrawal	4	1
Groundwater outflow to the glacial aquifer system	38	9
Groundwater outflow to the lower Hell Creek aquifer	148	33
Total discharge	446	100

[a]The percentage of total recharge or total discharge.

[b]Calculated as the difference between recharge and discharge.

Flowing Artesian Wells

The transient model was used to simulate discharge from 571 flowing artesian wells within the model area (figs. 6 and 20). Of the 571 established flowing artesian wells simulated by the model, 271 wells did not flow at any time during the simulation because hydraulic head was always below the land-surface altitude. As hydraulic head declined throughout the simulation, 68 of these wells responded by ceasing to flow by the end of 2005. The total simulated discharge for 571 flowing artesian wells ranged from 22.5 to 61.4 ft³/s, and the mean total simulated discharge was 55.1 ft³/s. The mean simulated discharge from the individual flowing wells ranged from 0.039 to 0.177 ft³/s, and the overall simulated mean from the individual flowing wells was 0.118 ft³/s. Of the 34 wells that were used for model calibration, the mean residual (observed minus simulated) was 0.014 ft³/s and ranged from -0.045 to 0.360 ft³/s. The positive mean residual for the transient model flowing wells indicates a tendency by the model to underestimate discharge to flowing artesian wells with measured discharge rates. The total simulated discharge to flowing artesian wells typically increased between 1961 and 1981 and began slowly decreasing in 1982 through the end of the transient simulation period (fig. 20). Simulated mean discharge to flowing artesian wells increased from 0.039 to 0.177 ft³/s between 1961 and 1975 and decreased to 0.102 ft³/s between 1975 and 2005. Decreases in discharge to flowing wells are consistent with pressure head declines observed at flowing artesian wells in the model area (Honeyman, 2007a, b, c).

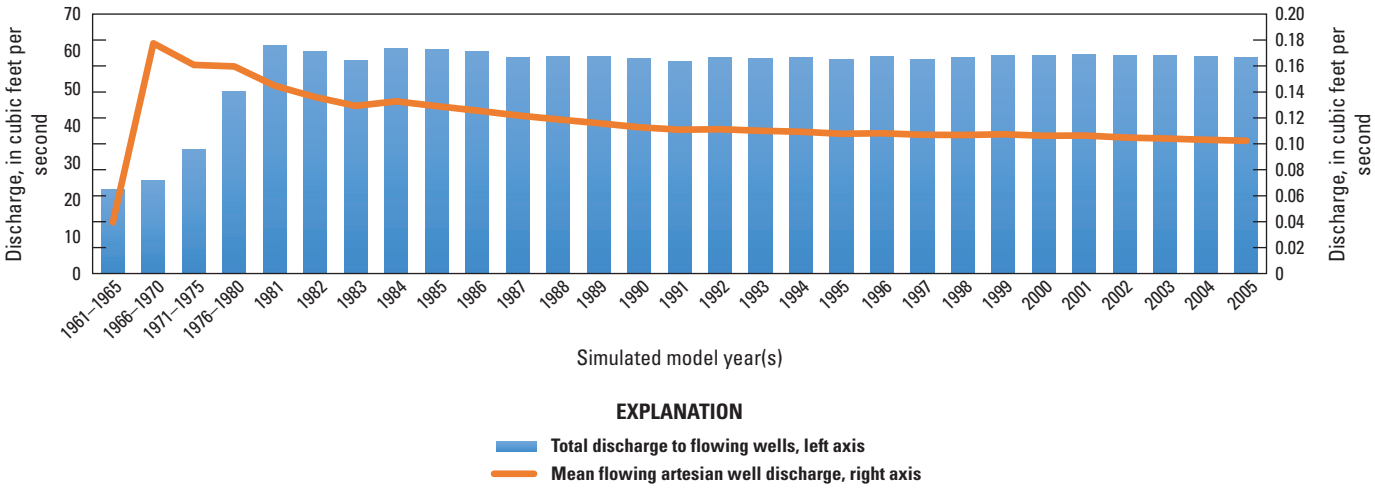

Figure 20. Total discharge to flowing artesian wells and mean flowing artesian well discharge as simulated by the Multi-Node Well Package for the transient model.

Parameter Sensitivity and Identifiability

A simulated observation is a simulated model-output value collocated in time and space with an observation. The Jacobian matrix is composed of sensitivity values relating each simulated observation to each parameter (Doherty, 2010). Sensitivity is defined as the change in simulated observations in response to changes in parameter values:

$$\frac{\partial y_i}{\partial p_j} \tag{1}$$

where

∂y	is an infinitesimal change in a simulated observation value,
∂p	is an infinitesimal change in a parameter value,
i	represents the ith observation (i=1, 2, …, *NOBS*),
j	represents the jth parameter (j=1, 2, …, *NPAR*),
NOBS	is the number of observations, and
NPAR	is the number of parameters.

The result of evaluating equation 1 for all combinations of parameters and simulated observations is the *NOBS* by *NPAR* Jacobian matrix. Sensitivity can also provide insight into which parameters have the greatest effect on modeled forecasts. In fact, sensitivity can be considered as one metric of parameter importance. A challenge is met in that parameters are often correlated with one another, so sensitivity can be misleading when used to evaluate parameter importance. Correlation is evaluated in pairs of parameters; therefore, with thousands of parameters, it is impractical to evaluate sensitivity and correlation independently.

Parameter identifiability, as described by Doherty and Hunt (2009), is more informative than simple sensitivity analysis because interference of parameter correlation is minimized. Parameter identifiability is based on SVD, which reassembles all parameters by combining them into linear combinations of new parameters, hereafter referred to as "SV parameters," that best describe the effect the model has on simulated observations. For clarity, the original parameters are hereafter referred to as "native parameters." The SV parameters are oriented along major axes of the overall variability of weighted native-parameter sensitivity, as defined by the Jacobian matrix and observation weights. In model calibration, SVD is useful because the SV parameters are ranked according to their effect on observations, and the calibration process focuses on the most influential SV parameters; for example, the 50 highest ranking SV parameters might be adjusted during model calibration, and the remaining SV parameters—having little effect on residuals—are ignored. For readers familiar with principle-component analysis (Davis, 2002), SVD is similar to a principal-component analysis applied to the Jacobian matrix.

Parameter identifiability is a metric that indicates qualitatively how much information from the overall set of observations is projected onto the native parameters during calibration. The identifiability value represents the projection of the most valuable information from observations onto the calibration space by analyzing the effect of the highest ranking SV parameters. The remaining information that is less useful is projected onto the null space, meaning native-parameter values can change potentially by large amounts without affecting the model outputs of interest.

Native parameters with high identifiability are well informed by the observations, whereas native parameters with low identifiability are ill informed by the observations and are generally held relatively constant during calibration by SVD. Identifiability values range from 0.0 (no projection of observation information onto native parameters) to 1.0 (complete projection of information onto native parameters). The solution and null spaces are defined by a cutoff value that determines how many of the highest ranked SV parameters will be included in the analysis. The high-ranking and low-ranking SV parameters correspond to what is considered information (calibration space) and noise (null space), respectively. If all SV parameters are included, then identifiability would be 1.0 for all parameters.

Parameter identifiability is shown in figure 21, where the overall height of each bar indicates the degree of parameter identifiability. The 28 most identifiable parameters (identifiability greater than 0.5) for the steady-state model when the number of SV parameters considered is 50 are shown in figure 21. Of these 28 parameters, three are for streambed hydraulic conductivity (st6, st25, and st44), two are recharge multipliers (rm1 and rm3), two are for vertical hydraulic conductivity (UHC_kz123 and FH_kz6a), and the remaining 21 are pilot points for horizontal hydraulic conductivity (table 11). The beginning capital letters in the names of the hydraulic-conductivity parameters refer to property zones (table 2), and "kx" and "kz" refer to horizontal hydraulic conductivity and vertical hydraulic conductivity, respectively. Details of these and other model parameters are documented in the electronic archive for the model (Davis and Long, 2018).

On each bar of the identifiability graph (fig. 21), the contribution to identifiability resulting from each SV parameter is displayed by color, where each additional SV parameter is separated by a black line. Warm colors (low values) indicate identifiability attributable to the most informative SV parameters, whereas cool colors indicate identifiability attributable to the least informative SV parameters; for example, parameters st6, rm3, and rm1 at the left end of figure 21 have an identifiability close to 1.0, and each are primarily represented by three or four SV parameters, indicated by the different colors on the plot. These three native parameters with the highest identifiability could be well calibrated if only 5 to 10 SV parameters are adjusted; therefore, bars that are made up almost entirely of warm colors can be qualitatively interpreted as having overall higher identifiability than those containing cool colors

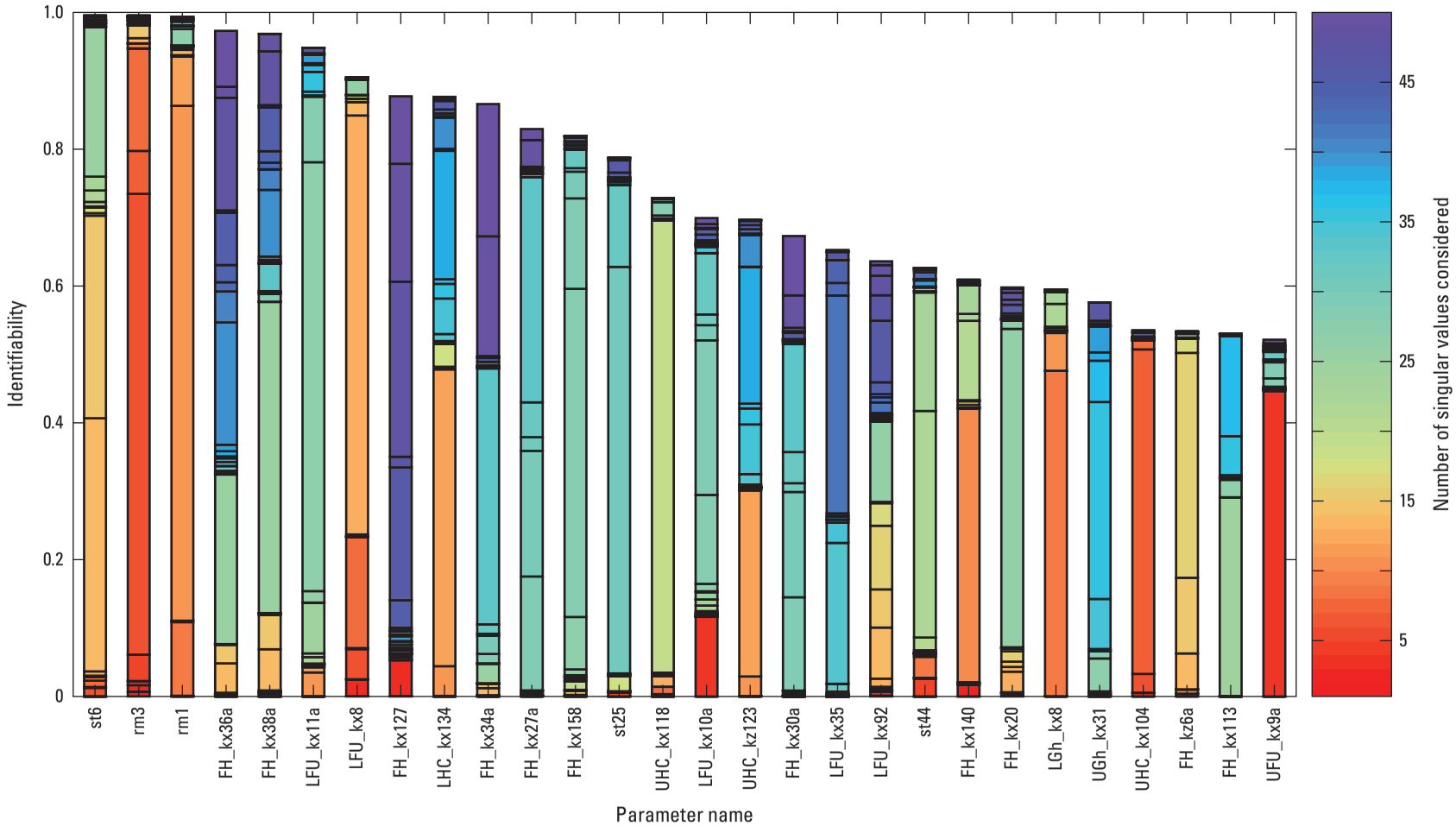

EXPLANATION

Streambed hydraulic conductivity (st) parameters are denoted using the convention "st" and the parameter number. Recharge multiplier (rm) parameters are denoted using the convention "rm" and the parameter number. Pilot point parameters are denoted using the property zone abbreviation, horizontal (kx) or vertical (kz) hydraulic conductivity identifier, and pilot point number. All parameters are defined in table 11. Pilot point parameters denoted with an "a" at the end are supplemental points and do not correspond to estimates provided by Thamke and others (2014).

FH, Fox Hills aquifer; LFU, lower Fort Union aquifer; LHC, lower Hell Creek aquifer; UHC, upper Hell Creek hydrogeologic unit; LGh, lower part of glacial aquifer system; UGh, upper part of the glacial aquifer system; UFU, upper Fort Union aquifer.

Figure 21. Identifiability of all parameters with values greater than 0.5 for the steady-state model, when the 50 highest ranking singular-value (SV) parameters are considered.

Table 11. Parameters with identifiability values greater than 0.5 for the steady-state model.

[Streambed hydraulic conductivity (st) parameters are denoted using the convention "st" and the parameter number; recharge multiplier (rm) parameters are denoted using the convention "rm" and the parameter number; pilot point parameters are denoted using the property zone abbreviation, horizontal (kx) or vertical (kz) hydraulic conductivity identifier, and pilot point number; pilot point parameters denoted with an "a" at the end are supplemental points and do not correspond to estimates provided by Thamke and others (2014); --, not applicable; FH, Fox Hills aquifer; LFU, lower Fort Union aquifer; LHC, lower Hell Creek aquifer; UHC, upper Hell Creek hydrogeologic unit; LGh, lower part of the glacial aquifer system-high; UGh, upper part of the glacial aquifer system-high]

Parameter name (fig. 21)	Parameter description	Property zone (table 2)	Parameter name used in Davis and Long (2018)
st6	Streambed hydraulic conductivity	--	st6
rm3	Spatial recharge multiplier for the lower Tertiary and Upper Cretaceous aquifer systems	--	rm3
rm1	Spatial recharge multiplier for the glacial aquifer system	--	rm1
FH_kx36a	Horizontal hydraulic conductivity pilot point	FH	8aKx36
FH_kx38a	Horizontal hydraulic conductivity pilot point	FH	8aKx38
LFU_kx11a	Horizontal hydraulic conductivity pilot point	LFU	5aKx11
LFU_kx8	Horizontal hydraulic conductivity pilot point	LFU	5Kx8
FH_kx127	Horizontal hydraulic conductivity pilot point	FH	8Kx127
LHC_kx134	Horizontal hydraulic conductivity pilot point	LHC	5Kx134
FH_kx34a	Horizontal hydraulic conductivity pilot point	FH	8aKx34
FH_kx27a	Horizontal hydraulic conductivity pilot point	FH	8aKx27
FH_kx158	Horizontal hydraulic conductivity pilot point	FH	8Kx158
st25	Streambed hydraulic conductivity	--	st25
UHC_kx18	Horizontal hydraulic conductivity pilot point	UHC	8Kx18
LFU_kx10a	Horizontal hydraulic conductivity pilot point	LFU	5aKx10
UHC_kz123	Vertical hydraulic conductivity pilot point	UHC	3Kz123
FH_kx30a	Horizontal hydraulic conductivity pilot point	FH	8aKx30
LFU_kx35	Horizontal hydraulic conductivity pilot point	LFU	5Kx35
LFU_kx92	Horizontal hydraulic conductivity pilot point	LFU	5Kx92
st44	Streambed hydraulic conductivity	--	st44
FH_kx140	Horizontal hydraulic conductivity pilot point	FH	8Kx140
FH_kx20	Horizontal hydraulic conductivity pilot point	FH	8Kx20
LGh_kx8	Horizontal hydraulic conductivity pilot point	LGh	g2_hx8
UGh_kx31	Horizontal hydraulic conductivity pilot point	UGh	g1_hx31
UHC_kx104	Horizontal hydraulic conductivity pilot point	UHC	6Kx104
FH_kz6a	Vertical hydraulic conductivity pilot point	FH	8Kz6A
FH_kx113	Horizontal hydraulic conductivity pilot point	FH	8Kx113
UFU_kx9a	Horizontal hydraulic conductivity pilot point	UFU	3Kx9A

because these parameters are well described by the fewest SV parameters.

Three of the top 28 most identifiable parameters are streambed hydraulic conductivity parameters used in the SFR package (fig. 21). In general, these parameters affected outputs that corresponded to calibration targets of base flow and hydraulic head. Streambed hydraulic conductivity parameter st6, the highest identifiable parameter, is present along the Moreau River (figs. 1 and 6) and its tributaries in the southern part of the model area near a substantial number of hydraulic head observation targets in layer 7 and layer 8 (fig. 13). In particular, this parameter has a substantial effect on the hydraulic head observation targets in that area because this parameter controls the amount of groundwater and surface-water interactions that can exist in that area.

Recharge multipliers rm1 and rm3 indicate high identifiability (fig. 21). Recharge is a vital component to the water balance and is expected to be an important process in the model. In particular, parameter rm1, the recharge multiplier for the glacial part of the model, indicates high identifiability. The SWB-estimated recharge in the model is low, and for this reason, it is easily recognized that small changes in simulated

recharge result in larger changes in calculated groundwater flow in the model.

Of the top 28 most identifiable parameters, 21 are horizontal hydraulic conductivity pilot points. Although the horizontal hydraulic conductivity pilot point parameters are not the most identifiable, they constitute a greater number of highly identifiable parameters than any other parameter type (fig. 21); therefore, it may be inferred that model calibration targets are greatly affected by these horizontal hydraulic conductivity parameters. Horizontal and vertical hydraulic conductivity affect how water moves throughout the groundwater system, and changes to these parameters has a strong effect on stream base flow, stream flux, and hydraulic head observation targets.

Model Limitations and Assumptions

The numerical model is a set of numerical equations designed to represent a complex natural system; nevertheless, the numerical model adequately simulated flow in the uppermost principal aquifer systems in the Williston Basin based on the comparison between the simulated and estimated groundwater-flow budget, the comparison between simulated and observed (estimated) potentiometric surfaces, and the results of the calibration process. As with any model, however, certain limitations should be considered. Model limitations arise from aspects of the conceptual model and from simplifications inherent in the construction and calibration of the numerical model. These limitations include uncertainties in many of the numerical model input parameters, such as aquifer hydraulic conductivity and storage properties, which greatly affected model results. Extensive prior information was not available for most parameters; therefore, these parameters were estimated or calculated using the literature and observation data that were available. Recharge was calculated by subtracting evapotranspiration from precipitation using the SWB method, which included assumptions and limitations inherent to the SWB method (Westenbroek and others, 2010).

The numerical model is limited in its application by simplifying assumptions that were necessary to represent the aquifers mathematically. Aquifer properties were averaged for a set of rectangular cells that represented a finite volume of aquifer material that could vary substantially within that volume. The materials that make up these aquifers were deposited in many discontinuous layers that ranged from impermeable clays to very permeable sands and gravels. Local hydraulic properties could vary substantially from the generalized representation in the model. Hydraulic connection between depositional layers could be very discontinuous. As a result, the actual response of the aquifers to local stress could vary substantially from that represented by the model. Ranges of hydraulic conductivity used in the numerical model were based on general ranges of previously published values, but final values were determined through model calibration. Model accuracy depends, in part, on the accuracy of the estimates of model input parameters; nevertheless, calibration of the model yielded hydraulic conductivity distributions that were deemed acceptable, given the data available. It is reasonable to assume that similar hydraulic conductivity distributions that also would yield satisfactory model results could exist.

The primary parameters used in the transient model were specific storage and specific yield. Spatially uniform values were used for the bedrock layers and for the zones in the glacial aquifers. Spatially varied values were not used in the transient model for three primary reasons: (1) local information for specific storage was not available, (2) long transient model run times made calibration of a large number of parameters difficult, and (3) groundwater-level changes generally were small or localized in the model area and did not provide a substantial amount of information for the calibration of the transient model. Spatial differences in aquifer storage (specific storage and specific yield) are likely to exist within the Williston Basin; however, the calibrated values were within the ranges of previously estimated values (tables 3, 4, and 6).

Boundary conditions that represented hydrologic features in the model were created with the best available data. Some boundary condition locations were assumed based on expert knowledge of the hydrologic system, and other boundary conditions were placed at locations that best represented known hydrologic features. Additionally, hydrologic features were represented at a scale that was coincident with the model grid. Simplifying assumptions were needed to downscale some hydrologic information for the inclusion in the model (for example, the number of wells represented by the steady-state model). A greater degree of variability exists than can be represented by boundary conditions at the scale of the model; however, it was assumed that for the purposes of a regionalized groundwater-flow model, the scale and the simplifying assumptions were necessary and appropriate.

Temporally, the model was discretized into 5-year and 1-year stress periods. This temporal discretization was determined primarily by data resolution but also by assuming that the 5-year and 1-year increments were appropriate for assessing groundwater availability at the regional scale. Each stress period incorporates mean input values for groundwater withdrawal, streamflow, and precipitation recharge. Additionally, calibration information was down-scaled so that only one calibration value for each target type was used per stress period. A greater degree of temporal variability exists than can be represented at the scale of the model, and no attempt was made to interpret model results at a greater variability than the stress-period lengths represented by the model.

Discharge from individual flowing artesian wells completed in the lower Hell Creek and Fox Hills aquifers was used in the calibration of the transient model. For many of these wells, measured flow rates were unavailable. Additionally, the actual number of flowing wells that exist in the model area is unknown (Wanek, 2009; Fischer, 2013). A potential source of error with the simulated flowing wells is that there is a high probability of groundwater originating from the Fox Hills and lower Hell Creek aquifers that is discharging to the

upper Hell Creek hydrogeologic unit or lower Tertiary aquifer system through compromised casings in older flowing wells (Fischer, 2013). This process is not simulated with the model because the flowing wells are only open to the Fox Hills and lower Hell Creek aquifers (layers 7 and 8).

Additional considerations apply where the numerical model represents the glacial aquifers, especially in areas where deposits are thin. In many stress periods, the thin areas in the glacial aquifer system (layers 1 and 2) were simulated as being dry; therefore, these areas may not be well represented by the model. Groundwater withdrawals in parts of the glacial aquifer system (layers 1 and 2) were reduced because of the model instability these withdrawals caused. The instability was likely a result of groundwater withdrawals in the thin and dry parts of the glacial aquifer system. The reduced groundwater withdrawals in the glacial aquifer system may affect the interaction of groundwater between the bedrock and glacial aquifers, but the potential change in interaction was assumed to be negligible.

Other model construction decisions were made that were not assumed to negatively affect the overall model results; for example, single water-level measurements were used for steady-state model calibration even though the measurements may have been taken during different periods. Also, data for wells on Indian reservations were not available for input because Native American Tribes are not required to report groundwater use or information on flowing wells. Lastly, evapotranspiration was not simulated explicitly because of the numerical instability it produced.

Summary

The U.S. Geological Survey developed a groundwater-flow model for the uppermost principal aquifer systems in the Williston Basin in parts of Montana, North Dakota, and South Dakota in the United States and parts of Manitoba and Saskatchewan in Canada as part of a detailed assessment of the groundwater availability of the area. The assessment was completed because of the potential for future dependency on groundwater for municipal and industrial needs in the area because of large-scale energy development. As a part of this assessment, a three-dimensional numerical groundwater-flow model was developed as a tool to understand groundwater availability that can be used to simulate how the groundwater-flow system responds to changes in hydrologic stresses at a regional scale.

The three-dimensional groundwater-flow model was developed using the U.S. Geological Survey's numerical finite-difference groundwater model with the Newton-Rhapson solver, MODFLOW–NWT, to represent the glacial, lower Tertiary, and Upper Cretaceous aquifer systems for steady-state (mean) hydrological conditions for 1981–2005 and transient (temporally varying) conditions using a combination of a steady-state period for pre-1960 and transient periods for 1961–2005. The numerical model framework was constructed based on existing and interpreted hydrogeologic and geospatial data and consists of eight layers: two layers representing the glacial aquifer system (upper part and lower part), three layers representing the lower Tertiary aquifer system (upper Fort Union aquifer, middle Fort Union hydrogeologic unit, and lower Fort Union aquifer), and three layers representing the Upper Cretaceous aquifer system (upper Hell Creek hydrogeologic unit, lower Hell Creek aquifer, and Fox Hills aquifer). The numerical model was constructed using a uniform grid with square cells that are about 1 mile (1,600 meters) on each side with a total of about 657,000 active cells.

Model calibration was completed by linking Parameter ESTimation (PEST) software with MODFLOW–NWT. The PEST software uses statistical parameter estimation techniques to identify an optimum set of input parameters by adjusting individual model input parameters and assessing the differences, or residuals, between observed (measured or estimated) data and simulated values. Steady-state model calibration consisted of attempting to match simulated values of (1) hydraulic head values, (2) hydraulic head differences between model layers, (3) stream infiltration, and (4) discharge to streams to observed values. Calibration of the transient model consisted of attempting to match simulated and observed values of temporally distributed hydraulic head changes, stream base flow, and groundwater discharge to flowing artesian wells. Hydraulic properties estimated through model calibration included horizontal hydraulic conductivity, vertical hydraulic conductivity, aquifer storage, and streambed hydraulic conductivity in addition to groundwater recharge and well skin.

The ability of the model to accurately simulate groundwater flow in the Williston Basin was assessed, primarily by its ability to match calibration targets for hydraulic head, stream base flow, and flowing artesian well discharge. The steady-state groundwater model also was used to assess the simulated potentiometric surfaces in the upper Fort Union aquifer, the lower Fort Union aquifer, and the Fox Hills aquifer. Additionally, a previously estimated regional groundwater-flow budget was compared with the simulated groundwater-flow budget for the Williston Basin. The simulated potentiometric surfaces typically compared well with the estimated potentiometric surfaces, and simulated and estimated potentiometric surfaces indicated localized groundwater-flow gradients that were topographically controlled in outcrop areas, and more generalized gradients where the aquifers were confined. Hydraulic head residuals (observed minus simulated values) indicated the steady-state model generally underestimated hydraulic head in the model area and was indicated by a positive mean residual of 11.2 feet for all model layers. Layer 7, which represents the lower Hell Creek aquifer, is the only layer for which the steady-state model overestimated hydraulic head. Simulated groundwater-level changes for the transient model matched within plus or minus 2.5 feet of the observed values for more than 60 percent of all measurements and to within plus or minus 17.5 feet for 95 percent of all measurements; however, the transient model underestimated

groundwater-level changes for all model layers. A comparison between simulated and estimated base flow for the steady-state and transient models indicated that the steady-state and transient models overestimated base flow in streams and underestimated annual fluctuations in base flow.

The estimated and simulated groundwater budgets indicate that the model area received a substantial amount of recharge from precipitation and stream infiltration. The steady-state model indicated reservoir seepage was a larger component of recharge in the Williston Basin than was previously estimated. Irrigation recharge and groundwater inflow from outside the Williston Basin accounted for a small part of total groundwater recharge. Most of the estimated and simulated groundwater discharge in the Williston Basin was to streams and reservoirs. Simulated groundwater withdrawal, discharge to reservoirs, and groundwater outflow in the Williston Basin accounted for a small part of total groundwater discharge.

The transient model was used to simulate discharge to 571 flowing artesian wells within the model area. Of the 571 established flowing artesian wells simulated by the model, 271 wells did not flow at any time during the simulation because hydraulic head was always below the land-surface altitude. As hydraulic head declined throughout the simulation, 68 of these wells responded by ceasing to flow by the end of 2005. Total mean simulated discharge for the 571 flowing artesian wells was 55.1 cubic feet per second (ft^3/s), and the mean simulated flowing well discharge at individual wells was 0.118 ft^3/s. Simulated discharge to individual flowing artesian wells increased from 0.039 to 0.177 ft^3/s between 1961 and 1975 and decreased to 0.102 ft^3/s by 2005. The mean residual for 34 flowing wells with measured discharge was 0.014 ft^3/s, which indicates the transient model overestimated discharge to flowing artesian wells in the model area.

Model limitations arise from aspects of the conceptual model and from simplifications inherent in the construction and calibration of a regional-scale numerical groundwater-flow model. Simplifying assumptions in defining hydraulic parameters in space and hydrologic stresses and time-varying observational data in time can limit the capabilities of this tool to simulate how the groundwater-flow system responds to changes in hydrologic stresses, particularly at the local scale; nevertheless, the steady-state model adequately simulated flow in the uppermost principal aquifer systems in the Williston Basin based on the comparison between the simulated and estimated groundwater-flow budgets, the comparison between simulated and estimated potentiometric surfaces, and the results of the calibration process.

References Cited

Alley, W.M., Evenson, E.J., Barber, N.L., Bruce, B.W., Dennehy, K.F., Freeman, M.C., Freeman, W.O., Fischer, J.M., Hughes, W.B., Kennen, J.G., Kiang, J.E., Maloney, K.O., Musgrove, MaryLynn, Ralston, Barbara, Tessler, Steven, and Verdin, J.P., 2013, Progress toward establishing a national assessment of water availability and use: U.S. Geological Survey Circular 1384, 34 p. [Also available at https://pubs.usgs.gov/circ/1384.]

Anna, L.O., 1981, Ground water resources of Billings, Golden Valley, and Slope Counties, North Dakota: North Dakota Geological Survey Bulletin 76, pt. 3, 56 p., 1 pl.

Anna, L.O., 2011, Effects of groundwater flow on the distribution of biogenic gas in parts of the Northern Great Plains of Canada and United States: U.S. Geological Survey Scientific Investigations Report 2010−5251, 24 p. [Also available at https://pubs.usgs.gov/sir/2010/5251/.]

Arcement, G.J., Jr., and Schneider, V.R., 1989, Guide for selecting Manning's roughness coefficients for natural channels and flood plains: U.S. Geological Survey Water-Supply Paper 2339, 38 p. [Also available at https://pubs.er.usgs.gov/publication/wsp2339/.]

Arihood, L.D., 2009, Processing, analysis, and general evaluation of well-driller logs for estimating hydrogeologic parameters of the glacial sediments in a ground-water flow model of the Lake Michigan Basin: U.S. Geological Survey Scientific Investigations Report 2008–5184, 26 p. [Also available at https://pubs.er.usgs.gov/publication/sir20085184.]

Armstrong, C.A., 1971, Ground-water resources of Burke and Mountrail Counties: North Dakota Geological Survey Bulletin 55, pt. 3, 86 p.

Bader, C.D., and Radig, S.A., 1991, Hydrologic assessment and delineation of wellhead protection areas for the city of Stanley, North Dakota: North Dakota State Water Commission, Ground-Water Studies no. 96, 102 p.

Barbosa, V.C.F., and Silva, J.B.C., 1994, Generalized compact gravity inversion: Geophysics, v. 59, no. 1, p. 57–68. [Also available at https://doi.org/10.1190/1.1443534.]

Croft, M.G., 1973, Ground-water resources of Mercer and Oliver Counties, North Dakota: North Dakota Geological Survey Bulletin 56, pt. 3, 81 p.

Croft, M.G., 1978, Ground-water resources of Adams and Bowman Counties, North Dakota: North Dakota Geological Survey Bulletin 65, pt. 3, 54 p.

Croft, M.G., 1985, Ground-water resources of McKenzie County, North Dakota: North Dakota Geological Survey Bulletin 80, pt. 3, 57 p.

Croft, M.G., and Wesolowski, E.A., 1970, Transmissivity and storage coefficient of aquifers in the Fox Hills Sandstone and Hell Creek Formation, Mercer and Oliver Counties, North Dakota, chap. B *of* Geological Survey Research 1970: U.S. Geological Survey Professional Paper 700–B, p. B190–B195.

Cummings, D.I., Russell, H.A.J., and Sharpe, D.R., 2012, Buried-valley aquifers in the Canadian Prairies—Geology, hydrogeology, and origin: Canadian Journal of Earth Sciences, v. 49, no. 9, p. 987–1004. [Also available at https://doi.org/10.1139/e2012-041.]

Davis, J.C., 2002, Statistics and Data Analysis in Geology (3d ed.): Hoboken, New Jersey., John Wiley & Sons, Inc., 638 p.

Davis, K.W., and Long, A.J., 2018, MODFLOW–NWT model used to assess groundwater availability in the uppermost principal aquifer systems of the Williston Basin, United States and Canada: U.S. Geological Survey data release, https://doi.org/10.5066/F75B01CZ.

Doherty, John, 2003, Ground water model calibration using pilot points and regularization: Ground Water, v. 41, no. 2, p. 170–177. [Also available at https://doi.org/10.1111/j.1745-6584.2003.tb02580.x.]

Doherty, J.E., 2010, PEST—Model-independent parameter estimation—User manual (5th ed.): Brisbane, Australia, Watermark Numerical Computing, accessed June 28, 2010, at http://www.pesthomepage.org/files/pestman.pdf.

Doherty, John, 2014, Addendum to the PEST manual: Brisbane, Australia, Watermark Numerical Computing, 316 p.

Doherty, J.E., and Hunt, R.J., 2009, Two statistics for evaluating parameter identifiability and error reduction: Journal of Hydrology, v. 366, no. 1–4, p. 119–127. [Also available at https://doi.org/10.1016/j.jhydrol.2008.12.018.]

Doherty, J.E., and Hunt, R.J., 2010, Approaches to highly parameterized inversion—A guide to using PEST for groundwater-model calibration: U.S. Geological Survey Scientific Investigations Report 2010–5169, 59 p. [Also available at https://pubs.usgs.gov/sir/2010/5169/.]

Downey, J.S., 1986, Geohydrology of bedrock aquifers in the Northern Great Plains in parts of Montana, North Dakota, South Dakota, and Wyoming: U.S. Geological Survey Professional Paper 1402–E, 87 p., 3 pls. [Also available at https://pubs.er.usgs.gov/publication/pp1402E.]

Eisenlohr, W.S., Jr., and Sloan, C.E., 1968, Generalized hydrology of prairie potholes on the Coteau du Missouri, North Dakota: U.S. Geological Survey Circular 558, 12 p. [Also available at https://pubs.er.usgs.gov/publication/cir558.]

Fischer, Kimberly, 2013, Groundwater flow model inversion to assess water availability in the Fox Hills-Hell Creek aquifer: North Dakota State Water Commission, Water Resource Investigation no. 54, 325 p.

Gesch, D.B., 2007, The National Elevation Dataset, *in* Maune, D.F., ed., Digital elevation model technologies and applications—The DEM user's manual (2d ed.): Bethesda, Md., American Society for Photogrammetry and Remote Sensing, p. 99–118.

Gesch, D.B., Oimoen, Michael, Greenlee, S.K., Nelson, C.A., Steuck, Michael, and Tyler, Dean, 2002, The National Elevation Dataset: Photogrammetric Engineering and Remote Sensing, v. 68, no. 1, p. 5–11.

Groundwater Information Network, 2012a, Waterwell databases—Manitoba: Groundwater Information Network database, accessed January 2013 at http://gin.gw-info.net/service/ngwds//en/downloadmanager/get/gw_mb.zip.

Groundwater Information Network, 2012b, Waterwell databases—Saskatchewan: Groundwater Information Network database, accessed January 2013 at http://gin.gw-info.net/service/ngwds//en/downloadmanager/get/gw_sk.zip.

Groundwater Information Center, 2013, Ground Water Information Center well data: Montana Bureau of Mines and Geology digital data, accessed January 10, 2013, at http://mbmggwic.mtech.edu.

Halford, K.J., and Hanson, R.T., 2002, User guide for the drawdown-limited, Multi-Node Well (MNW) Package for the U.S. Geological Survey's Modular Three-Dimensional Finite-Difference Ground-Water Flow Model, Versions MODFLOW–96 and MODFLOW–2000: U.S. Geological Survey Open-File Report 02–293, 33 p. [Also available at https://pubs.usgs.gov/of/2002/ofr02293/text.html.]

Harbaugh, A.W., 2005, MODFLOW-2005—The U.S. Geological Survey modular ground-water model−The ground-water flow process: U.S. Geological Survey Techniques and Methods 6–A16, variously paged. [Also available at https://pubs.usgs.gov/tm/2005/tm6A16/.]

Harrill, J.R., 1986, Ground-water storage depletion in Pahrump Valley, Nevada–California, 1962–75: U.S. Geological Survey Water-Supply Paper 2279, 53 p., 3 pls. [Also available at https://pubs.er.usgs.gov/publication/wsp2279.]

Honeyman, R.P., 2007a, Pressure head fluctuations of the Fox Hills-Hell Creek aquifer in Billings, Golden Valley, and Slope Counties, North Dakota: North Dakota State Water Commission Water Resource Investigation no. 42, 115 p.

Honeyman, R.P., 2007b, Pressure head fluctuations of the Fox Hills-Hell Creek aquifer in the Knife River Basin, North Dakota: North Dakota State Water Commission Water Resource Investigation no. 44, 86 p.

Honeyman, R.P., 2007c, Pressure head fluctuations of the Fox Hills-Hell Creek aquifer in McKenzie County, North Dakota: North Dakota State Water Commission Water Resource Investigation no. 43, 130 p.

Hutson, S.S., Barber, N.L., Kenny, J.F., Linsey, K.S., Lumia, D.S., and Maupin, M.A., 2004, Estimated use of water in the United States in 2000: U.S. Geological Survey Circular 1268, 52 p. [Also available at https://pubs.usgs.gov/circ/2004/circ1268/.]

Kehew, A.E., and Boettger, W.M., 1986, Depositional environments of buried-valley aquifers in North Dakota: Groundwater, v. 24, no. 6, p. 728–734. [Also available at https://doi.org/10.1111/j.1745-6584.1986.tb01688.x.]

Kenny, J.F., Barber, N.L., Hutson, S.S., Linsey, K.S., Lovelace, J.K., and Maupin, M.A., 2009, Estimated use of water in the United States in 2005: U.S. Geological Survey Circular 1344, 52 p. [Also available at https://pubs.usgs.gov/circ/1344/.]

Klausing, R.L., 1974, Ground-water resources of McLean County, North Dakota: North Dakota Geological Survey Bulletin 60, pt. 3, 73 p.

Klausing, R.L., 1979, Ground-water resources of Dunn County, North Dakota: North Dakota Geological Survey Bulletin 68, pt. 3, 48 p.

Konikow, L.F., Hornberger, G.Z., Halford, K.J., and Hanson, R.T., 2009, Revised multi-node well (MNW2) package for MODFLOW ground-water flow model: U.S. Geological Survey Techniques and Methods 6–A30, 67 p. [Also available at https://pubs.usgs.gov/tm/tm6a30/.]

Leaf, A.T., Fienen, M.N., Hunt, R.J., and Buchwald, C.A., 2015, Groundwater/surface-water interactions in the Bad River Watershed, Wisconsin: U.S. Geological Survey Scientific Investigations Report 2015–5162, 110 p. [Also available at https://doi.org/10.3133/sir20155162.]

Long, A.J., Aurand, K.R., Bednar, J.M., Davis, K.W., Mckaskey, J.D.R.G., and Thamke, J.N., 2014, Conceptual model of the uppermost principal aquifer systems in the Williston and Powder River structural basins, United States and Canada: U.S. Geological Survey Scientific Investigations Report 2014–5055, 41 p., with appendix. [Also available at https://doi.org/10.3133/sir20145055.]

Love, J.D., and Christiansen, A.C., 1985, Geologic map of Wyoming: U.S. Geological Survey, scale 1:500000. [Also available at https://ngmdb.usgs.gov/Prodesc/prodesc_16366.htm.]

McDonald, M.G., and Harbaugh, A.W., 1988, A modular three-dimensional finite-difference groundwater flow model: U.S. Geological Survey Techniques of Water-Resources Investigations, book 6, chap. A1, 586 p. [Also available at https://pubs.usgs.gov/twri/twri6a1/.]

McKay, Lucinda, Bondelid, Timothy, Dewald, Tommy, Johnston, Craig, Moore, Richard, and Rea, Alan, 2012, NHDPlus Version 2—User guide: United States Environmental Protection Agency, accessed September 20, 2012, at http://www.horizon-systems.com/NHDPlus/NHDPlusV2_documentation.php.

McWhorter, D.B., 1984, Specific yield by geophysical logging potential for the Denver Basin: Colorado Water Resources Research Institute Technical Completion Report no. 132, 32 p.

Montana Department of Environmental Quality, 2012, Public water systems digital database, accessed October 29, 2012, at http://deq.mt.gov/Water/PWSUB/pws.

Montana Department of Natural Resources and Conservation, 2015, Montana State Water Plan: Montana Department of Natural Resources and Conservation, 80 p., accessed March 24, 2017, at http://dnrc.mt.gov/divisions/water/management/docs/state-water-plan/2015_mt_water_plan.pdf.

Multi-Resolution Land Characteristics Consortium, 2011, National land cover database—Conterminous United States NLCD 2006 land cover: Multi-Resolution Land Characteristics Consortium, 20-m data, accessed September 26, 2011, at http://www.mrlc.gov/nlcd2006_downloads.php.

National Oceanic and Atmospheric Administration, 2014, Daily summaries station details—Williston Sloulin Field International Airport, ND US: National Oceanic and Atmospheric Administration digital data, accessed October 27, 2014, at https://www.ncdc.noaa.gov/cdo-web/datasets/GHCND/stations/GHCND:USW00094014/detail/.

Natural Resources Canada, 2012, National Hydro Network (NHN) (updated August 31, 2015): Department of Natural Resources, Canada, accessed August 2012 at http://open.canada.ca/data/en/dataset/a4b190fe-e090-4e6d-881e-b87956c07977/.

Niswonger, R.G., Panday, Sorab, and Ibaraki, Motomu, 2011, MODFLOW–NWT, A Newton formulation for MODFLOW–2005: U.S. Geological Survey Techniques and Methods 6–A37, 44 p. [Also available at https://pubs.usgs.gov/tm/tm6a37/.]

Niswonger, R.G., and Prudic, D.E., 2005, Documentation of the Streamflow-Routing (SFR2) Package to include unsaturated flow beneath streams—A modification to SFR1: U.S. Geological Survey Techniques and Methods 6–A13, 51 p. [Also available at https://pubs.er.usgs.gov/publication/tm6A13.]

North Dakota Information Technology Department, 2012, North Dakota Geographic Information Systems water data sites: North Dakota State Water Commission, accessed October 29, 2012, at https://gishubdata.nd.gov/dataset/ground-and-surface-water-data.

North Dakota State Water Commission, 2010, Surficial aquifers: North Dakota State Water Commission, accessed June 22, 2012, at https://gishubdata.nd.gov/dataset/surficial-aquifers.

North Dakota State Water Commission, 2013, Groundwater/surface water data: North Dakota State Water Commission, accessed June 11, 2013, at http://www.swc.nd.gov/info_edu/map_data_resources/groundsurfacewater/.

North Dakota State Water Commission, 2015, 2015 North Dakota State Water Management Plan: North Dakota State Water Commission, 119 p., accessed March 24, 2017, at http://www.swc.nd.gov/info_edu/state_water_plan/archives/pdfs/2015-2017%20Water%20Management%20Plan.pdf.

Peterson, J.A., 1984, Stratigraphy and sedimentary facies of the Madison Limestone and associated rocks in parts of Montana, Nebraska, North Dakota, South Dakota, and Wyoming: U.S. Geological Survey Professional Paper 1273–A, 34 p. [Also available at https://pubs.er.usgs.gov/publication/pp1273A.]

Prudic, D.E., Konikow, L.F., and Banta, E.R., 2004, A new Streamflow-Routing (SFR1) Package to simulate stream-aquifer interaction with MODFLOW–2000: U.S. Geological Survey Open-File Report 2004–1042, 104 p. [Also available at https://pubs.er.usgs.gov/publication/ofr20041042.]

Pugin, A.J.M., Oldenborger, G.A., Cummings, D.I., Russell, H.A.J., and Sharpe, D.R., 2014, Architecture of buried valleys in glaciated Canadian Prairie regions based on high resolution geophysical data: Quaternary Science Reviews, v. 86, p. 13–23. [Also available at https://doi.org/10.1016/j.quascirev.2013.12.007.]

Robson, S.G., 1987, Bedrock aquifers in the Denver Basin, Colorado—A quantitative water-resources appraisal: U.S. Geological Survey Professional Paper 1257, 73 p. [Also available at https://pubs.er.usgs.gov/publication/pp1257.]

Rossum, Guido van, and Drake, F.L., Jr., 2011, The Python language reference manual: United Kingdom, Network Theory Limited, 150 p.

Rutledge, A.T., 1998, Computer programs for describing the recession of ground-water discharge and for estimating mean ground-water recharge and discharge from streamflow records—Update: U.S. Geological Survey Water-Resources Investigations Report 98–4148, 52 p. [Also available at https://pubs.usgs.gov/wri/wri984148/.]

Saskatchewan Water Security Agency, 2012, Community water use records 1997 to 2011: Saskatchewan Water Security Agency, Saskatchewan Watershed Authority Report no. 25, 244 p., accessed November 26, 2013, at https://www.wsask.ca/About-WSA/Publications/Community-Water-Use-Records/.

Saskatchewan Water Security Agency, 2014, Observation well network: Saskatchewan Water Security Agency, accessed July 16, 2014, at https://www.wsask.ca/Water-Info/Ground-Water/Observation-Wells/.

Scott, J.C., 1990, Computerized stratified random site-selection approaches for design of ground-water-quality sampling network: U.S. Geological Survey Water-Resources Investigations Report 90–4101, 109 p. [Also available at https://pubs.er.usgs.gov/publication/wri904101.]

Sloan, C.E., 1972, Ground-water hydrology of prairie potholes in North Dakota: U.S. Geological Survey Professional Paper 585–C, 27 p. [Also available at https://pubs.er.usgs.gov/publication/pp585C.]

Smith, L.N., LaFave, J.I., Patton, T.W., Rose, J.C., and McKenna, D.P., 2000, Ground-water resources of the lower Yellowstone River area—Dawson, Fallon, Prairie, Richland, and Wibaux Counties, Montana: Montana Bureau of Mines and Geology, Montana Ground-Water Atlas no. 1, 93 p.

Solley, W.B., Merk, C.F., and Pierce, R.R., 1988, Estimated use of water in the United States in 1985: U.S. Geological Survey Circular 1004, 82 p. [Also available at https://pubs.er.usgs.gov/publication/cir1004.]

Solley, W.B., Pierce, R.R., and Perlman, H.A., 1993, Estimated use of water in the United States in 1990: U.S. Geological Survey Circular 1081, 76 p. [Also available at https://pubs.er.usgs.gov/publication/cir1081.]

Solley, W.B., Pierce, R.R., and Perlman, H.A., 1998, Estimated use of water in the United States in 1995: U.S. Geological Survey Circular 1200, 71 p. [Also available at https://pubs.er.usgs.gov/publication/cir1200.]

South Dakota Department of Environment and Natural Resources, 2013, South Dakota water well completion reports: South Dakota Department of Environment and Natural Resources database, accessed March 3, 2013, at http://denr.sd.gov/des/wr/dblogsearch.aspx.

Stoner, J.D., 1981, Horizontal anisotropy determined by pumping in two Powder River Basin coal aquifers, Montana: Groundwater, v. 19, no. 1, p. 34–40. [Also available at https://doi.org/10.1111/j.1745-6584.1981.tb03435.x.]

Thamke, J.N., LeCain, G.D., Ryter, D.W., Sando, Roy, and Long, A.J., 2014, Hydrogeologic framework of the uppermost principal aquifer systems in the Williston and Powder River structural basins, United States and Canada (ver. 1.1, December 2014): U.S. Geological Survey Scientific Investigations Report 2014–5047, 38 p. [Also available at https://doi.org/10.3133/sir20145047.]

Tikhonov, A.N., 1963a, Regularization of incorrectly posed problems: Soviet Mathematics, v. 4, no. 6, p. 1624–1637.

Tikhonov, A.N., 1963b, Solution of incorrectly formulated problems and the regularization method: Soviet Mathematics Doklady, v. 4, no. 4, p. 1035–1038.

Tonkin, M.J., and Doherty, John, 2005, A hybrid regularized inversion methodology for highly parameterized environmental models: Water Resources Research, v. 41, no. 10, paper W10412, 16 p., accessed August 28, 2015, at https://doi.org/10.1029/2005WR003995.

U.S. Army Corps of Engineers, 2013, Monthly project statistics−Garrison: U.S. Army Corps of Engineers, accessed November 8, 2013, at http://www.nwd-mr.usace.army.mil/rcc/projdata/garr.pdf.

U.S. Geological Survey, 2014a, National Elevation Dataset: U.S. Geological Survey, accessed September 24, 2014, at https://ned.usgs.gov/.

U.S. Geological Survey, 2014b, USGS water data for the Nation: U.S. Geological Survey National Water Information System database, U.S. Geological Survey, accessed July 10, 2014, at https://doi.org/10.5066/F7P55KJN.

Van der Kamp, Garth, and Hayashi, Masaki 1998, The groundwater recharge function of small wetlands in the semi-arid northern prairies: Great Plains Research—A Journal of Natural and Social Sciences, v. 8, p. 39–56.

Wanek, Alan, 2009, Recommended decision for the city of Alexander Water Permit Application no. 5990: North Dakota Office of the State Engineer report, 94 p.

Water Survey of Canada, 2013, HYDAT—Archived hydrometric data online: accessed March 3, 2013, at http://www.ec.gc.ca/rhc-wsc/default.asp?lang=En&n=9018B5EC-1.

Westenbroek, S.M., Kelson, V.A., Dripps, W.R., Hunt, R.J., and Bradbury, K.R., 2010, SWB—A modified Thornthwaite-Mather Soil-Water-Balance code for estimating groundwater recharge: U.S. Geological Survey Techniques and Methods 6–A31, 60 p. [Also available at https://pubs.usgs.gov/tm/tm6-a31/.]

Whitehead, R.L., 1996, Ground water atlas of the United States—Segment 8, Montana, North Dakota, South Dakota, Wyoming: U.S. Geological Survey Hydrologic Atlas 730, chap. I, 24 p.

Wilson, W.E., and Moore, J.E., eds., 1998, Glossary of hydrology: Alexandria, Virginia, American Geological Institute, 248 p.

Glossary

calibration target Observed (measured or estimated) values of hydraulic head, hydraulic head differences between model layers, stream infiltration, discharge to streams, and discharge to flowing wells that correspond to model-calculated values.

control volume Volume of the Earth consisting of the lower Tertiary and Upper Cretaceous aquifer systems and the overlying areas of the glacial aquifer system in the Williston Basin.

lake flux Rate of groundwater interaction with wetlands and lakes.

model area Spatial extent of the active model area.

objective-function value Sum of squared weighted differences (residuals) between observed values of hydrologic conditions and simulated equivalents.

observation data Measured or estimated values of hydrologic conditions used in model calibration.

pilot point Discrete locations distributed throughout the model area that represent surrogate parameters from which hydraulic property values are interpolated to the model grid.

steady-state model Numerical groundwater-flow model of the uppermost principal aquifer systems in the Williston Basin representing mean conditions for the period 1981–2005 with groundwater withdrawal.

stream flux Rate of groundwater interaction with streams.

SWB-estimated recharge Annual precipitation recharge for the Williston Basin for 1981–2011 estimated by Long and others (2014) using the Soil-Water-Balance (SWB) model.

transient model Numerical groundwater-flow model of the uppermost principal aquifer systems in the Williston Basin representing mean hydrological conditions for 1981–2005 without groundwater withdrawal and temporally-varying conditions for 1961–2005.

transient stress period A period simulated by the numerical model that represents the change from initial conditions at the beginning of the period to the end of the period.

vertical hydraulic head difference calibration target The difference in hydraulic head between separate model layers.

Appendixes 1–2

Appendix 1. Model Calibration Targets and Optimized Parameter Estimates

The tables are presented as a Microsoft® Excel workbook and can be downloaded from https://doi.org/10.3133/sir20175158.

Table 1–1. Groundwater-level calibration targets for the steady-state model and the transient model, in feet above the North American Vertical Datum of 1988.

Table 1–2. Groundwater-level change calibration targets for the transient model by stress period.

Table 1–3. Vertical hydraulic head difference calibration targets for the steady-state model.

Table 1–4. Estimated streambed hydraulic conductivity and estimated and simulated base flow or stream flux by reach for streams simulated by the Streamflow-Routing (SFR2), River, and Drain Packages.

Table 1–5. Estimated and simulated discharge to flowing artesian wells simulated using the Multi-Node Well Package.

References Cited

Davis, K.W., and Long, A.J., 2018, MODFLOW–NWT model used to assess groundwater availability in the uppermost principal aquifer systems of the Williston Basin, United States and Canada: U.S. Geological Survey data release, https://doi.org/10.5066/F75B01CZ.

Groundwater Information Center, 2013, Ground Water Information Center well data: Montana Bureau of Mines and Geology digital data, accessed January 10, 2013, at http://mbmggwic.mtech.edu.

Groundwater Information Network, 2012a, Waterwell databases—Manitoba: Groundwater Information Network Database, accessed January 2013 at http://gin.gw-info.net/service/ngwds//en/downloadmanager/get/gw_mb.zip.

Groundwater Information Network, 2012b, Waterwell databases—Saskatchewan: Groundwater Information Network Database, accessed January 2013 at http://gin.gw-info.net/service/ngwds//en/downloadmanager/get/gw_sk.zip.

North Dakota State Water Commission, 2013, Groundwater/surface water data: North Dakota State Water Commission, accessed June 11, 2013, at http://www.swc.nd.gov/info_edu/map_data_resources/groundsurfacewater/.

U.S. Geological Survey, 2014b, USGS water data for the Nation: U.S. Geological Survey National Water Information System database, U.S. Geological Survey, accessed July 10, 2014, at https://doi.org/10.5066/F7P55KJN.

Water Survey of Canada, 2013, HYDAT—Archived hydrometric data online: accessed March 3, 2013, at http://www.ec.gc.ca/rhc-wsc/default.asp?lang=En&n=9018B5EC-1.

Appendix 2. Model Calibration Weights

The tables are presented as a Microsoft® Excel workbook and can be downloaded from https://doi.org/10.3133/sir20175158.

Table 2–1. Data-quality rank assignment for water-level calibration data.

Table 2–2. Potentiometric assessment category for wells open to bedrock hydrogeologic units. Water levels were assessed in comparison to potentiometric surfaces from Thamke and others (2014).

Table 2–3. Assignment of observation groups A through F based on data-quality ranks 1–6 and potentiometric assessment categories "high," "medium," and "low."

Table 2–4. Observation weights for model calibration.

Weighting observation data is critical for the calibration process using Parameter ESTimation (PEST) software because the determination of observation weights guides the process by providing a balance of the resulting model fit to the different categories of observation data. Calibration weights were applied according to recommendations described by Doherty and Hunt (2010). Observations used in calibration were assigned to observation groups, which were weighted so that the total contribution to the objective-function value for each group was proportional to the data value of that group with respect to data accuracy or importance in modeling objectives. General observation categories consisted of groundwater levels, flow rates from free-flowing wells, and the exchange of groundwater and surface water.

The largest and most complex dataset was for groundwater levels; this dataset contains wells with a wide range of data quality. A stepwise process that considers many factors was developed to separate the wells from this dataset into six observation groups and assign a relative, or ranked, value to these groups. The first step of this process was to assign a data-quality rank from 1 to 6 (1 is high-value data) based on three criteria for steady-state calibration: the highest data-quality ranking was assigned to wells with a U.S. Geological Survey (USGS) site visit (criterion 1), a large number of measurements (criterion 2), and little change in water level for a well with multiple measurements (criterion 3; table 2–1). A USGS site visit was considered the primary criterion because a well without a site visit might have only a general location that was provided by a well driller, which can lead to an inaccurate land-surface altitude. Criterion 2 was considered important because a large number of measurements provides a reliable mean value, as well as good tracking of temporal changes. For criterion 3, wells with an annual mean water-level change of greater than or equal to (≥)0.4 foot (ft) were assigned a lower rank than those with less than (<)0.4 ft change (table 2–1). Criteria 1 and 2 were applied to steady-state and transient calibration data. Criterion 3 applied to steady-state calibration only because wells with little water-level change were assumed to best represent steady-state conditions.

The second step was to assign each well to the potentiometric assessment categories "high," "medium," and "low" based on water-level consistency with the estimated potentiometric surfaces (table 2–2); this analysis was independent of the data-quality ranking from step 1. The reason for this step was to consider the collective consistency of the data by comparison of the mean water level of each well to potentiometric surfaces, which required that the supporting data be spatially consistent. The mean water level for each well was used in this analysis. Wells that were used in developing the potentiometric surfaces were considered by Thamke and others (2014) to provide the highest-quality data and, by definition, were known to be consistent with the potentiometric surfaces; these wells were assigned to the potentiometric assessment category of "high." All other wells were assigned to the "medium" or "low" categories by first assigning all wells to groups I through IV according to criteria described in table 2–2. Next, groups I and IV were separated into two subgroups, which are also described in table 2–2. Because potentiometric surfaces were not available for the glacial aquifer system, the potentiometric assessment category of "medium" was assumed for all wells open to the glacial aquifer system.

The third step was to combine the data-quality ranks and potentiometric assessment categories from tables 2–1 and 2–2 to create six observation groups (A through F) that are differentiated by data quality, in which observation group A is considered to contain the highest quality data (table 2–3). The relative calibration weights for observation groups and actual observation weights for individual calibration targets are summarized in table 2–4.

Additional observation groups relate to head-dependent fluxes into and out of the groundwater system (table 2–4). The differences among the two potentiometric surfaces and simulated equivalents at selected points and simulated and measured flow rates from flowing wells (Honeyman, 2007a, 2007b, 2007c) were the seventh and eighth observation

groups, respectively. Simulated stream base-flow values were extracted from the simulation using the Gage Package and were calibrated to estimated values, as previously described; these were separated into the observation groups Gage-1, Gage-2, and Gage-3. Gage-1 and Gage-2 groups represented streamgages in the glacial and bedrock aquifers, respectively. Gage-3 represented large-flow streamgages for the Missouri and Yellowstone Rivers that were given a low observation-group weight, because the accuracy of base-flow estimates on these large rivers is questionable (Long and others, 2014). The observation group "stream flux" represented the rate of exchange of surface water and groundwater for Canada, which was simulated by the River and Drain Packages. Relative observation groups for the steady-state and transient calibration models were assigned before initial model calibration but were changed moderately during model calibration. The final relative observation weights are shown in table 2–4 along with the individual observation weights.

References Cited

Halford, K.J., and Hanson, R.T., 2002, User guide for the drawdown-limited, Multi-Node Well (MNW) Package for the U.S. Geological Survey's Modular Three-Dimensional Finite-Difference Ground-Water Flow Model, Versions MODFLOW–96 and MODFLOW–2000: U.S. Geological Survey Open-File Report 02–293, 33 p. [Also available at https://pubs.usgs.gov/of/2002/ofr02293/text.html.]

Harbaugh, A.W., 2005, MODFLOW-2005—The U.S. Geological Survey modular ground-water model−The ground-water flow process: U.S. Geological Survey Techniques and Methods 6–A16, variously paged, [Also available at https://pubs.usgs.gov/tm/2005/tm6A16/.]

Prudic, D.E., Konikow, L.F., and Banta, E.R., 2004, A new Streamflow-Routing (SFR1) Package to simulate stream-aquifer interaction with MODFLOW–2000: U.S. Geological Survey Open-File Report 2004–1042, 104 p. [Also available at https://pubs.er.usgs.gov/publication/ofr20041042.]

For additional information contact:

Director, South Dakota Water Science Center
U.S. Geological Survey
1608 Mountain View Rd.
Rapid City, SD 57702
https://sd.water.usgs.gov

Publishing support by:
The Rolla and Pembroke Publishing Service Centers

ISSN 2328-0328 (online)
https://doi.org/10.3133/sir20175158